Mechanical characterization of a Tire Derived Material and its Application in Vibration Reduction

by

Giuseppe Montella

A dissertation submitted in partial satisfaction of the

requirements for the degree of

Doctor of Philosophy

in

Construction Engineering

University of Naples, “Federico II”

Abstract

Mechanical characterization of a Tire Derived Material and its Application in Vibration Reduction

by

Giuseppe Montella

Doctor of Philosophy in Construction Engineering

University of Naples, "Federico II"

Tire Derived Materials (TDMs) deserve special interest as the reuse of tires is one of the most important topics in recycling and Environmental Engineering. This thesis describes the mechanical characterization of a new TDM based on appropriate experimental tests. Moreover a novel strain energy function is presented, based on the Hencky-logarithmic strain tensor, to model the response for moderately large deformations. TDM is a composite made by cold forging a mix of rubber fibers and grains, obtained by grinding scrap tires, and polyurethane binder. The mechanical properties are highly influenced by the presence of voids associated to the granular composition and low tensile strength due to the weak connection at the grain-matrix interface. For these reasons, TDM use is restricted to applications concerning a limited range of deformations.

Shear, compression and volumetric tests were performed on the material showing a stiffening behavior under compression, hysteresis and strain rate sensitivity of the material. A central feature of the response is connected to highly nonlinear behavior of the material under volumetric deformation which conventional hyperelastic models fail in predicting.

To further investigate this behavior, during the compression tests optical measurement techniques were used for the measurement of displacement fields allowing to evaluate the Poisson's coefficient in both the neighborhood of the undeformed state (linear Poisson's coefficient) and for large deformation (nonlinear Poisson's coefficient). The strain energy function presented here is a variant of the exponentiated Hencky strain energy proposed by Neff et al. [63], which for moderate strains, is as good as the quadratic Hencky model and in the large strain region it improves several important features from a mathematical point of view. One of the advantages of using the proposed form of the exponentiated Hencky energy is that it possesses a set of parameters uniquely determined in the infinitesimal strain regime and an orthogonal set of parameters to determine the nonlinear response that do not interfere with them.

The hyperelastic model is incorporated in a finite deformation viscoelasticty model based on the multiplicative decomposition of the deformation gradient into elastic and inelastic parts. It utilizes a nonlinear evolution equation as proposed by Reese and Govindjee [69].

Most of the parameters have a clear physical meaning, we choose the ones suggested by the experimental tests and allowed by the mathematical theory. The advantage is to overcome the difficulties related to finding a unique set of optimal parameters that are usually encountered fitting polynomial forms of strain energies. Moreover, by comparing the predictions from the proposed constitutive model with experimental data we conclude that the new constitutive model gives good prediction.

Finally a Finite element program is used to solve an optimization problem of railway track mat for light-weight lines.

To

my wife

Contents

List of Figures

List of Tables

Acknowledgments

I would like to express my sincere gratitude to Professor Giorgio Serino whom which I have had the pleasure of working with since 2009. He was the advisor of my first Masters thesis his guidance and encouragement have brought me this far.

I also would like to thank Professor Govindjee at UC Berkeley, he gave me the possibility to join his group and that was one of the best learning experiences I have ever had. He has always been full of suggestions and in a short time he became one of my inspirations.

I am also very grateful to Professor Neff at University of Duisburg-Essen for his help and enthusiasm. Part of this work on the strain energy functions comes from pleasant and stimulating discussions I had with him.

Additionally, I want to express my gratitude to Isolgomma s.r.l for providing the material objects of my study and in particular Gianfranca and Marco.

Finally, I want to thank my family all and in particular the best teammate I could have ever asked for my wife Raquel.

Thank you,
Giuseppe

Nomenclature

The notation used in this thesis is in agreement with the one used in Holzapfel [37] . The reader may want to refer to the book for a more extensive introduction to the algebra of Vectors and Tensors. Following the notations used throughout the thesis are explained. Scalars are typeset in standard letters(e.g. κ, μ), vectors are printed bold (e.g. $\mathbf{x}, \tau$) , second order tensors are set bold -face Latin (e.g. $\sigma, \mathbf{F}$).

Higher order tensors are set in blackboard bold letters (e.g.$\mathbb{C}, \mathbb{P}$). The quantities in the reference configuration are written in upper case letters, while the quantities in the actual configuration are written in lower case letters.

Indices designate components of the tensor quantities (e.g. $\sigma_{i,j}$=$\mathbf{e}_i \cdot \sigma \mathbf{e}_j$ is the $\{i, j\}$ component of the Cauchy stress σ).

The Kroenecker delta $\delta_{i,j}$ designates the components of the second order identity tensor $\mathbf{1}$ ($\delta_{i,j} = 1$ if $i = j$ and 0 elsewhere).

Parenthesis define function arguments (e.g. $f(x)$ is a function f with argument x).

Operators

$\langle \bullet \rangle$	Macaulay brackets
$(\bar{\bullet})$	Isochoric part
$(\dot{\bullet})$	Total time derivative
$(\bullet)'$	Deviator
$(\bullet)^{\mathrm{T}}$	Transpose
$(\bullet)_{\mathrm{vol}}$	Volumetric part
$(\bullet) : (\clubsuit)$	Double contraction
$(\bullet) \cdot (\clubsuit)$	Contraction
$(\bullet) \otimes (\clubsuit)$	Tensor product
$(\bullet) \times (\clubsuit)$	Vector cross product
$\bigtriangledown(\bullet)$	Gradient
abs$(\bullet)$	Absolute value
adj$(\bullet)$	Adjugate
D$(\bullet)$	Total derivative
det$(\bullet)$	Determinant
eig$(\bullet)$	Eigenvalues
grad$(\bullet)$	Gradient
ln$(\bullet)$	Natural logarithm
tr$(\bullet)$	Trace

Chapter 1

Introduction

This thesis is part of the project Dottorato in Azienda funded by POR Campania 2007. The aim of this thesis is to improve the understanding of Tire Derived Material including the modeling of the mechanical behavior and the application of simulation tools to improve the design.

This thesis provides a suitable model formulation based on appropriate experimental tests for the material including the parameter determination of the viscoelastic constitutive equations and finally the use of Finite Element theory to solve design problems.

Currently there is a lack of information on the behavior of Tire derived Material and no constitutive models have been proposed for this kind of material yet. Tire Derived Materials (TDMs) deserve special interest as the reuse of tires is one of the most important topics in recycling and Environmental Engineering.

According to the European Tire and Rubber Manufacturers Association, in 2012, the European Union generated approximately 3,418 million tons of scrap tires. However, 37% of these scrap tires are used for energy recovery mainly as fuel in kilns to produce cement, 39% are used as recycling materials for Civil Engineering work and product applications, almost the 5% is disposed to landfill or is illegally dumped and the remaining quota is traded or sold abroad [24] .

Also, the energy recovered from exhausted tires by waste-to-energy plants is a quarter of the energy needed for their production and the process itself raises obvious pollution concerns. Moreover, tires are not desired at landfills because of their large volume and 75% void space, which quickly consume areas. Also the chemical released from scrap tires can damage landfill liners that are generally installed to prevent the pollution of local surface and ground water.

In response to these problems research on uses of scrap tires has created many new markets and innovative applications [55] [32] [16]. The US Environmental Protection Agency has conducted research projects on scrap tires including rubberized asphalts and protection

systems against erosion of bridge piers [50]. The US Department of Energy has conducted research on innovative scrap tire uses. They investigated the development of methods for treating rubber from scrap tires in order to use it as automotive seals and gaskets, sealants, adhesives. Recycled rubber is also used to make absorptive sound barriers, playground surfaces, athletic and recreational applications [80].

Recently this kind of material has also been used to make low-cost devices for structural isolation [14] [15] [47]. Despite the advantages, a main drawback is that the recycled rubber is generally treated with procedures that require much more energy than the production of the polymers it replaces.

Different kinds of materials can be obtained by recycling used tires. The aim of this paper is to investigate the mechanical behavior of a TDM with a low cost and an easy to implement production process. This material can be very appealing for the production of low cost anti vibration-devices in replacement of the ones made of natural rubber especially in massive applications like railway track systems [56].

1.1 Outline of the thesis

The first two chapters introduce the reader to the new material and its applications and the mechanics of continuous deformable body that will be used throughout this thesis.

Chapter 2

This chapter gives an overview of the tire disposal issue and all the efforts of government agencies in helping state and local governments reduce the economic burdens and environmental risks associated with scrap tire piles on their landscapes.

New environmentally safe application for scrap tires have been introduced in the past three decades are described, they can be organized in three markets: Tire-derived fuel, Civil engineering application and Ground rubber application/rubberized asphalt. Despite of the that there is a lot more to be done to solve the issue of reusing scrap tires.

The new Tire Derived Material (TDM) object of study is introduced including its applications in railway track and seismic protection of structures. This new TDM claims a simple and easy to implement production process that can make the material very appealing from the economic point of view.

Chapter 3

The basic aspects of nonlinear continuum mechanics are presented. It starts with the introduction of kinematic quantities and continues with the stress measures. Thereafter constitutive equation used throughout the thesis are explained and eventually the elasticity tensor are defined.

Chapter 4 describe the experimental tests campaign on TDM while in chapter 5 the fitting on hyperelastic model is presented along with the new hyperelastic model based on Hencky strain.

Chapter 4

This chapter shows the experimental campaign performed on the TDMs. For this particular material there is a lack of information on the mechanical behavior. The need of explore the potential of the material in order to find new application motivated the choice of extensive testing.

The material due to its composition is suitable only for some of the testing procedure. Experiments were carried out in compression, tension and shear underlining the benefits and the limits of the new material. Furthermore, volumetric tests were performed in order to evaluate the bulk modulus of the material.

Tests showed great nonlinearity in the volumetric deformation, for this reason compression tests were repeated using optical measurement to estimate the Poisson's ratio in the infinitesimal and large deformation regime.

Chapter 5

Four conventional hyperelastic constitutive models including slight compressibility have been chosen to fit the experimental data from TDM in compression, shear and volumetric tests. These models have been chosen because they are representative, but not exhaustive, of the widely used hyperelastic models in Finite Element software.

Moreover not one of the chosen hyperelastic models was able to fit the three test data together with a single set of parameters. A new model based on exponentiated logarithmic strain allowed us to reach that goal. The new model is a modification of the Exponentiated Hencky strain energy proposed by Neff [62] in which the volumetric part has been changed to better describe the behavior of TDM.

The new model has been proven to have good mathematical properties beside all the advantages deriving from the logarithmic measures.

Chapter 6 describe the viscoelastic framework used in this thesis while in chapter 8 there is an optimization problem with TDM.

Chapter 6

The new model is inserted in a viscous framework. A new rheological model is proposed which is modification to the classical Standard Linear Solid model where there is a non-linear spring in series with two Maxwell element representing the two main process occurring in the material subjected to load: grain interaction at the material scale and intermolecular interplay at grains scale.

In this thesis we use a finite deformation model that utilizes a nonlinear evolution equation law as suggested by Reese and Govindjee [69]. The integration methodology for the nonlinear evolution law is based on the operator split of the material time derivative in an elastic predictor, in which only the elastic part of the model is used, and an inelastic corrector.

The parameter sets found give a good approximation of the material behavior in a certain range of frequency when compared with cyclic shear tests and compression tests.

Chapter 7

Describe the use of a commercial finite software (Abaqus) to solve an optimization problem regarding a railway mat made of TDM.

The problem concern finding a new shape different from the solid rectangular one in order to reduce the vertical stiffness of the mat. Lower stiffness are required when dealing with light rail system. The problem due to the high constrains degree imposed by the production process has been solved with a trial and error approach testing the few option available.

Despite of that a good solution was found which allows to have the desired stiffness both in the static and the dynamic regime. This allowed TDM to expand the range of application to a section previously occupied only by elastomeric foams.

Chapter 8

Summarizes eventually the achievements of the present work and rises open question that need future investigation.

Chapter 2

Tire Derived Material

Tire Derived Materials (TDMs) deserve special interest as the reuse of tires is one of the most important topics in recycling and Environmental Engineering. According to the European Tire and Rubber Manufacturers Association, in 2006, the European Union generated approximately 3,213 million tons of scrap tires.

However, 37% of these scrap tires are used as Tire-Derived Fuel, the 39% are used as recycling materials for Civil Engineering work, almost the 5% is disposed to landfill or is illegally dumped and the remaining quota is traded or sold abroad [24] (Figure2.1).

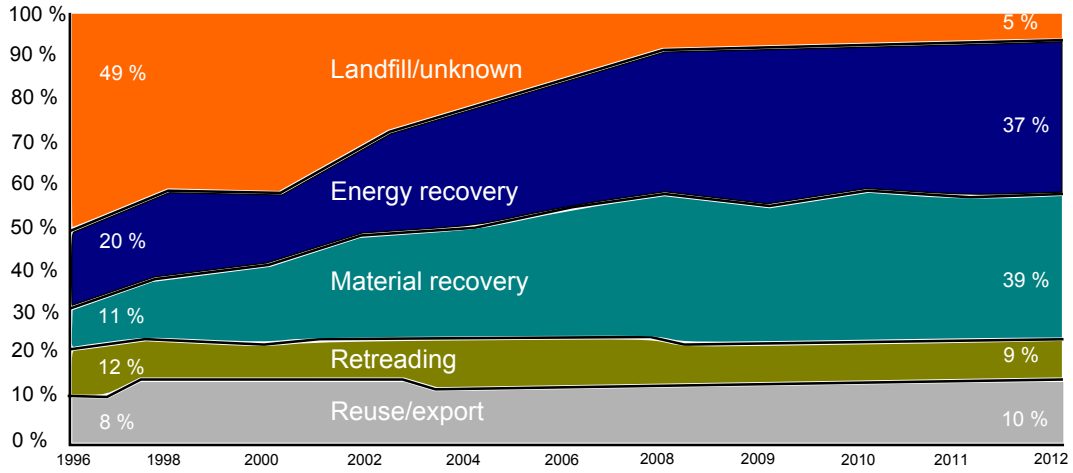

Figure 2.1: EU Treatment routes for used tires (1996-2012).

Also, the energy recovered from exhausted tires by waste-to-energy plants is a quarter of the energy needed for their production and the process itself raises obvious pollution concerns. Moreover, tires are not desired at landfills because of their large volume and 75% void space, which quickly consume areas. Also the chemical released from scrap tires can damage landfill liners that are generally installed to prevent the pollution of local surface

and ground water. In response to these problems research on uses of scrap tires has created many new markets and innovative applications [55] [32] [16].

The US Environmental Protection Agency has conducted research projects on scrap tires including rubberized asphalts and protection systems against erosion of bridge piers [50] (Figure 2.2). The US Department of Energy has conducted research on innovative scrap tire uses. They investigated the development of methods for treating rubber from scrap tires in order to use it as automotive seals and gaskets, sealants, adhesives. Recycled rubber is also used to make absorptive sound barriers, playground surfaces, athletic and recreational applications [80].

(a) (b)

Figure 2.2: Other application of scrap tires: (a) Rubberized asphalt, Modesto, Ca (b) Marshland protection from wave action, Gaillard island, AL

New Tire Derived Material

The material investigated here is composed by recycled rubber and polyurethane binder. The rubber is obtained from scrap tires and rubber factory leftovers, it can be in form of granules or big fibers.

The production process of the proposed material consists of the following phases:

1. tires are shredded into chips, mostly 50 mm in size using a rotary shear shredder with two counter-rotating shafts;

2. tire chips enter a granulator and are reduced to a size smaller than 10 mm while most of the steel cords are liberated by a combination of shaking screens and wind shifters;

3. the rubber granules are selected according to their dimensions to fit the desired design mix;

4. polyurethane binder is added to the rubber granules mix until the mixture becomes an homogenous compound;

5. pads of required size and shape are obtained by hot pressing or cold forging the compound.

The compound is first leveled by a roller and then it is hot pressed together.

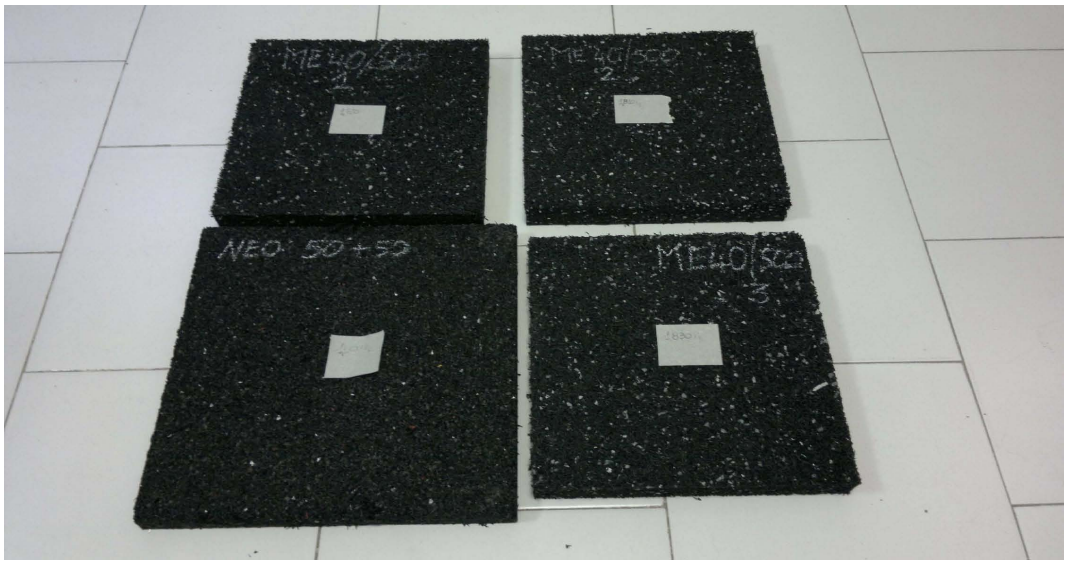

Figure 2.3: Tire Derived Material pad, Sample for lab testing.

For binding optimization, hot steam is used and pressure is applied until the polymerization of the binder is complete. Cold forging requires the mixture to be pressured in a mold. The industrial process previously described is particular feasible for the production of low-cost devices: it requires low energy consumption and low labor demand. It is also noted, that by changing rubber aggregates, binders, temperature and applied pressure, it is possible to produce materials with different mechanical characteristics.

The elastomer used in the process is usually tire derived Styrene Butadiene Rubber (SBR). A similar process can be applied to industrial leftovers made of Ethylene-Propylene Diene Monomer (EPDM), a rubber used for the production of a wide variety of seals.

The physical properties of the TDMs are greatly influenced by the technologies used in manufacturing. Tests have shown that the density and the mixture composition of the material are the parameters that affect the most of its mechanical properties.

In this thesis, three different types of TDMs were considered, which were obtained by using the same compositions (Figure 2.4) but three different densities. All the materials were made by means of the cold forging process. A different density of the material was obtained by pressing in the mold a different quantity of rubber, grains and fibers, and polyurethane binder.

Figure 2.4: Tire Derived Material pad, particular of composition 90% SBR fibers and 10% grains.

Table 2.1 lists in details the different materials compositions and specifications.

Table 2.1: Tire Derived Material description

Material	Density (kgm^{-3})	Composition
500	500	90% SBR fibers 10% SBR grains
600	600	
800	800	

2.1 Main applications of new Tire Derived Material

The vision of a new sustainable construction industry is motivating researchers and practitioner in developing novel eco-friendly materials and utilizations. In this trend, the re-use of rubber tires is gaining momentum, while the installation of low-cost TDM pads is spreading to different construction engineering applications.

The main use of the TDMs is by far the application to railway engineering. In railway engineering, the TDM is used instead of other elastomers to reduce the vibration transmitted by the trains moving on the railway track [56]. Elastomers are included in railway track with different configurations according to the transportation characteristics and surrounding conditions. For instance, in traditional railway systems elastomers are placed underneath the

ballast. The system successfully reduces the amount of ballast needed for the construction of high performance tracks. In ballastless track system the material is placed under a thick concrete slab. Thanks to a minimum maintenance requirement, the system is generally adopted where there are exceptional maintenance difficulties, for example in tunnels. Also, the life cost of this system can be lower than that of traditional railway tracks [23].

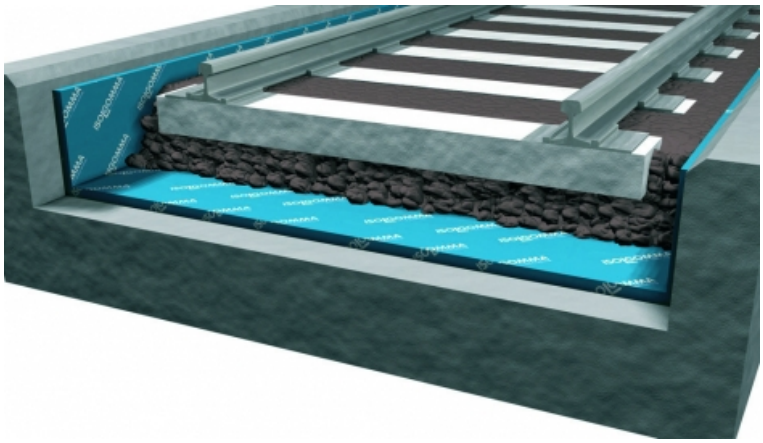

Figure 2.5: TDM antivibration mat for railway track application [43].

Successful applications of TDMs in railway track include a section of the Bologna-Firenze and a section of the Roma-Napoli high speed railway in Italy. Also TDMs have been used in many tramway track in Italy and metro railway track in Spain. In some application TDMs are used in floor insulations to avoid transmission of either solid and acoustic vibration in buildings (Figure 2.6). Few applications of TDMs consist of foundations insulation to mitigate vibration from industrial buildings. In other applications TDMs are used for the production of sound and noise barriers.

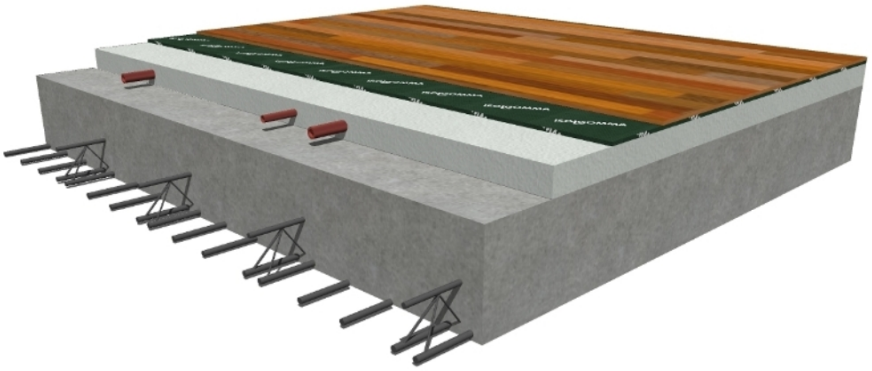

Figure 2.6: TDM antivibration mat for floor insulation [43].

They are also considered for playground pavements and for other recreational facilities such as race track or special sports applications [43]. Recently this kind of material has also been used to make low-cost devices for structural isolation (Figure 2.7).

Figure 2.7: Prototypes of seismic Isolators made of TDM [14].

Chapter 3

Nonlinear Continuum Mechanics

This chapter gives a brief overview into the theory of nonlinear continuum mechanics. The necessary quantities and objects that will be used in the subsequent chapters are presented. For a more complete introduction into this field the reader is referred to the classic text-books of (nonlinear) continuum mechanics [66].

The notation used in the present work is inspired by the one used in Holzapfel [37], a textbook which gives a good introduction into tensor analysis and solid mechanics.

3.1 Kinematics

Consider a body Ω_0 in the (undeformed) reference configuration with material points $P \in \Omega_0$. In a Cartesian coordinate system with basis vectors $e_i, i = 1; \ldots; 3$, each point P is described by its coordinates $\mathbf{X}$ (Figure 3.1).

Under an imposed load Ω_0 experiences a deformation and maps into the deformed (current) configuration Ω where the material points p are described by vectors $\mathbf{x}(\mathbf{X}, t)$.

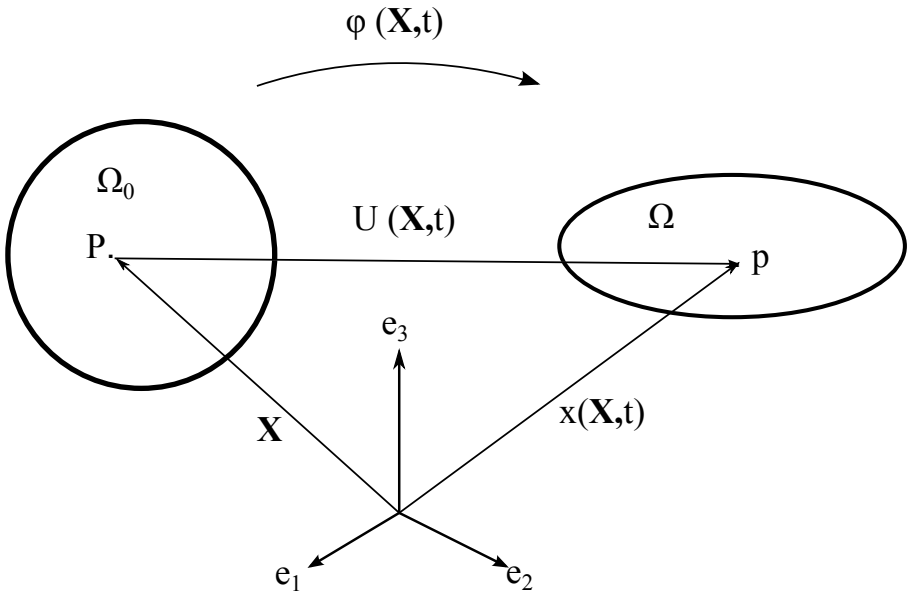

Figure 3.1: Reference configuration of a body Ω_0 and its mapping into a deformed configuration Ω.

Displacement

The transition from the reference to the current configuration is described by the mapping $\varphi(\mathbf{X}, t)$, called motion, such that $\mathbf{x} = \varphi(\mathbf{X}, t)$; $\mathbf{x}$ is a function of $\mathbf{X}$ and the time t. The displacement $\mathbf{U}(\mathbf{X}, t)$ of a point $\mathbf{X}$ is therefore defined as $\mathbf{U}(\mathbf{X}, t) = \mathbf{x}(\mathbf{X}, t) - \mathbf{X}$. In the following the function arguments will be omitted if not necessary for clarity.

Deformation gradient

We now define the mapping of an infinitesimal line-element $d\mathbf{X}$ in the reference configuration into an infinitesimal line-element dx in the deformed configuration.

$$d\mathbf{x} = \frac{\partial \varphi}{\partial \mathbf{X}} d\mathbf{X} = \left(1 + \frac{\partial \mathbf{U}}{\partial \mathbf{X}}\right) d\mathbf{X} = \mathbf{F} d\mathbf{X} \tag{3.1}$$

where $\mathbf{1}$ is the second order identity and $\mathbf{F}$ is called the deformation gradient. $\mathbf{F}$ can be decomposed in

$$\mathbf{F} = \mathbf{R}\mathbf{U} = \mathbf{v}\mathbf{R} \tag{3.2}$$

where $\mathbf{R}$ is a proper orthogonal tensor describing a rotation and $\mathbf{U}$ and $\mathbf{v}$ are the right and left stretch tensors, respectively. Thus, $\mathbf{F}$ describes the stretch and rotation of an infinitesimal line element $d\mathbf{X}$.

Volume ratio

The determinant of the deformation gradient $\mathbf{F}$ is the volume ratio J, i.e. the ratio between the volume of a deformed infinitesimal volume element and its volume in the reference configuration:

$$J = det\,(\mathbf{F}) = dV/dV_0 \tag{3.3}$$

Stretch measures

Since only stretches (but not pure rotations) contribute to the deformation energy a body takes under a superimposed load, it is customary to define a right and left Cauchy-Green deformation tensor $\mathbf{C}$ and $\mathbf{b}$, respectively, that depend only on the stretches

$$\mathbf{C} := \mathbf{F^T F} = \mathbf{U^T U} \tag{3.4}$$

$$\mathbf{b} := \mathbf{F F^T} = \mathbf{v v^T} \tag{3.5}$$

Polar decomposition

A local motion can be decomposed into a pure stretch and a pure rotation. At each point $\mathbf{X} \in \Omega_0$ and each time t, we have the following unique polar decomposition of the deformation gradient $\mathbf{F}$:

$$\mathbf{F} = \mathbf{R U} = \mathbf{v R} \tag{3.6}$$

$$\mathbf{R^T R} = \mathbf{I} \tag{3.7}$$

$$\mathbf{U} = \mathbf{U^T} \tag{3.8}$$

$$\mathbf{v} = \mathbf{v^T} \tag{3.9}$$

In (3.7) U and v define unique, positive definite, symmetric tensors, which are called right (or material) stretch tensor and left (or spatial) stretch tensor respectively. They measure local stretching along their mutually orthogonal eigenvectors. The right stretch tensor U is defined respect to the reference configuration while the left stretch tensor v is defined on the current configuration.

We also have the following properties:

$$\mathbf{U}^2 = \mathbf{U U} = \mathbf{C} \qquad \text{and} \qquad \mathbf{v}^2 = \mathbf{v v} = \mathbf{b} \tag{3.10}$$

Principal stretches and directions

The deformation gradient $\mathbf{F}$ can be written in terms of its eigenvalues λ_i, the principal stretches, and vectors $\mathbf{n}_i$ and $\mathbf{N}_i, i = 1 \ldots 3$

$$\mathbf{F} = \sum_{i=1}^{3} \lambda_i \mathbf{n}_i \otimes \mathbf{N}_i \tag{3.11}$$

The $\mathbf{N}_i$ are vectors defined in the reference configuration while the $\mathbf{n}_i$ are vectors defined in the deformed configuration. It follows directly for the right and left Cauchy-Green deformation tensors

$$\mathbf{C} = \sum_{i=1}^{3} \lambda_i^2 \mathbf{N}_i \otimes \mathbf{N}_i \tag{3.12}$$

$$\mathbf{b} = \sum_{i=1}^{3} \lambda_i^2 \mathbf{n}_i \otimes \mathbf{n}_i \tag{3.13}$$

from where can be seen that the eigenvalues of $\mathbf{C}$ and $\mathbf{b}$ are the squares of the eigenvalues $\mathbf{n}_i$ of the deformation gradient $\mathbf{F}$.

Often materials tests, e.g. uniaxial tensile tests, result in strain/stress states where the directions of the principal axes are knows. It is customary to describe such tests in terms of the principal strain/stress values. The deformation gradient $\mathbf{F}$, the right and left Cauchy-Green deformation tensor $\mathbf{C}$ and $\mathbf{b}$, respectively, might be split into an isochoric (distortional) and a volumetric part, $(\bar{\bullet})$ and $(\bullet)_{vol}$, respectively [25]:

$$\mathbf{F} = \mathbf{F_{vol}}\bar{\mathbf{F}} = J^1/3\ \mathbf{1}\bar{\mathbf{F}} \tag{3.14}$$

$$\mathbf{C} = \mathbf{C_{vol}}\bar{\mathbf{C}} = J^2/3\ \mathbf{1}\bar{\mathbf{C}} \tag{3.15}$$

$$\mathbf{b} = \mathbf{b_{vol}}\bar{\mathbf{b}} = J^2/3\ \mathbf{1}\bar{\mathbf{b}} \tag{3.16}$$

It can easily be demonstrated that the determinants of the deviators equal unity for all deformations

$$\det\left(\bar{\mathbf{F}}\right) = \det\left(\bar{\mathbf{C}}\right) = \det\left(\bar{\mathbf{b}}\right) \equiv 1 \tag{3.17}$$

3.2 Stress measures

If we imagine a body Ω in a (deformed) configuration where external loads $\mathbf{F}_{ext}^{(i)}$ ext are applied. If one virtually cuts that body into two parts, $\Omega^{(1)}$ and $\Omega^{(2)}$ two cutting surfaces $\partial\Omega^{(1)}$ and $\partial\Omega^{(2)}$ can be defined. Internal forces $\mathbf{F}_{int}^{(1)}$ and $\mathbf{F}_{int}^{(2)}$ such that $\mathbf{F}_{int}^{(1)} = -\mathbf{F}_{int}^{(2)}$ are necessary to hold the two parts together (Figure 3.2).

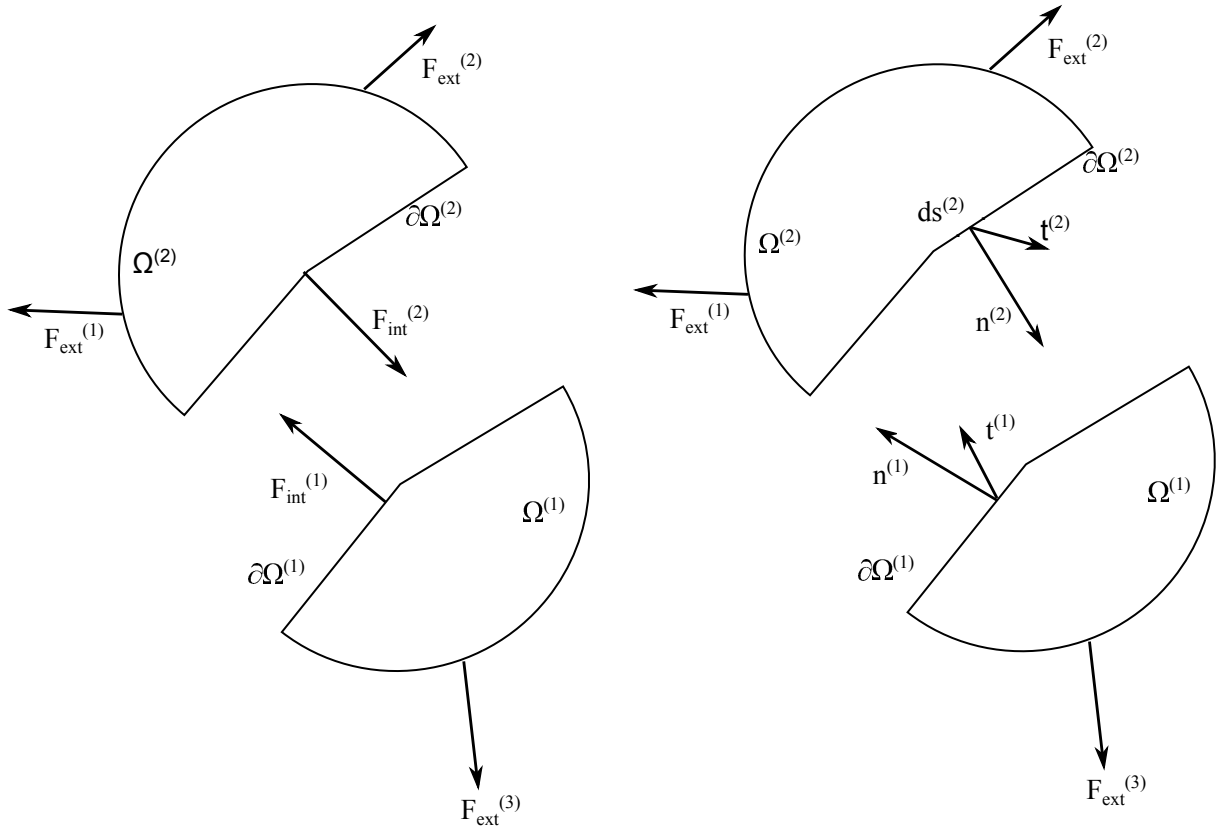

Figure 3.2: Virtual cut of a body Ω in two parts $\Omega^{(1)}$ and $\Omega^{(2)}$

On the cutting surfaces $\partial\Omega^{(i)}$ infinitesimal surface areas $ds^{(i)}$ with unit outward normals $\mathbf{n}^i$ can be defined. On each surface area a traction $\mathbf{t}^i$ acts that has the physical dimension of force per area. Here again holds $\mathbf{n}^1 = -\mathbf{n}^{(2)}$ and $\mathbf{t}^{(1)} = -\mathbf{t}^2$ The integration of all traction vectors over the cutting surface gives the internal forces:

$$\mathbf{F}^i_{int} = \int_{\partial\Omega^{(i)}} \mathbf{t}^i d\mathbf{s}^i \tag{3.18}$$

The tractions $\mathbf{t}^i$ defined in the current configuration are called Cauchy traction vectors. Pseudo traction vectors $\mathbf{T}$, called first Piola-Kirchhof traction vectors, measure the current force per unit area d$\mathbf{S}$ in the reference configuration. The tractions depend on the position, outward normal and time

$$\mathbf{t} = \mathbf{t}\left(\mathbf{x}, \mathbf{n}, t\right) \tag{3.19}$$

$$\mathbf{T} = \mathbf{T}\left(\mathbf{X}, \mathbf{N}, t\right) \tag{3.20}$$

Cauchy's stress theorem says that unique second-order tenors σ and $\mathbf{P}$ exist such that

$$\mathbf{t} = \sigma\mathbf{n} \tag{3.21}$$

$$\mathbf{T} = \mathbf{P}\mathbf{N} \tag{3.22}$$

σ is called the Cauchy (or true) stress and $\mathbf{P}$ the first Piola- Kirchhhof(or nominal) stress. By using the balance law of the angular momentum one can show that σ is symmetric (while $\mathbf{P}$ is in general asymmetric but satisfies the condition $\mathbf{PF^T} = \mathbf{FP^T}$). Nanson's formula, $ds = J\mathbf{F^{-T}}d\mathbf{S}$, which connects surface elements in different configurations (and especially surface elements in the current and the reference configuration) yields a relation between the two stress measures:

$$\mathbf{P} = J\sigma\mathbf{F^{-T}} \tag{3.23}$$

The so called second Piola-Kirchhoff stress $\mathbf{S}$ has no direct interpretation but proves to be very useful for many applications. Its relation to the previously introduced stress measures is given by

$$\mathbf{S} = J\mathbf{F^{-1}}\sigma\mathbf{F^{-T}}\mathbf{S} = \mathbf{F^{-1}}\mathbf{P} \tag{3.24}$$

3.3 Constitutive relations

Constitutive equations describe the relation between the strains undergone by a certain material and the resulting stress.

Linear elasticity

The most simple and best known constitutive relation is the one for isotropic, linear elastic materials. Hook's law describes a linear relationship between the deformations (strains) ε and the true stress σ:

$$\sigma = 2\mu\varepsilon + \lambda tr(\varepsilon)1 \tag{3.25}$$

The strain ε is defined as

$$\varepsilon = \frac{1}{2}\left(\bigtriangledown u + (\bigtriangledown u)^T\right) \tag{3.26}$$

The Lamé constants μ [MPa] and λ [MPa] are given in terms of the (more classic) Young's modulus E [MPa] and Poisson's ratio ν [-]:

$$\mu = \frac{1}{2}\frac{E}{1+\nu} \qquad \lambda = \frac{E\nu}{(1-2\nu)(1+\nu)} \tag{3.27}$$

Green-elasticity for isotropic materials

Elastic materials that deform with negligible energy dissipation are called Green- or hyperelastic. For such materials the stress can be deduced from a strain energy density (the Helmholtz free-energy per unit reference volume) by taking its derivative with respect to the deformation (for notational ease, here and in the following, different strain energy functions will be written with the same symbol Ψ):

$$\mathbf{P} = \frac{\partial\Psi(\mathbf{F})}{\partial\mathbf{F}} \qquad \mathbf{S} = 2\frac{\partial\Psi(\mathbf{C})}{\partial\mathbf{C}} \tag{3.28}$$

By the fact that Ψ should not depend on superimposed rigid body motions (material frame indifference) it is possible to show that it must depend on the right stretch tensor $\mathbf{U}$ only. Typically,Ψ is written as a function of the right Cauchy-Green deformation tensor $\mathbf{C}$ which depends on $\mathbf{U}$ only:

$$\Psi = \Psi\left(\mathbf{U}\left(\mathbf{F}\right)\right) = \Psi\left(\mathbf{C}\left(\mathbf{F}\right)\right) \tag{3.29}$$

The invariance of Ψ under transformations that respect the material symmetries (in case of isotropic materials this are arbitrary rotations) leads to a representation that depends only on the so called invariants of C or b:

$$\Psi = \left(I_1\left(\mathbf{C}\right), I_2\left(\mathbf{C}\right), I_3\left(\mathbf{C}\right)\right) = \left(I_1\left(\mathbf{b}\right), I_2\left(\mathbf{b}\right), I_3\left(\mathbf{b}\right)\right) \tag{3.30}$$

with

$$I_1 = tr\left(\mathbf{C}\right) = \lambda_1^2 + \lambda_2^2 + \lambda_3^2 \tag{3.31}$$

$$I_2 = \frac{1}{2}\left(\left(\mathbf{C}\right)^2 - \mathrm{tr}\left(\mathbf{C}^2\right)\right) = \lambda_1^2\lambda_2^2 + \lambda_1^2\lambda_3^2 + \lambda_2^2\lambda_3^2 \tag{3.32}$$

$$I_3 = J^2 = \det\left(\mathbf{C}\right) = \lambda_1^2\lambda_2^2\lambda_3^2 \tag{3.33}$$

From $\Psi\left(I_1, I_2, I_3\right)$ the first Piola-Kirchhoff stress $\mathbf{P}$ can be obtained by taking the derivative with respect to the deformation gradient

$$\mathbf{P} = 2\Psi_{,1} + 2\Psi_{,2}\left(I_1\mathbf{F} - 2\mathbf{F}\mathbf{C}\right) + J\Psi_{,3}\mathbf{F}^{-T} \tag{3.34}$$

where $\Psi_{,i}$ depicts the partial derivative of Ψ with respect to the i'th invariant I_i. By the multiplicative split of the right Cauchy-Green tensor $\mathbf{C}$ it is possible to write the strain energy Ψ in an uncoupled form

$$\Psi = U\left(J\right) + \bar{\Psi}\left(\bar{I}_1, \bar{I}_2\right) \tag{3.35}$$

Here U is the response of the material to volume changes and Ψ depends only on the isochoric part of the deformation. $\bar{I}_1$ and $\bar{I}_2$ are the invariants of the unimodular (isochoric) part $\bar{\mathbf{C}}$ of the right Cauchy-Green deformation tensor $\mathbf{C}$:

$$\bar{I}_1 = \mathrm{tr}\left(\bar{\mathbf{C}}\right) \qquad \bar{I}_2 = \frac{1}{2}\left(\left(\mathrm{tr}\left(\bar{\mathbf{C}}\right)\right)^2 - \mathrm{tr}\left(\bar{\mathbf{C}}^2\right)\right) \tag{3.36}$$

The first Piola-Kirchhoff stress reads in this uncoupled form [1]

$$\mathbf{P} = JU_{,J}\mathbf{C}^{-1} + 2J^{-2/3}\bar{\Psi}_{,1}\left(\mathbf{F} - \frac{1}{3}I_1\mathbf{F}^{-T}\right) + 2J^{-4/3}\bar{\Psi}_{,2}\left(I_1\mathbf{F} - \frac{2}{3}I_2\mathbf{F}^{-T} - \mathbf{F}\mathbf{C}\right) \tag{3.39}$$

[1] If the second Piola-Kirchhoff stress S is considered the extra terms reveal their nature:

$$\mathbf{S} = JU_{,J}\mathbf{C}^{-1} + \left(\bar{\Psi}_{,1}\frac{\partial\bar{I}_1}{\partial\bar{\mathbf{C}}} + \bar{\Psi}_{,2}\frac{\partial\bar{I}_2}{\partial\bar{\mathbf{C}}}\right) : \frac{\partial\bar{\mathbf{C}}}{\partial\mathbf{C}} = \tag{3.37}$$

$$= JU_{,J}\mathbf{C}^{-1} + J^{-2/3}\mathbb{P} : \left(\bar{\Psi}_{,1}\frac{\partial\bar{I}_1}{\partial\bar{\mathbf{C}}} + \bar{\Psi}_{,2}\frac{\partial\bar{I}_2}{\partial\bar{\mathbf{C}}}\right) \tag{3.38}$$

P is the projection tensor in the reference configuration which makes the respective stress components deviatoric. This means that the stress components originating from a dependency on $\bar{I}_1$ or $\bar{I}_2$ are independent on a volume change.

For fully incompressible materials the constitutive pressure cannot be deduced from the constitutive equations but has to be determined using the boundary conditions. In Equation (3.39) the term including $U_{,J}$ has to be replaced by the unknown pressure p.

Polynomial models

The polynomial models are truncated Taylor-series of the isochoric strain energy density $\bar{\Psi}$ around the initial state where $I_1 = 3[-]$ and $I_2 = 3[-]$ [58] [70]:

$$\bar{\Psi}(\bar{I}_1, \bar{I}_2) = \overbrace{\bar{\Psi}(\bar{I}_1 = 3, \bar{I}_2 = 3)}^{=0} + \sum_{i+j=1}^{\infty} \underbrace{\left(\frac{1}{i!j!} \frac{\partial^{i+j} \bar{\Psi}}{\partial \bar{I}_1^i \partial \bar{I}_2^j} \right)_{\bar{I}_1=3, \bar{I}_2=3}}_{=c_{ij}} \cdot \left(\bar{I}_1 - 3\right)^i \left(\bar{I}_2 = 3\right)^j . \quad (3.40)$$

The partial derivatives of $\bar{\Psi}$ at the reference state together with the preceding constants are treated as parameters c_{ij} [MPa]:

$$\bar{\Psi}_P = \sum_{i+j=1}^{N} c_{ij} \left(\bar{I}_1 - 3\right)^i \left(\bar{I}_2 = 3\right)^j + U(J). \quad (3.41)$$

Here again the volumetric energy U(J) was used. The small strain shear modulus μ equals $2(c_{10}+c_{01})$ in this model. The expression for the first Piola-Kirchhoff stress of the polynomial model P_P is given in Table 3.1. As shown by Yeoh [85] the dependency on the second invariant is generally much smaller than on the first, such that often only the latter is taken into account, the reduced polynomial model:

$$\bar{\Psi}_{RP} = \sum_{i+j=1}^{N} c_{ij} \left(\bar{I}_1 - 3\right)^i + U(J). \quad (3.42)$$

Some of the most often used models for isotropic materials are obtained by a limitation of equation (3.42) to only the first terms. The Mooney-Rivlin model restricts N to one, such that:

$$\bar{\Psi}_{MR} = c_{10} \left(\bar{I}_1 - 3\right) + c_{10} \left(\bar{I}_2 - 3\right) + U(J). \quad (3.43)$$

An even simpler model is the Neo-Hookean where only the first term of the Reduced polynomial model is considered:

$$\bar{\Psi}_{NH} = c_1 \left(\bar{I}_1 - 3\right) + U(J). \quad (3.44)$$

Remark Equations (3.43) and (3.44) are generalizations of the Mooney-Rivlin and Neo-Hookean materials, respectively, for the compressible response. The original forms of these materials were for the incompressible response.

The Ogden model

Ogden proposed a different model that does not use the invariants I_1 and I_2 but the principal stretches λ_i as arguments:

$$\bar{\Psi}_O = \frac{2\mu_i}{\alpha_i^2}\left(\bar{\lambda}_1^{\alpha_i} + \bar{\lambda}_2^{\alpha_i} + \bar{\lambda}_3^{\alpha_i} - 3\right) + U(J). \tag{3.45}$$

The parameters μ_i [MPa] have the dimension of a pressure, the $\alpha_i[-]$, i = 1,...,N, are dimensionless. The small strain shear modulus of this model is given by $\mu = \sum_{i=1}^{N} \mu_i$ Note that for the special case $N = 1[-]$ and $\alpha_1 = 2[-]$ the Neo-Hookean model (cf. Eq. (3.44)) is regained. Table 3.6 shows the expression for the first Piola-Kirchhoff stress of the Ogden model P_O.

Michromechanical models

The most successful model based on michromechanical theory is the expression of a strain energy function based on the non-Gaussian approach of the statistical molecular theory proposed by Arruda and Boyce [3], which the fifth order approximation expression is:

$$\bar{\Psi}_A = \mu \frac{c_i}{\lambda_m^{2i-2}}\left(\bar{I}_1 - 3\right)^i + U(J). \tag{3.46}$$

Where:

$$\mu = \mu_0 \left(1 + \frac{3}{5\lambda_m^2} + \frac{99}{175\lambda_m^4} + \frac{513}{875\lambda_m^6} + \frac{42039}{67375\lambda_m^8}\right)^{-1} \tag{3.47}$$

$$c_1 = \frac{1}{2}, c_2 = \frac{1}{20}, c_3 = \frac{11}{1050}, c_4 = \frac{19}{7000}, c_5 = \frac{519}{673750} \tag{3.48}$$

In the formula μ_0 is the initial shear modulus and λ_m is the locking stretch. This function, based on the non-Gaussian approach of the statistical molecular theory, was developed starting out from a representative volume element where eight chains emanate from the center of a cube to its corners for this reason it is also called the "8-chain" model. The Arruda Boyce potential depends only on the first invariant I_1, the physical interpretation is that the eight chains, which undergo tensile stretching for all imposed deformations, are stretched equally under the action of a general deformation state.

3.4 Elasticity tensors

The solution of finite (in-) elasticity problems requires often the use of numerical methods, e.g. the finite element (FE) method. It achieves solutions that satisfy the weak form of static or dynamic equilibrium by solving iteratively the nonlinear problem. Trial solutions

are checked if they fulfill the equilibrium condition and if not a Newton-Raphson algorithm is used to find a correction.

This strategy relies on the treatment of the linearized constitutive equations, which involves the derivative of the stress with respect to the deformation measures, the so called elasticity (or stiffness) tensors. The material elasticity tensor $\mathbb{C}$, which is a fourth-order tensor, is defined by

$$\mathbb{C} = 2\frac{\partial \mathbf{S}(\mathbf{C})}{\partial \mathbf{C}} = 4\frac{\partial^2 \Psi(\mathbf{C})}{\partial \mathbf{C} \otimes \partial \mathbf{C}} \tag{3.49}$$

The last equality in (3.49) holds only true for the case of a hyperelastic material. Numerical methods often use the spatial elasticity tensor c which is obtained by applying a Piola transformation on each slot of $\mathbb{C}$:

$$\mathbb{c}_{ijkl} = J^{-1} F_{iI} F_{jJ} F_{kK} F_{lL} C_{IJKL} \tag{3.50}$$

A user implementation of constitutive equations for use with a FE program needs good knowledge on the required quantities. For the derivation of stiffness quantities for a certain material the reader is pointed to textbooks (e.g. Holzapfel [37] and others). Also for experienced users it is advantageous to test an implementation with a benchmark program.

3.5 Elasticity tensor in terms of principal stretches

If we consider an isotropic hyperelastic material charcterized by the strain-energy function $\Psi = \Psi(\lambda_1, \lambda_2, \lambda_3)$ with $\lambda_1, \lambda_2, \lambda_3$ being the principal stretches. The spectral form of the elasticity tensor $\mathbf{C}$ in this case, in the material description, is:

$$\begin{aligned}\mathbb{C} = &\sum_{i,j=1}^{3} \frac{1}{\lambda_j}\frac{\partial \mathbf{S}}{\partial \lambda_j} \mathbf{N}_i \otimes \mathbf{N}_i \otimes \mathbf{N}_j \otimes \mathbf{N}_j + \\ &+ \sum_{i,j=1;i\neq j}^{3} \frac{S_j - S_i}{\lambda_j^2 - \lambda_i^2}\frac{\partial \mathbf{S}}{\partial \lambda_j} \left(\mathbf{N}_i \otimes \mathbf{N}_j \otimes \mathbf{N}_i \otimes \mathbf{N}_j + \mathbf{N}_i \otimes \mathbf{N}_j \otimes \mathbf{N}_i \otimes \mathbf{N}_j\right)\end{aligned} \tag{3.51}$$

with the principal Piola-Kirchooff stresses:

$$S_i = 2\frac{\partial \Psi}{\partial \lambda_i^2} = \frac{1}{\lambda_i}\frac{\partial \Psi}{\partial \lambda_i} \qquad i = 1, 2, 3 \tag{3.52}$$

and the set $\mathbf{N}_i, i = 1, 2, 3$ of orthonormal eigenvectors of the right Cauchy-Green tensor $\mathbf{C}$. They define principal referential directions at point $\mathbf{X}$, with the conditions $|\mathbf{N}_i = 1|$ and $\mathbf{N}_i \cdot \mathbf{N}_j = \delta_{ij}$. The proof of relation (3.51) can be found in Holzapfel [37]. In the same way as (3.50) the spatial tensor of elasticities can be obtained as the push-forward operation of $\mathbb{C}$ times a factor of J^{-1}.

3.6 Dissipative materials

Rubber-like materials and many others have inelastic behavior. In particular in this thesis the viscoelastic behavior of TDM is studied based on the concept of internal variables. the thermodynamic state of a thermoelastic material can be determined by the current value of the deformation gradient F and the temperature T, these values that are directly measurable are called external variable.

The current state of a dissipative material in addiction can be determined by a finite number of internal variables. These variables, which we denote ξ, are not directly measurable and are used to describe aspects of the internal structure of the materials associated with irreversible dissipative effects. Inelastic strain or stress, dashpot displacement etc. can be associated with an internal variable in viscoelasticity. The concept of internal variables postulates that the current thermodynamic state of a dissipative materials is described by the current values of the deformation gradient F the temperature T and the internal variables ξ.

The concept of internal variable introduced here serve as a basis for the development of the finite viscoelasticity theory that will be introduced in the following section.

Relaxation Creep and Hysteresis

For inelastic materials a non-equilibrium status that evolves with time is postulated to describe their behavior. Two main irreversible process which govern the non-equilibrium states are relaxation and creep.

Relaxation is the decrease of stress with time at fixed strain (Figure 3.3) while creep is the phenomenon for which strain increases with time at fixed constant stress (Figure 3.4)

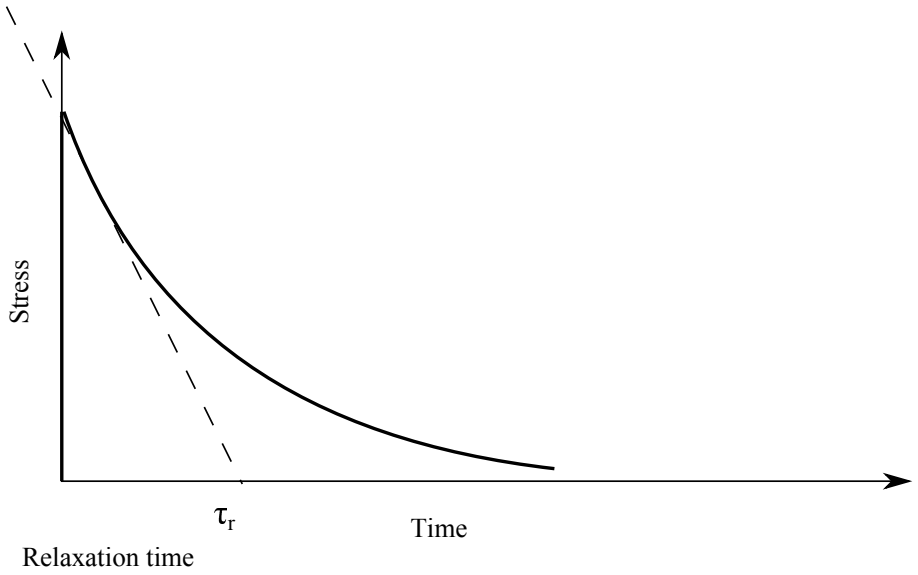

Figure 3.3: Relaxation Process

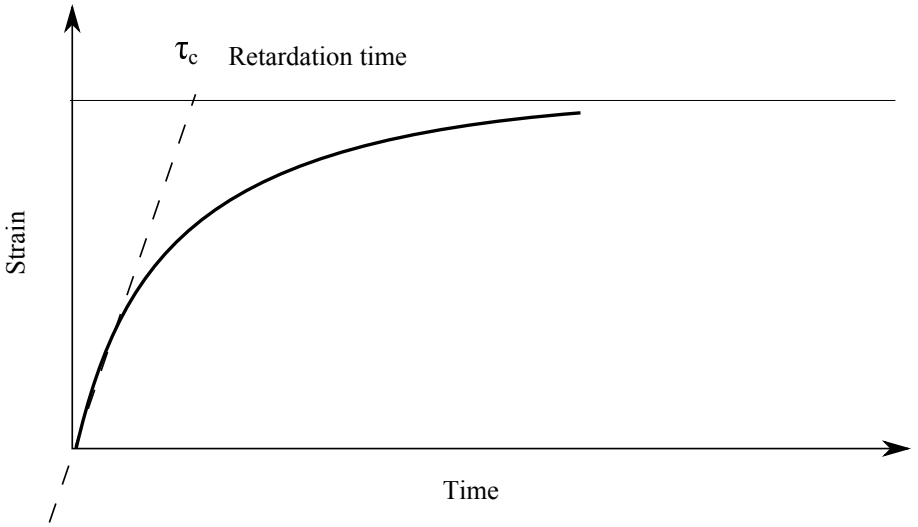

Figure 3.4: Creep Process

The rate of decay of the stress and strain in a viscoelastic process is characterized by the so-called relaxation time τ_r with dimension of a time while the parameter associated with the creep is the so-called retardation time τ_c. A viscoelastic behavior of a material is also characterized by hysteresis, in which the loading and the unloading path do not coincide. The area in the center of a hysteresis loop (Figure 3.5) is the energy dissipated due to material internal friction.

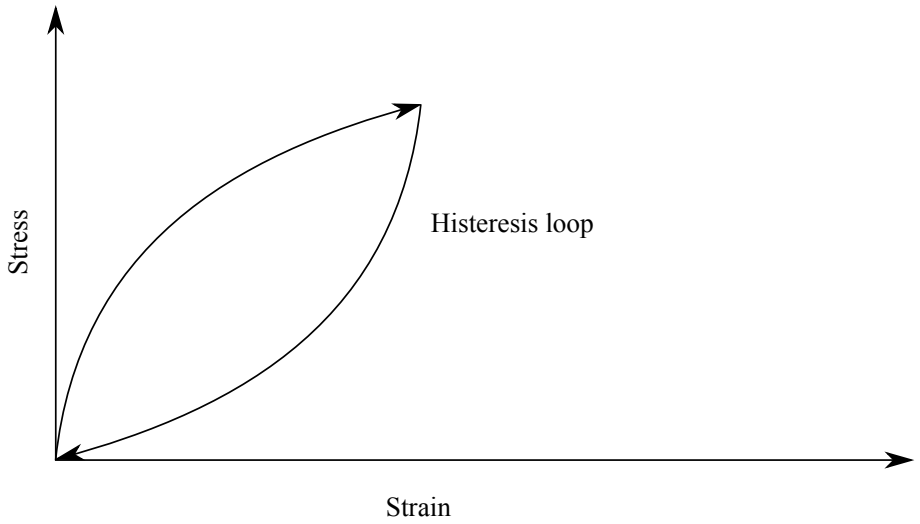

Figure 3.5: Hysteresis Process

Most of the models that are used to approximate the inelastic behavior or real nonlinear inelastic materials are developed on the basis of internal variable.

In this work we do not consider the effects of temperature on the material. In chapter 6 it will be introduced a viscoelasticity thoery based on the multiplicative split of the free energy into an equilibrium and a non-equilibrium part where the strain associated to the non-equilibrium part represents the internal variable. Hence we postulate the Helmholtz free-energy function as:

$$\bar{\Psi} = \Psi\left(\mathbf{F}, \xi_1, \ldots, \xi_m\right) \tag{3.53}$$

Evolution equation

Evolution equation is a relation which describes the evolution of the involved internal variable ξ_i and the associated dissipation mechanism. The only restriction to the evolution equation is the thermodynamic admissibility which is a statement concerning the irreversibility of natural processes when energy dissipation is involved. It can be written in the form:

$$\dot{\xi}_i = \chi_i\left(\mathbf{F}, \xi_1, \ldots, \xi_m\right), \qquad i = 1, \ldots, m \tag{3.54}$$

The evolution of the system is described by $\chi_i, i = 1, \ldots, m$ which are tensor valued functions of 1+m tensor variables. Every system tends towards the equilibrium state where the external and internal variables reach equilibrium under constant stress or strain. Hence the equilibrium is a limiting case and requires the introduction of an additional condition:

$$\chi_i\left(\mathbf{F}, \xi_1, \ldots, \xi_m\right) = 0, \qquad i = 1, \ldots, m \tag{3.55}$$

Table 3.1: 1st Piola-Kirchhoff stresses for the constitutive models

Polynomial Model

$$\mathbf{P_p} = JpF^{-T} + \sum_{i+j=1}^{N} ic_{ij}\left(\bar{I}_1 - 3\right)^{i-1}\left(\bar{I}_2 - 3\right)^{j}\frac{\partial \bar{I}_1}{\partial F} + \sum_{i+j=1}^{N} jc_{ij}\left(\bar{I}_1 - 3\right)^{i}\left(\bar{I}_2 - 3\right)^{j-1}\frac{\partial \bar{I}_2}{\partial F}$$

Ogden Model

$$\mathbf{P_O} = \sum_{a=1}^{3}\frac{1}{\lambda_a}\frac{\partial \Psi_O}{\partial \lambda_a}\mathbf{n_a}\otimes\mathbf{N_a} \qquad \text{with} \qquad \frac{\partial \Psi_O}{\partial \lambda_a} = \sum_{i=1}^{N}\frac{2\mu_i}{\alpha_i}\left(J^{-1/3}\hat{\lambda}_a^{\alpha_i - 1} - \frac{1}{3\lambda_a}\left(\bar{\lambda}_1^{\alpha_i} + \bar{\lambda}_2^{\alpha_i} + \bar{\lambda}_3^{\alpha_i}\right)\right)$$

Arruda Model

$$\mathbf{P_p} = JpF^{-T} + i\mu\frac{c_i}{\lambda_m^{2i-2}}\left(\bar{I}_1 - 3\right)^{i-1}\frac{\partial \bar{I}_1}{\partial F}$$

Chapter 4

Experiments on Tire derived Materials

The physical properties of the TDMs are greatly influenced by the technologies used in manufacturing. Tests have shown that the density and the mixture composition of the material are the parameters that affect the most of its mechanical properties.

Due to the lack of information on this material, experiments are required to identify an adequate form for a theoretical stress-strain curve. Here we study the rate-independent behavior of the material using hyperelastic constitutive models.

The principal application of TDM is in railway track system where recycled rubber pads are mainly subjected to compression loads. Therefore, for a first assessment of the material's mechanical characteristics, compression tests were performed. Under compression, as the aspect ratio of the pads is large, the main quota of the deformation is due to an high compressibility of the rubber. For this reason, volumetric tests were also conducted.

Moreover, as the pads work as antivibration material, the assessment of their overall behavior is crucial. For this reason, and for the lack of information on the material performances, an extensive experimental campaign was conducted.

Experiments were carried out in compression, tension and shear underlining the benefits and the limits of the low-cost elastomeric material. Furthermore, volumetric tests were performed in order to evaluate the bulk modulus of the material.

4.1 Uniaxial tension tests

A set of tensile tests were performed to determine the tensile strength of the TDM. ASTM D412 [5] describes the procedures to evaluate the uniaxial properties of rubber.

According to the standard, since the experiment is intended to load the specimen up to failure, dumbbell shaped samples should be used to prevent failure of the rubber in the clamps. Therefore, specific size requirements are described in detail in order to compare the mechanical behavior of the different materials.

Due to the fact that it was exceptionally difficult to manufacture TDMs in a dumbbell shape and also there was no need to make reference to any specific size requirements, tests were performed on straight specimens. The length of all the tested specimens was L_{tot}=350 mm. The width and the thickness were 20 mm (Figure 4.1).

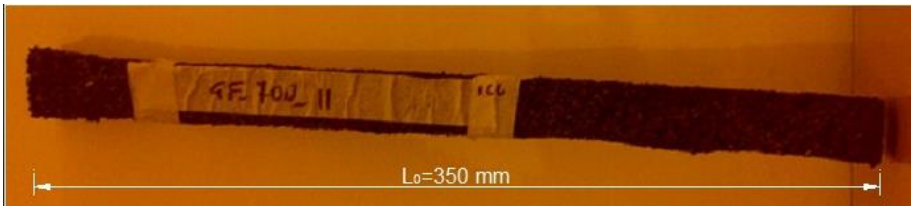

Figure 4.1: Specimen used in tension tests

The specimen clamps give an indeterminate state of stress and strain in the region surrounding the clamps (due to gripping). Considering that, the tensile strain of the specimen ($\Delta L/L_0$) was measured by means of a non-contacting strain measuring device away from the extremities, where a pure tension strain state occurred (L_0=100mm). The force was measured by a load cell.

The tests were carried out using displacement control at a constant rate of velocity until failure, with the rate of displacement of 5 mm/min (strain rate of $8.3 \cdot 10^{-4}\text{sec}^{-1}$). Tests were performed on a set of three specimens for every density.

Table 4.1: Mechanical properties of TDM in tension

Material	Ultimate elongation Avg. (%)	Tensile failure stress Avg. (MPa)
500	0.75	0.18
600	0.87	0.46
800	0.95	0.8

Table 4.1 indicates that the tensile strength of the TDM is much lower when compared to that of natural rubber and depends significantly on the density of the compound, being higher for higher densities and also depending on function of the inert shapes. Also, the ultimate deformation of TDMs is in the range from 0.4-1% (Figure 4.2).

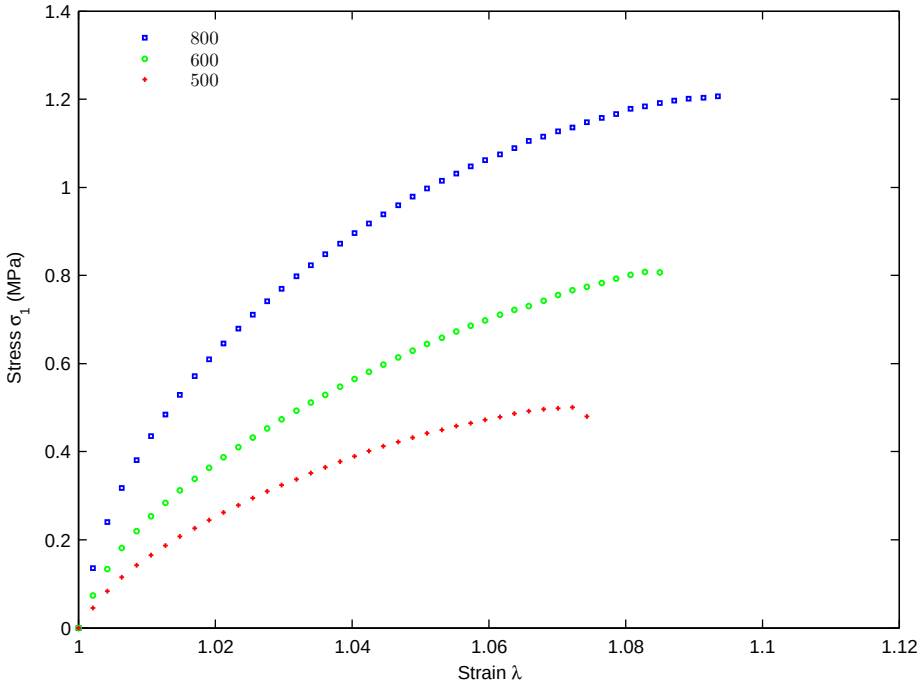

Figure 4.2: Tension tests TDMs

This is some orders of magnitude lower than that of natural rubber ($100 - 600\%$). It is evident to see that no devices subjected to tensile loads should be produced using this low-cost material. A visual inspection of the tested samples clarified that the polyurethane binder failed at the grains interface, without any failure surface dividing the grains. None of the grains were broken and only few fibers were.

4.2 Compression tests

Gathering specimens with the same cylindrical shape, 15 mm height and 27 mm diameter, were cut off from a TDM mat and were tested under homogeneous compression.

In order to obtain specimens of uniform diameter a cork borer was used. It had a thin wall thickness of ≈ 0.5 mm and the cutting edge at the center of the cork borer wall. Also, the cork borer was lubricated with detergent before cutting the sample in order reduce the strains developing in the elastomer as the borer becomes embedded in the rubber, which may produce tapered samples.

Tests were carried out using a computer controlled servo hydraulic testing machine with a 15 kN load cell. The specimens were subjected to a three cycles of load and unload at 9 mm/min (strain rate of $0.01s^{-1}$) up to a strain of 50% prior to the actual test. This was necessary as the TDMs showed a stiffening behavior that tended to stabilize after a few cycles with most of the stiffening occurring during the first cycle.

It is deemed that this phenomenon can be mainly accounted on the presence of voids, in fact, TDMs tend to get compacted when they are loaded, in a measure strictly connected to the material density and regardless of the inert shape. As matter of fact residual strains occurred after the preloading cycles with height changes of the samples ranging from about 13% for the low densities to almost no height change for the high densities (Figure 4.3-4.5).

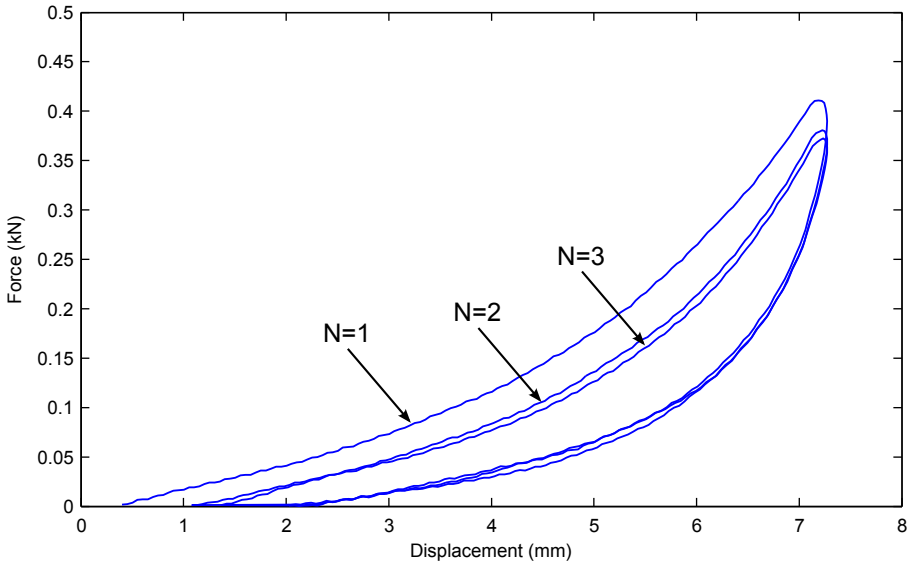

Figure 4.3: Preload cycles on TDM 500 (N=cycle number)

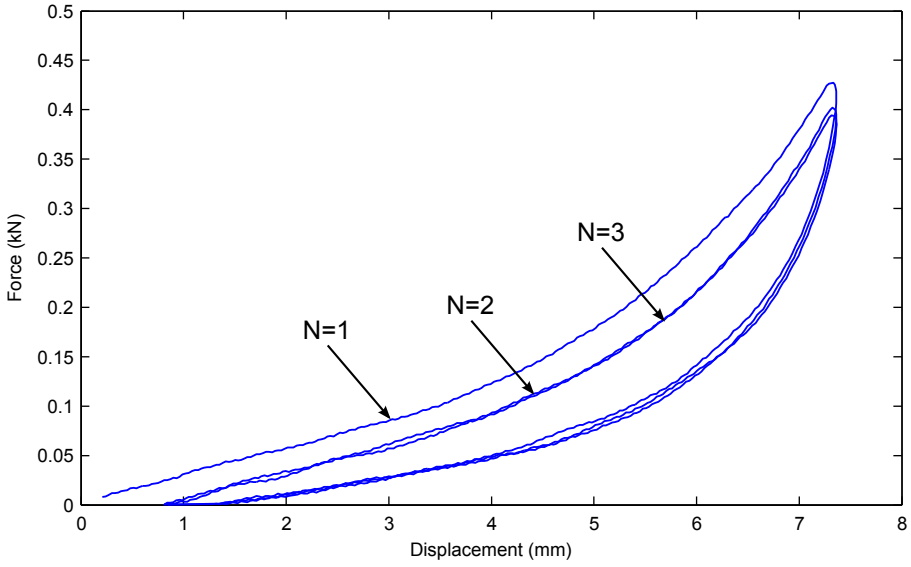

Figure 4.4: Preload cycles on TDM 600 (N=cycle number)

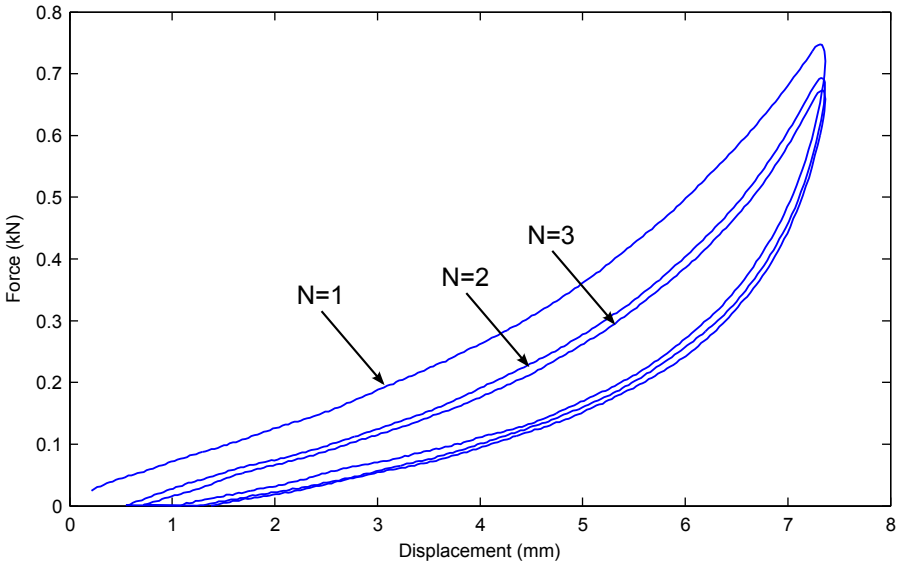

Figure 4.5: Preload cycles on TDM 800 (N=cycle number)

The stroke rate of the actuator for the compression tests ranged from 9mm/min (strain rate of $0.001s^{-1}$) to 90 mm/min (strain rate of $0.1s^{-1}$). Displacements up to a strain of 80% were applied in the vertical direction. The corresponding force in the specimens were obtained from the load cell.

In order to get homogeneous compression the loaded ends of the specimen were required to slide freely. For this reason, a frictionless contact between the plates and the sample surfaces was needed. The frictionless constraints were obtained by placing Polytetrafluoroethylene (PTFE) sheets with lubricant on the top and bottom of the sample.

During the tests from a visual inspection the unloaded surfaces seemed to not bulge under the compression load.

However, a check on the stress field has been done by testing two specimens with different shape factor S. The shape factor, S, is a dimensionless measure given by the ratio of the loaded area over the unloaded area of the sample. For a cylindrical specimen $S = \frac{r}{2t}$ where r is the radius and t is the thickness of the specimen. The first specimen had the same dimension as the one tested in compression, which was 27 mm in diameter and 15 mm in height leading to a shape factor $S = 0.45$. The second specimen was cut from a mat of 25 mm in height keeping the diameter of 27 mm and leading to a shape factor $S = 0.27$.

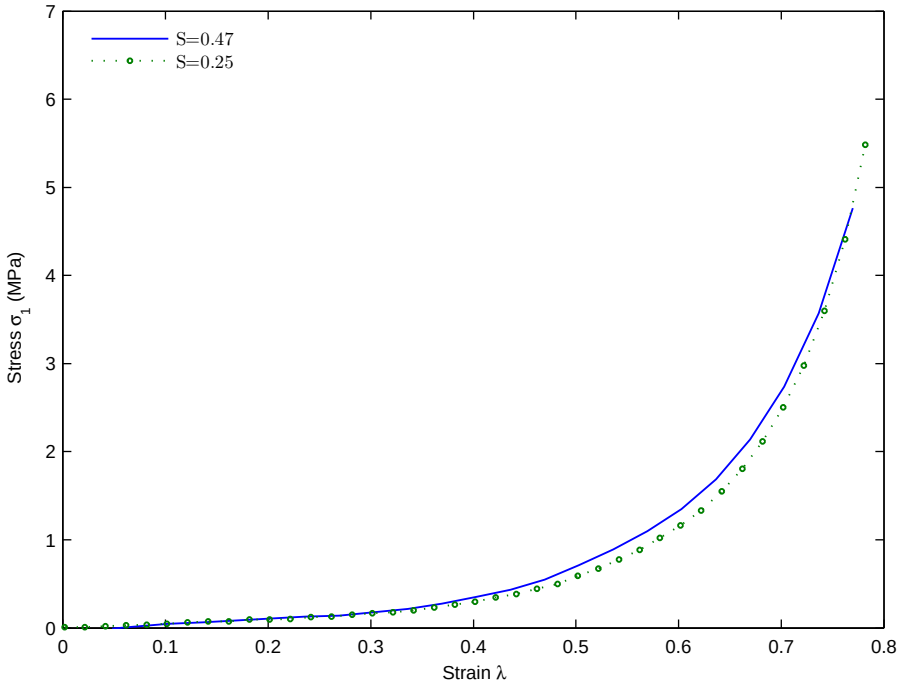

Figure 4.6: Comparison between two specimens of TDM 500 with different shape factors S under compression.

The responses for the two specimens were very close to each other with a variation about the mean of 3.2% (Figure 4.6). This example demonstrated that, since the stress strain response is a strong function of the shape factor for bonded specimens [26] and it is independent of the shape factor for homogeneous compression, samples were subjected with good approximation to an homogeneous compression stress field [12].

Tests were performed on a set of three specimens for every density. Compression tests showed that the compression strength of the TDM was lower when compared to the natural rubber, depending on the density of the compound and it is higher for higher densities (Figure 4.7-4.9).

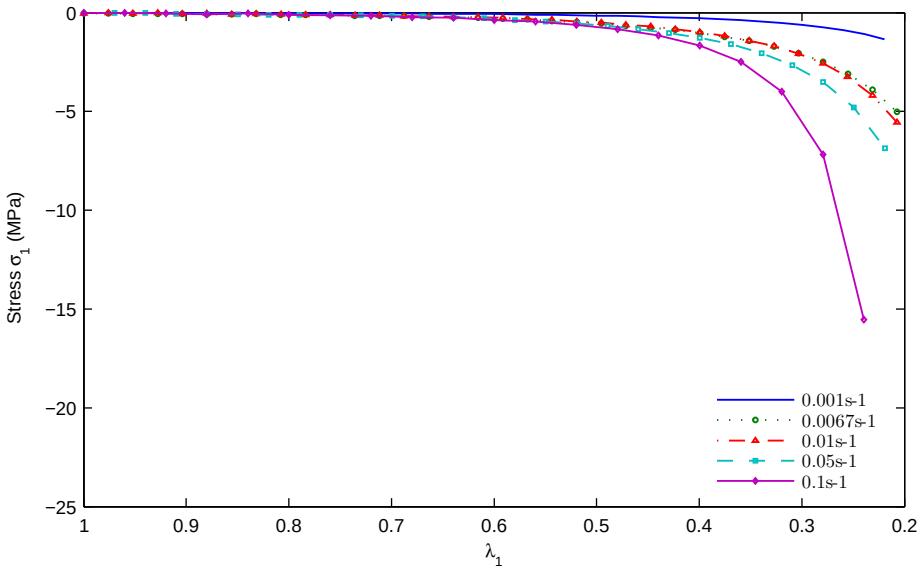

Figure 4.7: Compression tests at different strain rate TDM 500

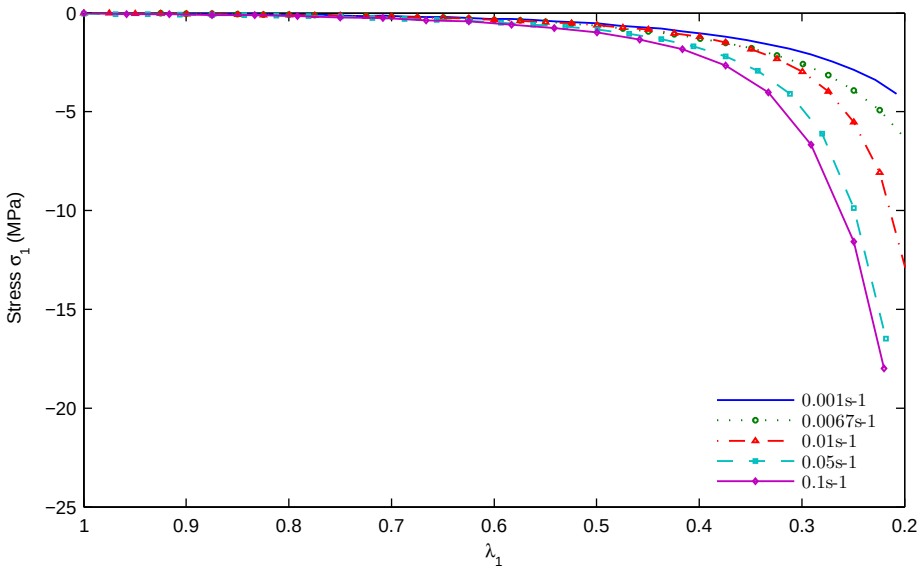

Figure 4.8: Compression tests at different strain rate TDM 600

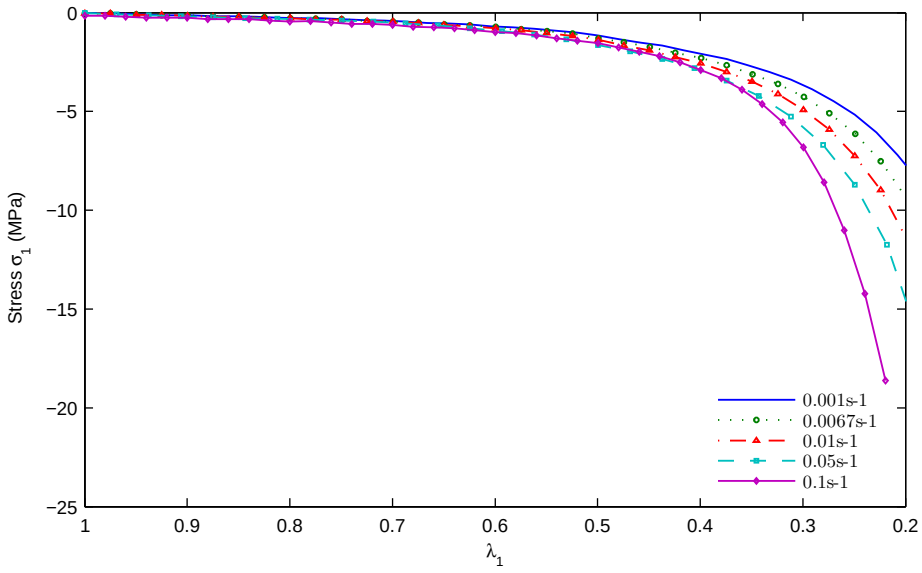

Figure 4.9: Compression tests at different strain rate TDM 800

Table 4.2: Mechanical properties of TDM in compression

Material	E_{sec} Avg. 10% strain (MPa)	E_{sec} Avg. 30% strain (MPa)	E_{sec} Avg. 50% strain (MPa)	E_{sec} Avg. 80% strain (MPa)
500	0.44	0.51	1.01	6.10
600	0.53	0.59	1.08	6.25
800	1.26	1.51	2.42	7.5

Table 3 shows the secant compression modulus E_{sec} for the different materials at different strain levels.

4.3 Relaxation tests and optical measurement

The need of evaluating the nonlinear behavior of TDM in compression suggested to perform Relaxation test in compression. The tests were performed at *UC Berkeley*.

In rubbers, the presence of a significant, but unknown extent of material viscosity makes it difficult to specify a loading rate that is slow enough for obtaining the rate-independent response. To overcome this problem, a multi-step relaxation test was employed in this study.

This approach eliminates the necessity of performing uniaxial test trials in specifying a slow loading rate.

In the present study, TDMs with different densities were tested up to 70% of strain levels. Figure 4.3 shows the applied stretch and the resultant stress histories of the tests. It is observed that at the end of each relaxation interval of 600 sec duration, each stress history converges to an almost constant state in all specimens. The corresponding force in the specimens were obtained from the load cell. In order to get homogeneous compression the loaded ends of the specimen were required to slide freely. For this reason, a frictionless contact between the plates and the sample surfaces was needed. The frictionless constraints were obtained by placing Polytetrafluoroethylene (PTFE) sheets with lubricant on the top and bottom of the sample. Tests were performed on a set of three specimens for every density.In every step the strain level is increased of 0.05 at strain rate $\epsilon = 0.001\, s^{-1}$ up to 0.7 strain level. In between every step there is a 10 mins interval.

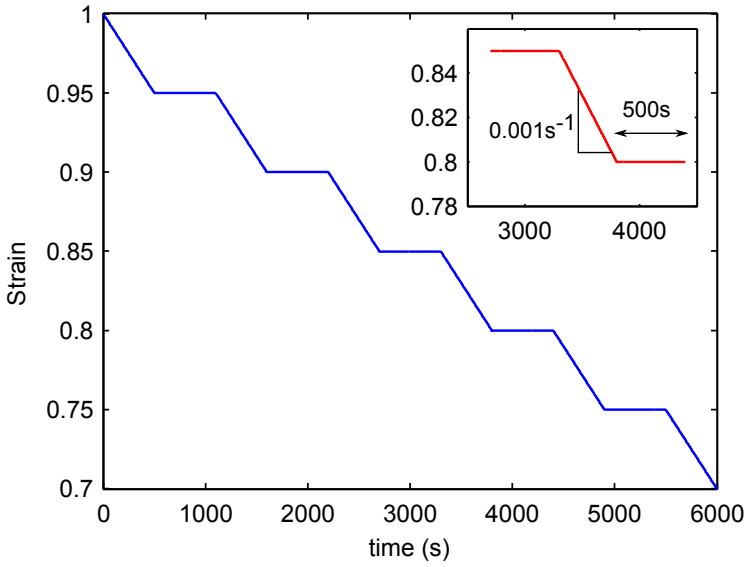

Figure 4.10: Strain history relaxation test.

The digital images were processed using the image processing toolbox in MATLAB. By using the MATLAB command im2bw, the original images were converted to gray scale, which is an intensity image. The gray scale images were then converted into black and white binary images by thresholding; the output binary image has values of 0 (black) for all pixels image with intensity levels less than the threshold, and 1 (white) for all other pixels. Based on visual inspection of the original and processed images, the threshold level was chosen to be 0.87.

Figure 4.3 shows the images taken with the camera and the same images after processing. The white area, measured in pixels, is the region occupied by the sample, and was determined for each image. Pictures were taken at the end of every relaxation period with a digital

camera mounted on a tripod. The digital images were processed using the image processing toolbox in Matlab [53].

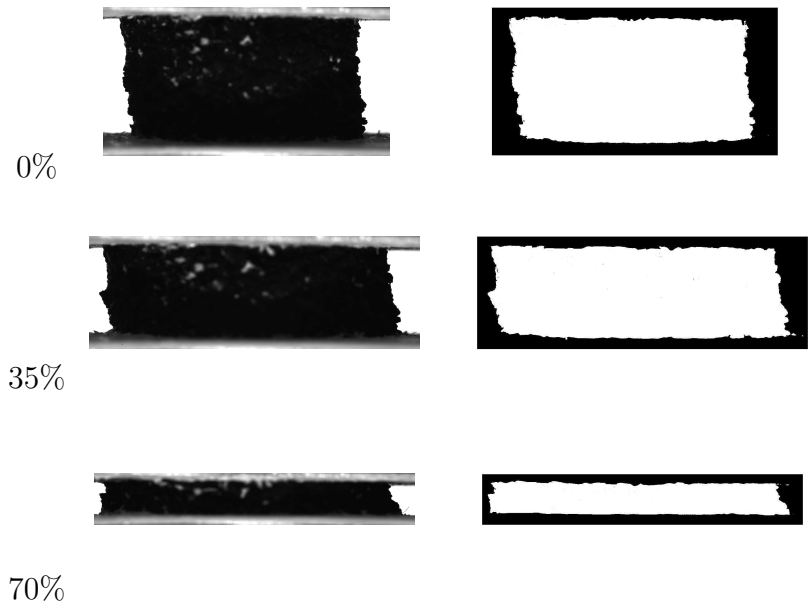

Figure 4.11: Original image from the digital camera vs Image after processing for TDM 600.

The vertical strain in each image was specified in the experiment. TDM for their composition are very difficult to cut and usually the samples have not a straight edge. For these reasons using the processed images we evaluate the average width of the sample as:

$$\widehat{w} = \frac{A}{h} \tag{4.1}$$

And the average lateral strain as:

$$\widehat{\epsilon}_{22} = \widehat{\epsilon}_{33} = \frac{\widehat{w} - \widehat{w}_0}{\widehat{w}_0} \tag{4.2}$$

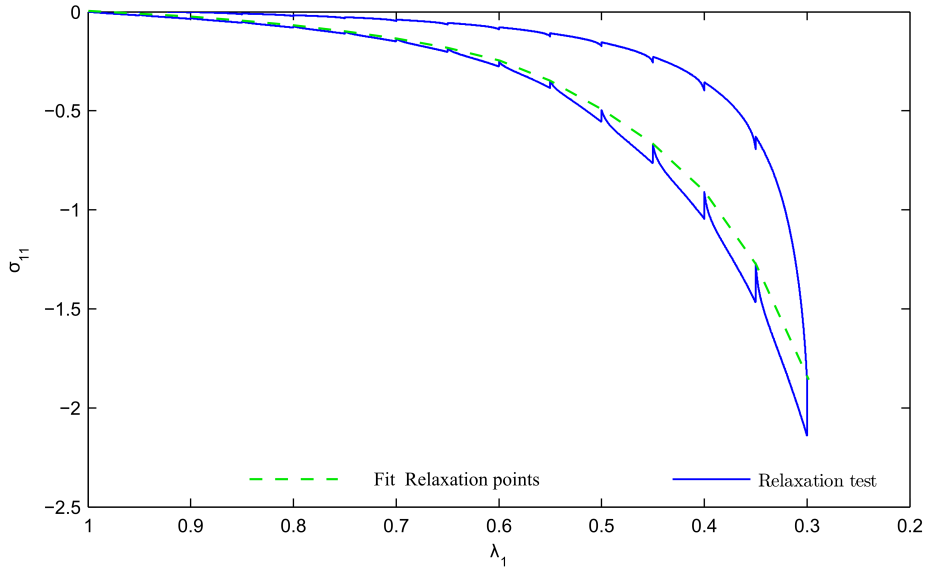

Figure 4.12: Relaxation tests TDM 500

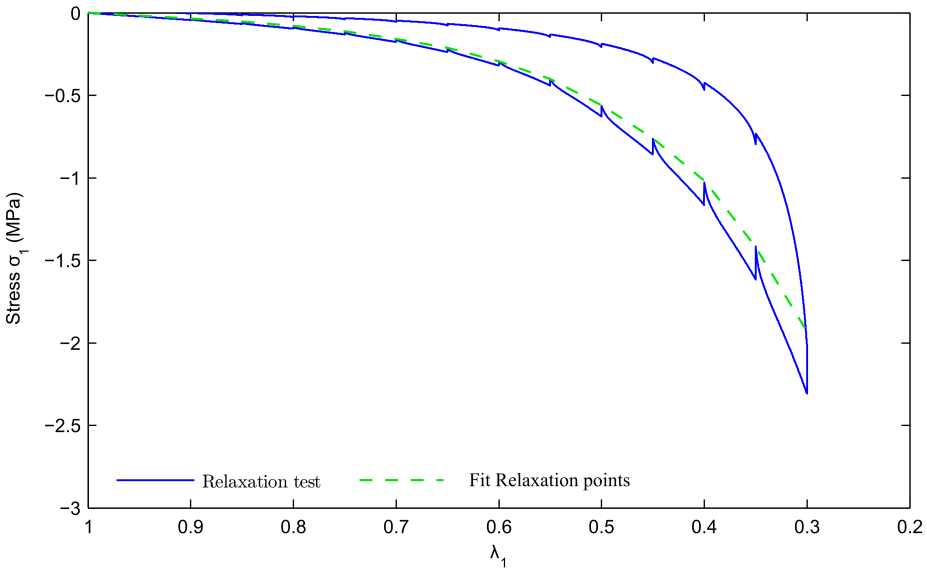

Figure 4.13: Relaxation tests TDM 600

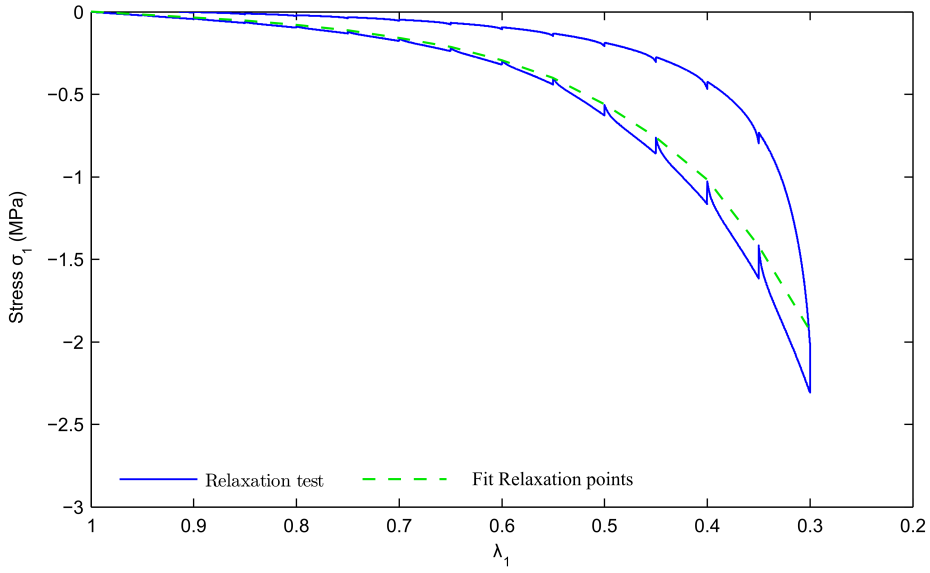

Figure 4.14: Relaxation tests TDM 800

The results were compared with the ones obtained during the compression tests described in the previous paragraph, we found that the fit of the relaxation points overlap the results of the compression tests suggesting that the material in both cases is close to the relaxed state.

4.4 Shear tests

Shear tests were carried out at *Tun Abdul Razak Research Centre* in Hertford (UK). The samples were tested with the classical dual lap simple shear tests configuration commonly used in the tire industry.

The test consisted of three steel plates with two pads bonded between them, in testing the two external plates were clamped to the stationary part of the test fixture, and the single central plate was displaced by the machine, Figure 4.15 shows the complete test setup.

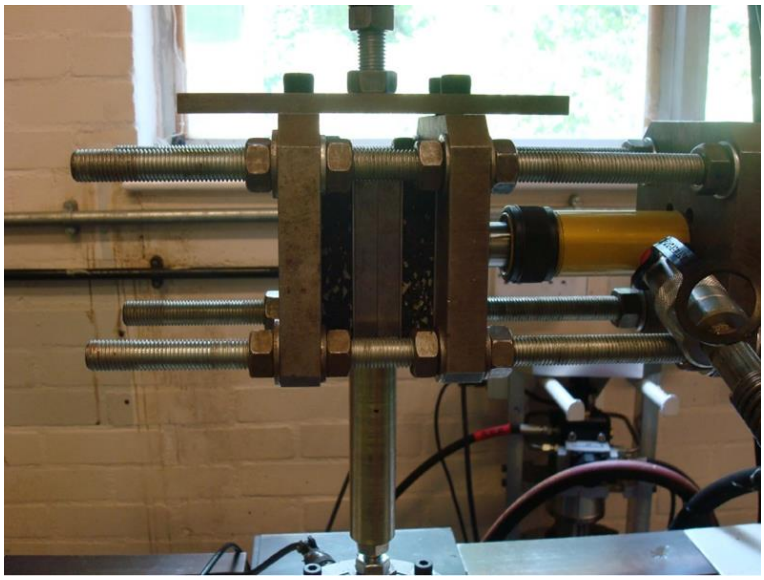

Figure 4.15: Simple shear tests setup

This test procedure does not allow the measurement of compressibility and it is not failure oriented [16].

To avoid any bending effect, the samples used for shear tests were of rectangular shape of 90 mm x 50 mm planar dimensions and 20 mm in thickness [17]. Samples were sheared at shear strain amplitude of 100% of the initial rubber thickness at the deformation rate of 8 mm/min (strain rate of $6.7 \cdot 10^{-3} s^{-1}$). Tests were performed on a set of three specimens for every density.

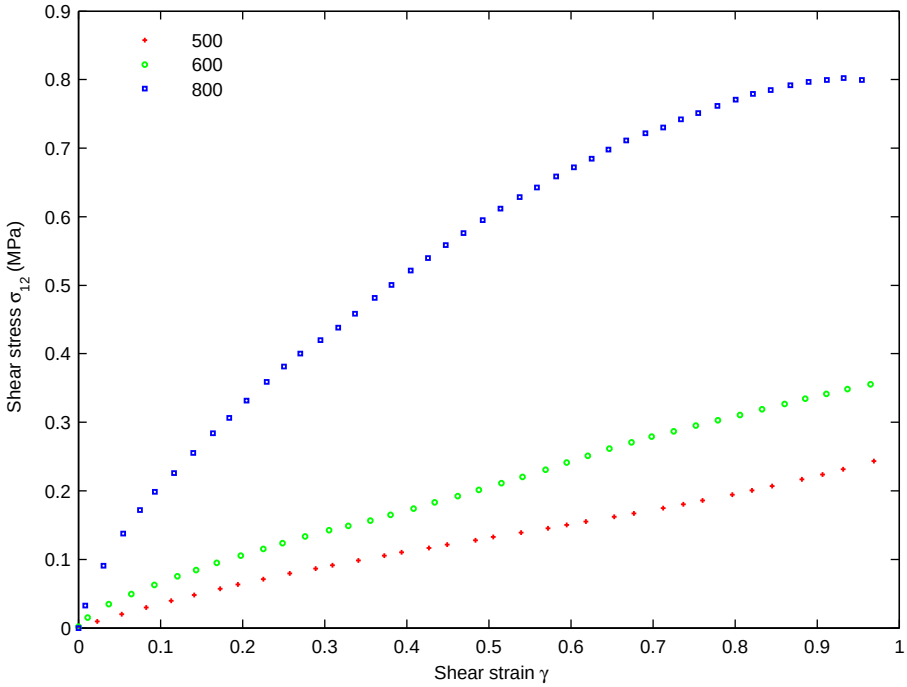

Figure 4.16: Shear test results

As clear from Figure 4.16, tests showed that specimens with higher density have higher shear stiffness with a secant shear modulus in the range from 0.4-1.1 MPa for a deformation of 100% .

Table 4.3: Mechanical properties of TDM in shear

Material	G_{sec} Avg. 10% strain (MPa)	G_{sec} Avg. 33% strain (MPa)	G_{sec} Avg. 66% strain (MPa)	G_{sec} Avg. 100% strain (MPa)
500	0.38	0.38	0.30	0.24
600	0.42	0.40	0.40	0.38
800	1.00	0.95	0.80	0.40

Table 4 shows the values of the secant shear modulus G_{sec} for different values of strain.

4.5 Volumetric tests

Volumetric tests involved the compression in the axial direction of lubricated cylinder specimens within a rigid cylinder (Figure 4.17).

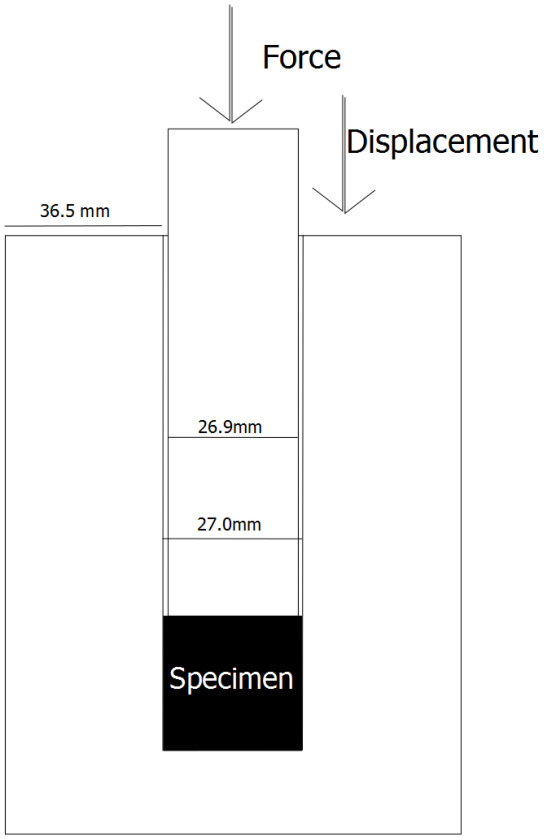

Figure 4.17: Volumetric test scheme

This test required an easy to implement testing apparatus, but has some disadvantages which can make the results inaccurate.

The first problem is connected to the presence of friction at the cylinder-specimen interface. This has to be negligible in order to consider the resulting deformation homogeneous.

The second problem is connected to the capacity of reproducing an hydrostatic stress field. During the test, as the sample is loaded, its lateral surfaces tend to bulge. The presence of the steel cylinder acting as a constrain generates a stress field on the contact surfaces of the side as well as the top and bottom of the sample. As a result, the stress field is quasi-hydrostatic as the stress on the lateral surfaces is lower than that at the top and bottom. Even if both volumetric and deviatoric deformations are present, for natural rubber, the deviatoric stress usually is much smaller than the hydrostatic stress. This is due to a bulk modulus that is several orders of magnitude higher than the shear modulus [39].

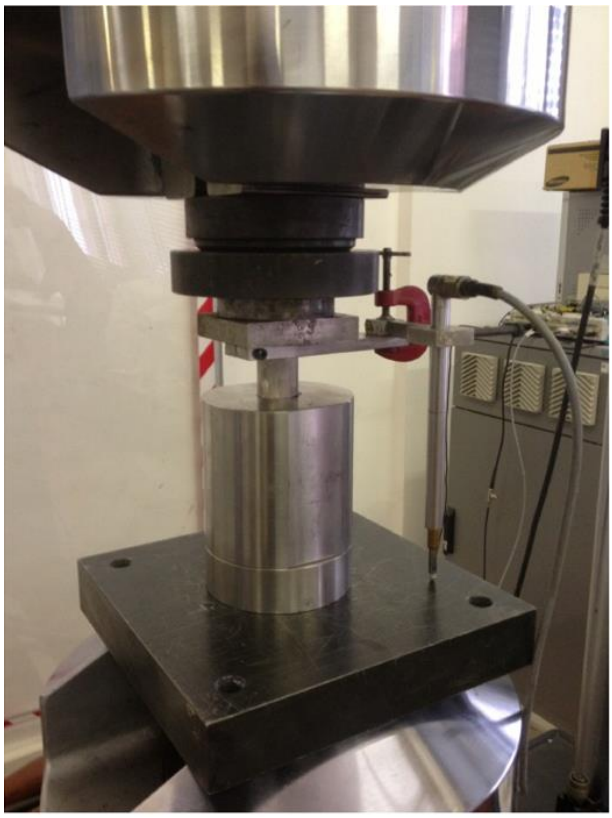

Figure 4.18: Volumetric test apparatus

Conversely, TDMs for low applied pressure, are more compressible than natural rubber. For this reason the values of compressibility in this range of pressure might be inaccurate.

A cylinder of recycled rubber compound of nominal height equal to 25 mm and a diameter of 27 mm was cut from a TDM mat with the same procedure as the sample used previously for compression tests.

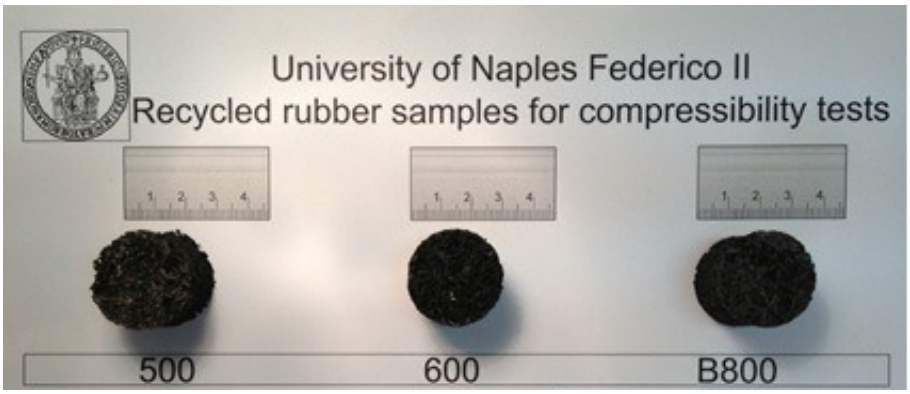

Figure 4.19: Volumetric tests samples

The sample was lubricated and fitted tightly into a thick–wall steel cylinder with a close fitting piston (Figure 4.19). The specimens were subjected to a three cycles of load and unload at 15 mm/min (volume ratio rate of $0.01s^{-1}$) up to a strain of 50% prior to the actual test. During the test the force was applied on top of the piston using a MTS810 test machine with a 500kN load cell at a rate of 10 mm/minute (volume ratio rate $6.7 \cdot 10^{-3}s^{-1}$).

Displacement was measured by an auxiliary Linear Variable Displacement Transducer (LVDT) that was placed directly between the platens.

A smooth passage of the piston in the cylinder was ensured by using a spherical hinge as a contact point between the piston and the loading plate. This procedure is suggested in different references(e.g.,[29]).

Tests were performed on a set of three specimens for every density. The force deflection plot for each of the tested materials is approximately linear up to a certain value of force, then the stiffness increases holding it to an almost constant value (Figure 4.20).

Table 4.4: Bulk Modulus of TDM

Material	K_{sec1} Avg. (MPa)	K_{sec2} Avg. (MPa)
500	6.7	297
600	9.0	315
800	7.9	281

The secant bulk modulus in the region below the sharp upturn K_{sec1} was calculated at about 0.8 of volume ratio J. The secant bulk modulus above the sharp upturn K_{sec2} was obtained from a tangent to the curve at a strain of about 0.7-0.75 of volume ratio J.

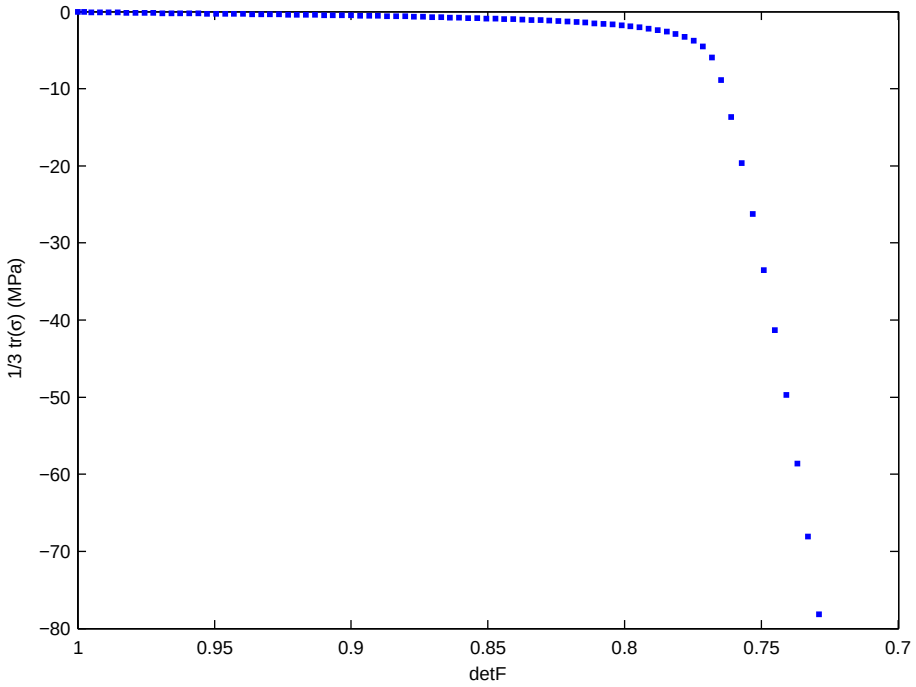

Figure 4.20: Volumetric tests results TDM 500

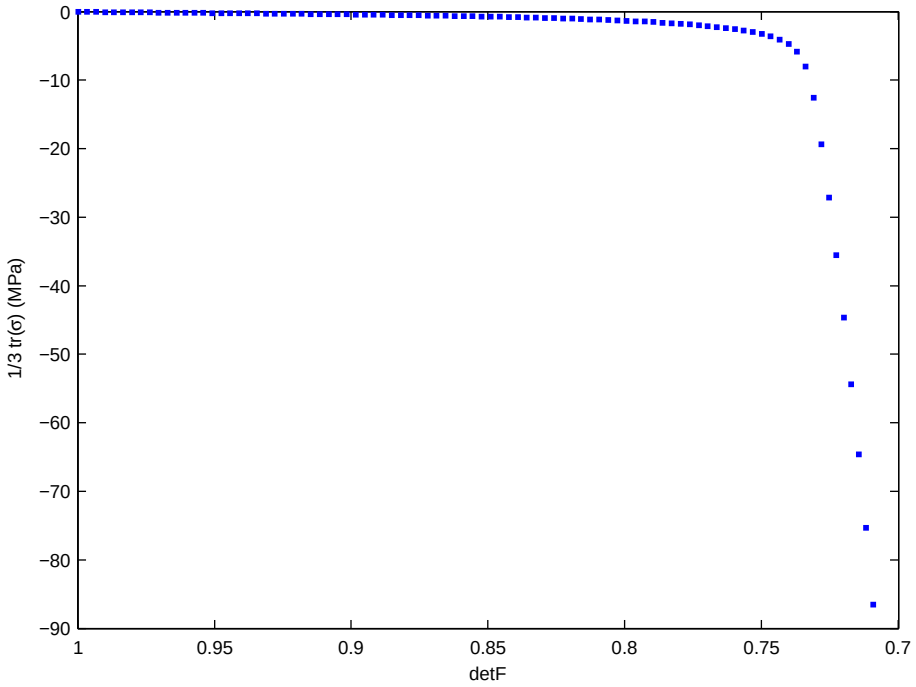

Figure 4.21: Volumetric tests results TDM 600

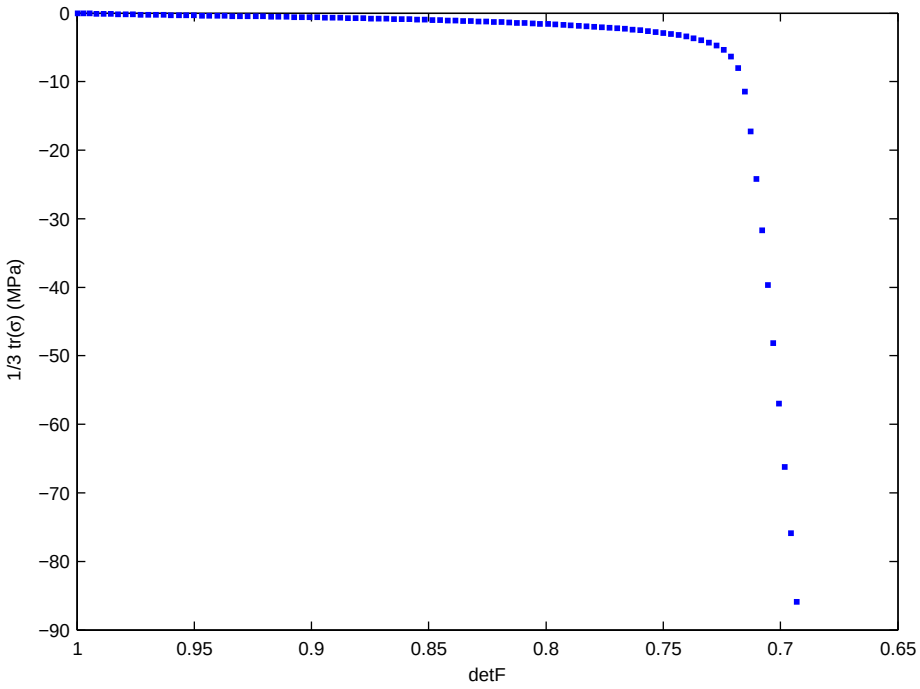

Figure 4.22: Volumetric tests results TDM 800

Chapter 5

Hyperelastic models

5.1 Conventional Hyperelastic models

Four conventional hyperelastic constitutive models including slight compressibility have been chosen to fit the experimental data from TDM in compression, shear and volumetric tests. These models have been chosen because they are representative, but not exhaustive, of the widely used hyperelastic models in Finite Element software.

The constitutive model considered are: the one proposed by Arruda and Boyce (3.46), Mooney-Rivlin (3.43), Ogden (3.45) and a particular forms of the polynomial model that can be obtained setting some coefficient to zero (3.42). If all C_{ij} with $j = 0$ are set to zero we get the reduced polynomial form which depends only on the first strain invariant.

Uniaxial tension tests data were discarded due to the low strength and ultimate deformation of TDMs in this regime of stress. Moreover not one of the chosen hyperelastic models was able to fit the three other test data together, therefore there is a necessity to find a new model to describe the behavior of TDMs for both compression and shear deformation.

The values of the hyperelastic parameters were evaluate considering the compression tests with strain rate of $6.7 \cdot 10^{-3} s^{-1}$ which is also the strain rate at which the volumetric tests were performed. Following the four constitutive models are presented. Many different constitutive models have been proposed to reflect deviations from incompressibility on assuming that the material is homogeneous, isotropic and hyperelastic. The performance of each constitutive model in representing the compression and volumetric response of the material is presented in Figs. 5.1 and 5.4 respectively.

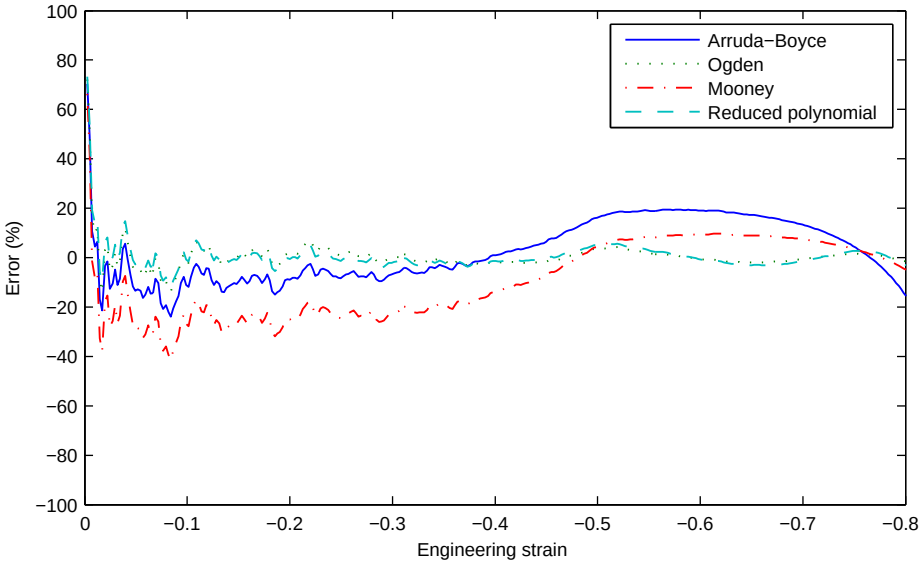

Figure 5.1: Error Constitutive models compression TDM 500

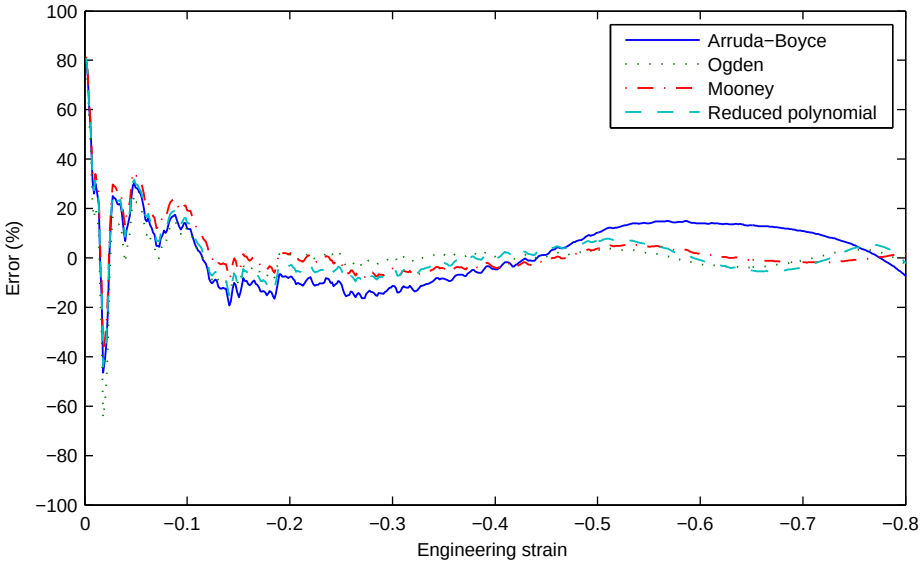

Figure 5.2: Error Constitutive models compression TDM 600

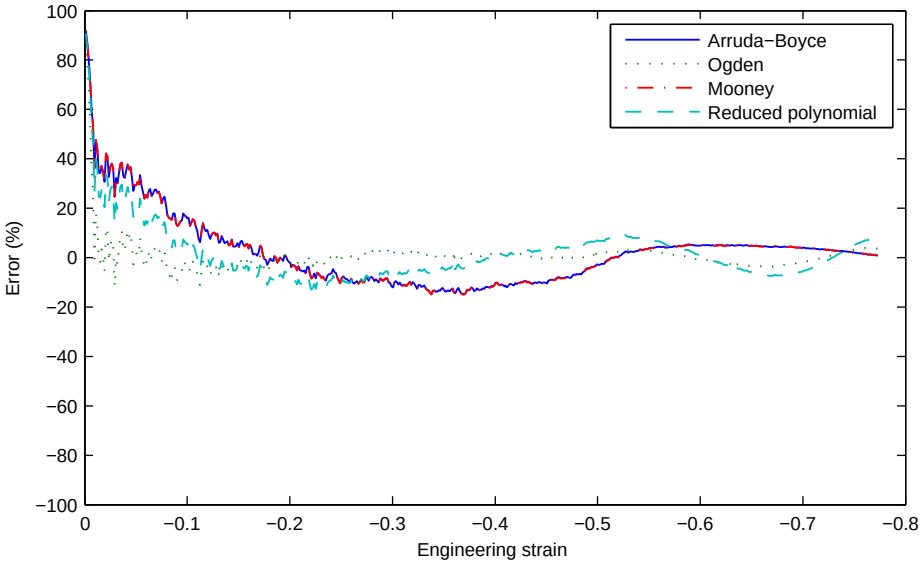

Figure 5.3: Error Constitutive models compression TDM 800

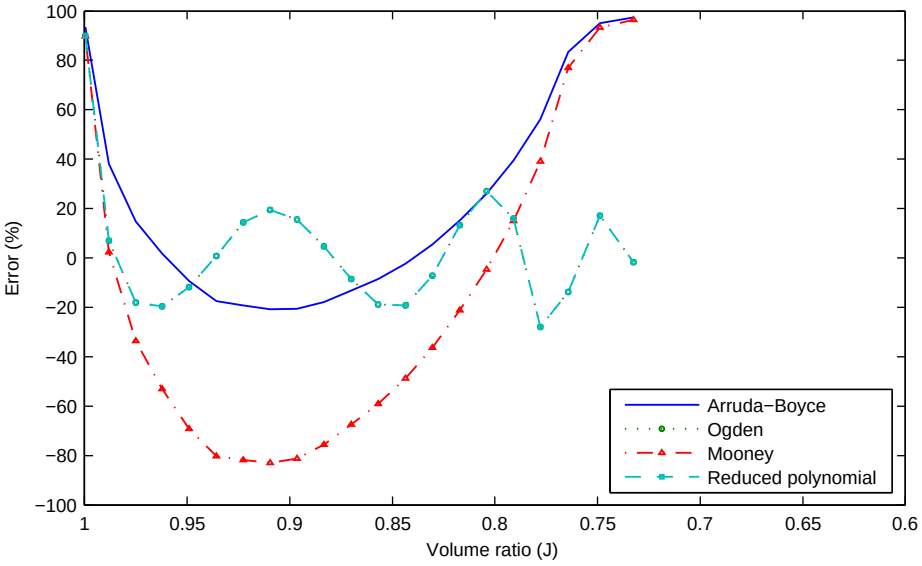

Figure 5.4: Error Constitutive models volumetric TDM 500

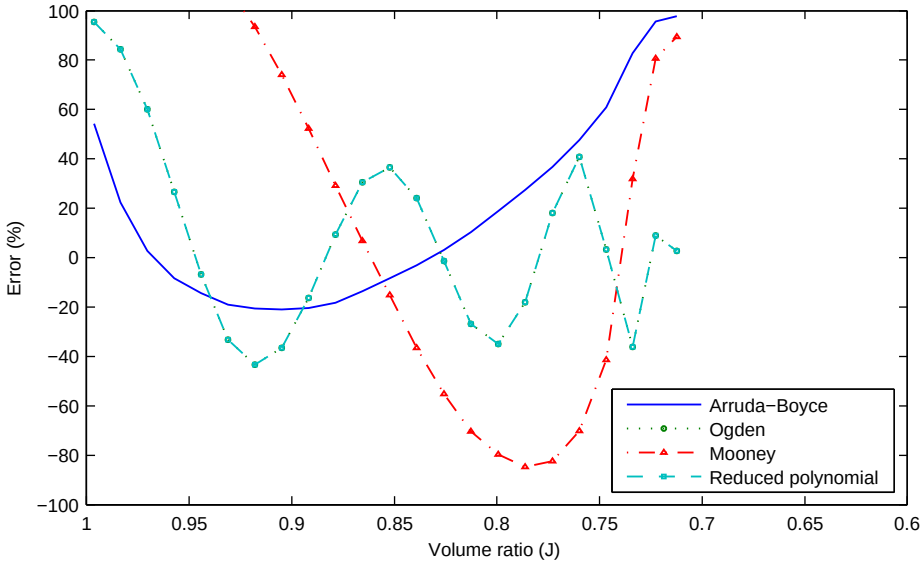

Figure 5.5: Error Constitutive models volumetric TDM 600

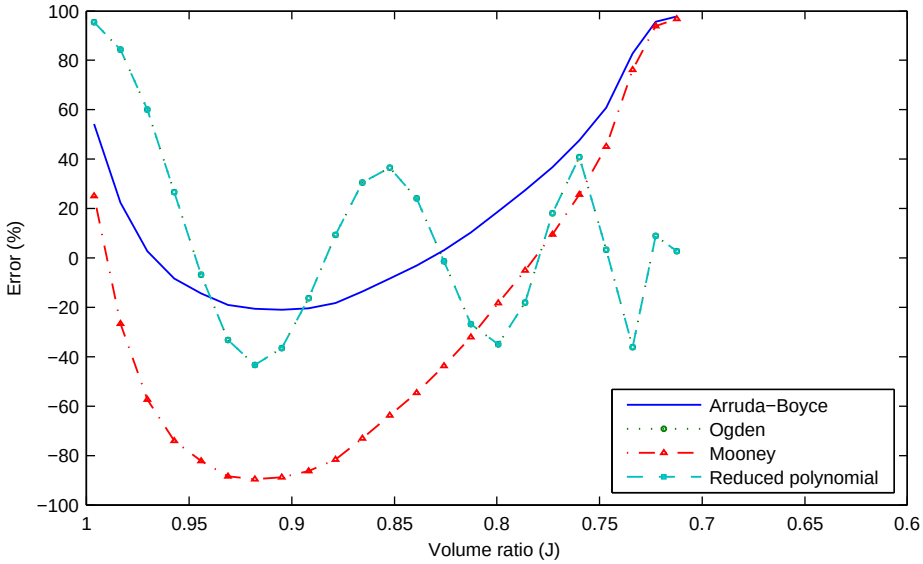

Figure 5.6: Error Constitutive models volumetric TDM 800

The error of a constitutive equation was defined as follows for each kind of homogeneous loading as:

$$\text{Error} = \frac{\sigma_{\text{exp}} - \sigma_{\text{mod}}}{\sigma_{\text{exp}}} \text{x}100 \tag{5.1}$$

where σ_{exp} is the experimental stress and σ_{mod} is the simulated stress for the evaluated model.

Compression tests at high strain level are relatively well depicted by all constitutive equations. The comparison shows the inadequacy of the hyperelastic models in representing the stress strain response at low strain level (up to -0.1). Moreover the Arruda and Mooney hyperelastic models describe better the behavior of TDM with higher densities because, due to the lower presence of voids, they behave more like natural rubber in compression.

Indeed Ogden and Reduced Polynomial model have the same performance for all the densities since polynomial of higher degree can fit better the behavior of lower densities material for which there is a longer softening path on the strain stress curve at low strain.

On the other hand the comparison with volumetric test results clearly indicates that none of the hyperelastic models are able to fit the data with good accuracy. For Arruda and Mooney model this is due to the form of the volumetric term of the strain energy function that can predict only a linear relation between pressure and volume change [39]. Ogden and Reduced Polynomial give better performances with errors less than 50% for almost all the volume ratio range.

5.2 Hencky strain

Logarithmic strain, typically referred as a "true strain", was proposed for the first time by Ludvik [52] to measure the extension of a rod of length l and was defined via the integral:

$$\epsilon_{\text{true}} \int_{l_0}^{l} \frac{dl}{l} = ln\left(\frac{l}{l_0}\right). \tag{5.2}$$

Today is also named after Hencky [33] who extended the measure to a three dimensional analysis by defining the logarithmic strains for the three principal directions.

The one dimensional nominal strain on the other hand is given by:

$$\epsilon = \left(\frac{l - l_0}{l_0}\right). \tag{5.3}$$

The Hencky strain satisfied the additivity of strain even for large deformations, it also has many interesting properties, one of the most important is that it allows to realize a fully uncoupled split of the volumetric and the deviatoric deformation.

Moreover Hencky proposed a strain energy function which, as demostrated by Anand [2], is in good agreement with experiment for a wide class of materials for moderately large deformations:

$$\Psi(\mathbf{F})_{\text{H}} := \widehat{\Psi}_{\text{H}}(\mathbf{U}) := \mu \,||\, \text{dev}_3 \log \mathbf{U}||^2 + \frac{\kappa}{2} \left[\text{tr}(\log \mathbf{U})\right]^2 \tag{5.4}$$

The introduction of the quadratic Hencky strain energy based on the logarithmic strain tensor $\log \mathbf{V}$ is a milestone in the development of nonlinear elasticity theory in the first half of the 20^{th} century. Since the original manuscripts are written in German, they are not easily accessible today.

5.3 New strain energy function

The most common hyperelastic material models used in Finite Element codes failed in describing TDMs in different deformation modes with a unique set of parameters [57].

Fitting experimental data of elastomeric solid to polynomial strain energy function is not an easy question and can lead to high-orders polynomials with parameters that may not have any physical meaning [67].

Here logarithmic measure are used to describe the mechanical behaviour of the TDMs. In a series of articles [63, 64, 61, 62] it is investigate a family of isotropic volumetric-isochoric decoupled strain energies

$$\mathbf{F} \mapsto \Psi_{\mathrm{eH}}(\mathbf{F}) := \widehat{\Psi}_{\mathrm{eH}}(\mathbf{U}) := \begin{cases} \dfrac{\mu}{k}\, e^{k\,\|\operatorname{dev}_n \log \mathbf{U}\|^2} + \dfrac{\kappa}{2\,\widehat{k}}\, e^{\widehat{k}\,[\operatorname{tr}(\log \mathbf{U})]^2} & \text{if} \quad \det \mathbf{F} > 0, \\ \\ +\infty & \text{if} \quad \det \mathbf{F} \leq 0, \end{cases} \tag{5.5}$$

based on the Hencky-logarithmic (true, natural) strain tensor $\log \mathbf{U}$, where $\mu > 0$ is the infinitesimal shear modulus, $k = \frac{2\mu+3\lambda}{3} > 0$ is the infinitesimal bulk modulus with λ the first Lamé constant, $k, \widehat{k}$ are dimensionless parameters, $\mathbf{F} = \nabla\varphi$ is the gradient of deformation, $\mathbf{U} = \sqrt{\mathbf{F}^T\mathbf{F}}$ is the right stretch tensor and $\operatorname{dev}_n \log \mathbf{U} = \log \mathbf{U} - \frac{1}{n}\operatorname{tr}(\log \mathbf{U}) \cdot \mathbb{1}$ is the deviatoric part of the strain tensor $\log \mathbf{U}$.

In this paper a variation to the volumetric part of (5.5) is proposed to describe the mechanical behavior of TDM:

$$\mathbf{F} \mapsto \Psi_{\mathrm{eHm}}(\mathbf{F}) := \widehat{\Psi}_{\mathrm{eHm}}(\mathbf{U}) := \begin{cases} \dfrac{\mu}{k}\, e^{k\,\|\operatorname{dev}_n \log \mathbf{U}\|^2} + \dfrac{\kappa}{2\,\widehat{k}}\, e^{\widehat{k}\,[\operatorname{tr}(\log \mathbf{U})]^2} + \\ + \dfrac{\kappa_1}{m\,\tilde{k}}\, e^{\tilde{k}\left([\operatorname{tr}|\log \mathbf{U}|^2]\right)^{\frac{m}{2}}} & \text{if} \quad \det \mathbf{F} > 0, \\ \\ +\infty & \text{if} \quad \det \mathbf{F} \leq 0, \end{cases} \tag{5.6}$$

where k_1 is the value of the bulk modulus for large deformations and $\tilde{k}$ is a dimensionless parameters.

The main advantage of using the exponentiated Hencky energy comes from the fact that the shear and bulk modulus are already uniquely determined in the infinitesimal strain regime, while k_1 is dimensionless constants which determine the nonlinear response, without interfering with μ and k.

Additionally to the well-known properties of the Henky strain energy function, the exponentiated-Hencky strain energy has more attractive properties. Recently was found that the Hencky energy (not the logarithmic strain itself) exhibits a fundamental property. By purely differential geometric reasoning, in forthcoming papers [59, 60, 65] (see also [9, 49])

it will be shown that

$$\begin{aligned}\operatorname{dist}^2_{\text{geod}}\left((\det \mathbf{F})^{1/n}\cdot \mathbb{1}, \mathrm{SO}(n)\right) &= \operatorname{dist}^2_{\text{geod},\mathbb{R}_+\cdot\mathbb{1}}\left((\det \mathbf{F})^{1/n}\cdot \mathbb{1}, \mathbb{1}\right) = |\log\det \mathbf{F}|^2,\\ \operatorname{dist}^2_{\text{geod}}\left(\frac{\mathbf{F}}{(\det \mathbf{F})^{1/n}}, \mathrm{SO}(n)\right) &= \operatorname{dist}^2_{\text{geod},\mathrm{SL}(n)}\left(\frac{\mathbf{F}}{(\det \mathbf{F})^{1/n}}, \mathrm{SO}(n)\right) = \|\operatorname{dev}_n \log \mathbf{U}\|^2, \quad (5.7)\end{aligned}$$

where $\operatorname{dist}_{\text{geod}}$ is the canonical left invariant geodesic distance on the Lie group $\mathrm{GL}^+(n)$ and $\operatorname{dist}_{\text{geod},\mathrm{SL}(n)}$, $\operatorname{dist}_{\text{geod},\mathbb{R}_+\cdot\mathbb{1}}$ denote the corresponding geodesic distances on the Lie groups $\mathrm{SL}(n)$ and $\mathbb{R}_+\cdot\mathbb{1}$, respectively (see [60, 65]). For small elastic strains, Ψ_{eH} approximates the classical quadratic Hencky strain energy Ψ_{H}, which is not everywhere rank-one convex, moreover in [63], we have also pointed out that the quadratic Hencky energy has some other serious shortcomings.

These points being more or less well-known, it is clear that there cannot exist a general mathematical well-posedness result for the quadratic Hencky model Ψ_{H}. Of course, in the vicinity of the identity, an existence proof for small loads based on the implicit function theorem will always be possible. All in all, the status of Hencky's quadratic energy is put into doubt. This state of affairs, on the one hand the preferred use of the quadratic Hencky energy and its fundamental property (5.7), on the other hand its mathematical shortcomings, motivated our search for a modification of Hencky's energy.

The best candidate for now is Ψ_{eH} defined by (5.5). Up to moderate strains, for principal stretches $\lambda_i \in (0.7, 1.4)$, our new exponentiated Hencky formulation (5.5) is de facto as good as the quadratic Hencky model Ψ_{H} and in the large strain region it improves several important features from a mathematical point of view. The main features that have been shown in [63] is that the exponentiated Hencky energy (5.5) satisfies the LH-condition (rank-one convexity) in planar elasto-statics, i.e. for $n = 2$. In the second part of the series of papers [64] it is aimed to complete this investigation by showing that the planar elasto-static formulation is, in fact, polyconvex and satisfies a coercivity estimate which allows us to show the existence of minimizers. Unfortunately, some aspects of the three-dimensional description remain open, since the formulation is not globally rank-one convex.

However, in the three-dimensional case, results indicating the loss of ellipticity only for extreme distortional strains suggest that the coupling with plasticity is most natural: permanent deformation sets in, based on a criterion of distortional energy (Huber-Hencky-von Mises-type) $\|\operatorname{dev}_3 \tau_{\text{eH}}\|^2 \leq \frac{2}{3}\boldsymbol{\sigma}_{\mathbf{y}}^2$ with τ_{eH} the Kirchhoff stress tensor, and former results suggest that $\Psi_{\text{eH}}(\mathbf{F}_e)$ never reaches the non-elliptic domain in any elasto-plastic process. This is in sharp contrast to the loss of ellipticity of the quadratic Hencky energy Ψ_{H}, which is not related to the distortional energy alone. As it turns out, for the overall non-elliptic energy Ψ_{eH} (in three dimensions) plasticity provides a natural relaxation mechanism, which prevents loss of ellipticity in the elastic domain.

Moreover, in the above defined elastic domain characterized by $\|\operatorname{dev}_3 \tau_{\text{eH}}\|^2 \leq \frac{2}{3}\boldsymbol{\sigma}_{\mathbf{y}}^2$, the constitutive relation $\log \mathbf{B}_e \mapsto \sigma(\log \mathbf{B}_e)$ remains monotone ($\mathbf{B}_e = \mathbf{F}_e\mathbf{F}_e^T$, i.e. the true-stress-true-strain monotonicity condition (TSTS-M$^+$) is also satisfied in this domain (see [63, 81, 82, 44]), as observed in experiments.

Beside the above mathematical properties, the exponentiated Hencky energy (5.5) have also the following attractive constitutive properties [63] beyond those of the quadratic Hencky energy: planar pure Cauchy shear stress produces biaxial pure shear strain and $\nu = \frac{1}{2}$ corresponds to exact incompressibility; there exists a special ($k = \frac{2}{3}\widehat{k}$) three parameter subset of energies of our family $\Psi_{\rm eH}$ such that uniaxial tension leads to no lateral contraction if and only if the Poisson's ratio $\nu = 0$, as in linear elasticity. Moreover, some other properties (see [63]) such as uniqueness in the hydrostatic loading problem [66, 18] confirm the status of the exponentiated Hencky formulation as a useful energy in plane elasto-statics and give a new perspective in three dimensions.

For the exponentiated-Hencky strain energy proposed, the Kirchhof stress tensor is given by:

$$\tau = D_{\log\mathbf{U}}\Psi_{\rm eHm}(\log\mathbf{U}) = 2\,\mu\, e^{k\,\|\,\mathrm{dev}_3\log\mathbf{U}\|^2}\cdot \mathrm{dev}_3\log\mathbf{U} + \kappa\, e^{\widehat{k}\,[\mathrm{tr}(\log\mathbf{U})]^2}\mathrm{tr}(\log\mathbf{U}) + \tag{5.8}$$

$$+\,\kappa_1\, e^{\tilde{k}\left[\mathrm{tr}|\log\mathbf{U}|^2\right]^{\frac{m}{2}}}\frac{|\mathrm{tr}(\log\mathbf{U})|^m}{\mathrm{tr}(\log\mathbf{U})}\cdot\mathbb{1} \tag{5.9}$$

while the Cauchy stress tensor is:

$$\sigma = e^{-\mathrm{tr}(\log\mathbf{U})}\tau = 2\,\mu\, e^{k\,||\mathrm{dev}_3\log\mathbf{U}||^2-\mathrm{tr}(\log\mathbf{U})}\cdot\mathrm{dev}_3\log\mathbf{U} + \kappa\, e^{\widehat{k}\,[\mathrm{tr}(\log\mathbf{U})]^2-\mathrm{tr}(\log\mathbf{U})}\mathrm{tr}(\log\mathbf{U}) +$$

$$\kappa_1\, e^{\tilde{k}\left[\mathrm{tr}(\log\mathbf{U})^2\right]^{\frac{m}{2}}-\mathrm{tr}(\log\mathbf{U})}\frac{|\mathrm{tr}(\log\mathbf{U})|^m}{\mathrm{tr}(\log\mathbf{U})}\cdot\mathbb{1} \tag{5.10}$$

Following we consider three deformation modes in which the TDM has been tested.

5.4 Comparison with experimental data

Simple shear

Shear tests were carried out at *Tun Abdul Razak Research Centre* in Hertford (UK). The samples were tested with the classical dual lap simple shear tests configuration commonly used in the tire industry. Samples were sheared at shear strain amplitude of 100% of the initial rubber thickness at the strain rate of $6.7\cdot 10^{-3}s^{-1}$. Tests were performed on a set of three specimens for every density.

In simple shear the direction of applied displacements does not coincide with the direction of the principal stretches; rather it involves a rotation of axes. The polar decomposition of $\mathbf{F} = \mathbf{R}\cdot\mathbf{U}$ gives the right Biot stretch tensor $\mathbf{U} = \sqrt{\mathbf{F}^T\mathbf{F}}$ of the deformation and the orthogonal polar factor $\mathbf{R}$:

$$\mathbf{U} = \frac{1}{\sqrt{\gamma^2+4}}\begin{bmatrix} 2 & \gamma & 0 \\ \gamma & \gamma^2+2 & 0 \\ 0 & 0 & \sqrt{\gamma^2+4} \end{bmatrix} \tag{5.11}$$

$$\mathbf{R} = \frac{1}{\sqrt{\gamma^2+4}} \begin{bmatrix} 2 & \gamma & 0 \\ -\gamma & 2 & 0 \\ 0 & 0 & \sqrt{\gamma^2+4} \end{bmatrix} \tag{5.12}$$

$\mathbf{U}$ can be orthogonally diagonalized to find:

$$\log\mathbf{U} = \frac{1}{\sqrt{\gamma^2+4}} \begin{bmatrix} -\gamma\log\lambda_1 & 2\log\lambda_1 & 0 \\ 2\log\lambda_1 & \gamma\log\lambda_1 & 0 \\ 0 & 0 & 0 \end{bmatrix} \tag{5.13}$$

Where $\lambda_1 = \frac{1}{2}\left(\sqrt{\gamma^2+4}+\gamma\right)$ is the first eigenvalue of $\mathbf{U}$.

Simple shear does not imply change in volume for this reason $\det\mathbf{F} = \mathbf{1}$ and $\mathrm{tr}(\log\mathbf{U}) = 0$ then the Kirchhoff stress τ from equation (5.8) is given by:

$$\tau\left(\log\mathbf{U}\right) = 4\,\mu\, e^{2\,k\log^2\left[\frac{1}{2}\left(\sqrt{\gamma^2+4}+\gamma\right)\right]} \cdot \frac{\log\left[\frac{1}{2}\left(\sqrt{\gamma^2+4}+\gamma\right)\right]}{\sqrt{\gamma^2+4}} \tag{5.14}$$

TDMs behave like a granular material in which particle rotation determinates the response. For this reason, the shear modulus for infinitesimal deformation is high due to the initial interparticle rolling resistance. This phenomenon is more marked as the density increases.

Here the value of μ is evaluated when the effect of the initial resistance vanishes Figure 5.7.

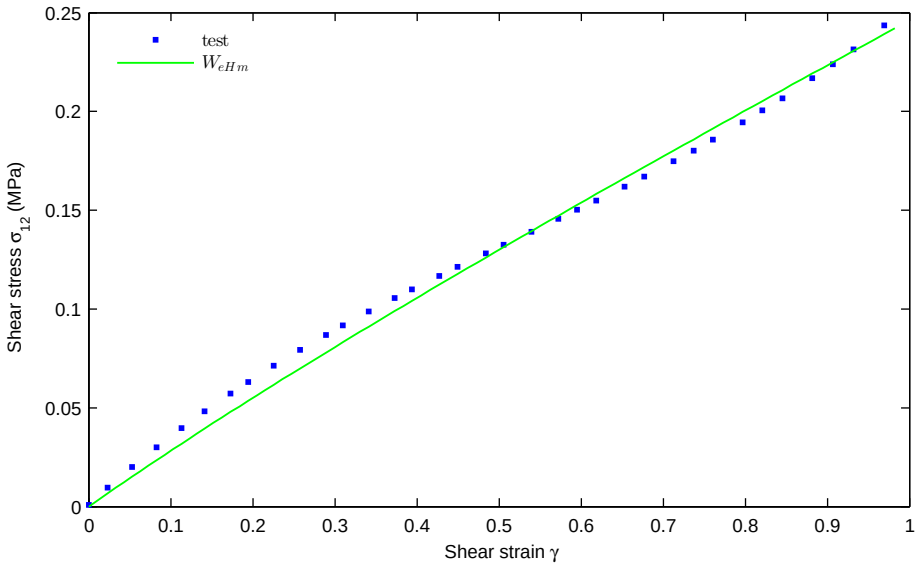

Figure 5.7: Comparison between shear stress corresponding to exponentiated Hencky energy Ψ_{eHm}, equation (5.14), and experimental tests for TDM 500.

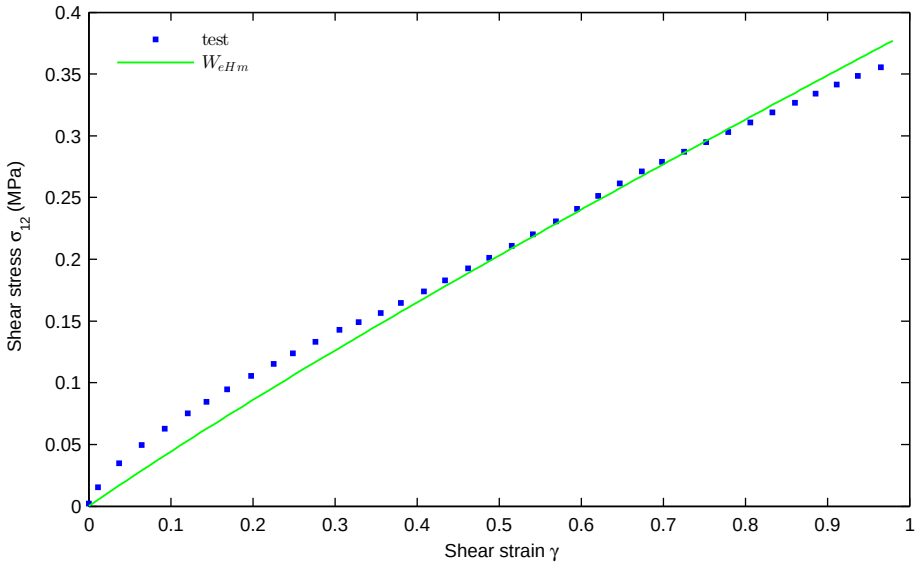

Figure 5.8: Comparison between shear stress corresponding to exponentiated Hencky energy Ψ_{eHm}, equation (5.14), and experimental tests for TDM 600.

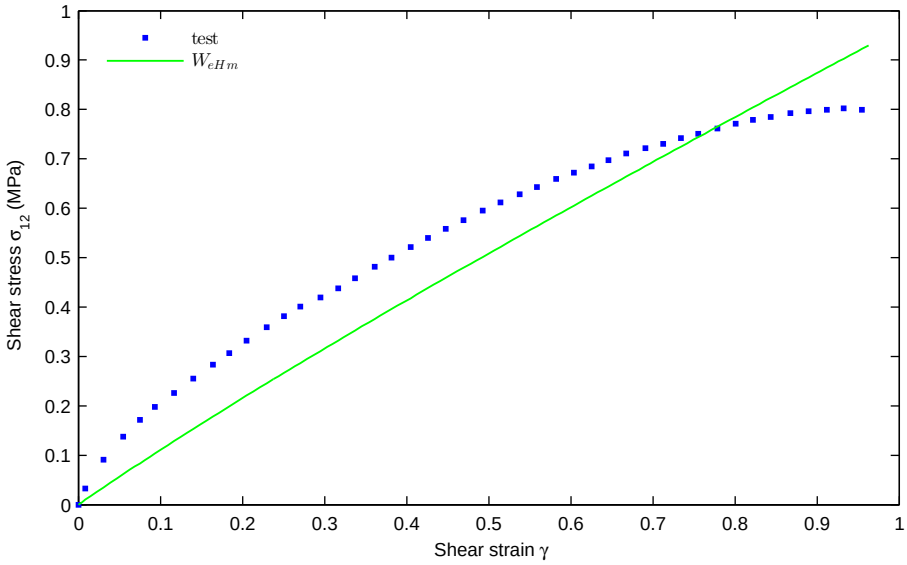

Figure 5.9: Comparison between shear stress corresponding to exponentiated Hencky energy Ψ_{eHm}, equation (5.14), and experimental tests for TDM 800.

We have also compared [63] the simple shear stress σ_{12} corresponding to the amount of shear for the energies $\Psi_{\text{eHm}}, \Psi_{\text{eH}}$, for the Mooney-Rivlin energy and for Neo-Hooke energy and we have obtained that our results are more closely related to the experimental data for the simple shear deformation of vulcanized rubber, measured in 1944 by L.R.G. Treloar [76] and in 1975 by L.R.G. Treloar and D.F. Jones [45] (see also [77, 78]).

Compression

From equation (5.10), if we consider s the value of the Cauchy stress, by projection on the Lie-algebras $\mathfrak{sl}(n)$ and $\mathbb{1} \cdot \mathbb{R}$,we have:

$$2\,\mu\, e^{k\,||\,\mathrm{dev}_3\,\log\mathbf{U}||^2-\mathrm{tr}(\log\mathbf{U})}\,\mathrm{dev}_3\,\log\mathbf{U} = \mathrm{dev}_3\,\sigma = \begin{pmatrix} \frac{2}{3}s & 0 & 0 \\ 0 & -\frac{1}{3}s & 0 \\ 0 & 0 & -\frac{1}{3}s \end{pmatrix} \tag{5.15}$$

If we consider the folllowing ansatz for $\mathbf{U}$:

$$\mathbf{U} = \begin{pmatrix} e^{a+\frac{1}{3}x} & 0 & 0 \\ 0 & e^{-\frac{1}{2}a+\frac{1}{3}x} & 0 \\ 0 & 0 & e^{-\frac{1}{2}a+\frac{1}{3}x} \end{pmatrix} = e^{\frac{1}{3}x} \begin{pmatrix} e^{a} & 0 & 0 \\ 0 & e^{-\frac{1}{2}a} & 0 \\ 0 & 0 & e^{-\frac{1}{2}a} \end{pmatrix} \tag{5.16}$$

equation (5.15) becomes:

$$3\,\mu\, e^{k\,\frac{3}{2}\,a^2-x} a = s, \tag{5.17}$$

Which in terms of Poisson's coefficient ν and Young's Modulus $E > 0$ gives:

$$\frac{3}{2}\,\frac{E}{1+\nu}\, e^{k\,\frac{3}{2}\,a^2-x} a = s, \tag{5.18}$$

where the linear Poisson's coefficient is $\nu = -\dfrac{\widehat{\epsilon_{22}}}{\epsilon_{11}}$ with ϵ_{11} and $\widehat{\epsilon_{22}}$ evaluated for infinitesimal deformation.

Table 5.1: Linear Poisson's coefficient and Young's Modulus

Material	ν	E (MPa)
500	0.031	1.10
600	0.033	1.05
800	0.041	2.49

We define the non linear Poisson's coefficient as negative ratio of the lateral extension and axial contraction measured in the logarithmic strain we have:

$$\widehat{\nu}(s) = -\frac{(\log\mathbf{U})_{22}}{(\log\mathbf{U})_{11}} = \frac{\dfrac{1}{2}a - \dfrac{1}{3}x}{a + \dfrac{1}{3}x} \tag{5.19}$$

The linear Poisson's ratio for many materials is positive and not strain sensitive until nonelastic effects intervene [74, 46]. The graphic of the map $\dfrac{s}{E} \mapsto \widehat{\nu}(\dfrac{s}{E})$ is tangent to the line $\widehat{\nu}(0) = \nu$, decreases for positive (linear) Poisson's ration, while for negative (linear) Poisson's ratio the map increases.

Moreover, the nonlinear Poisson's ratio $\widehat{\nu}$ remains positive whenever $\nu = \widehat{\nu}(0)$ is positive and it remains negative whenever ν is negative.

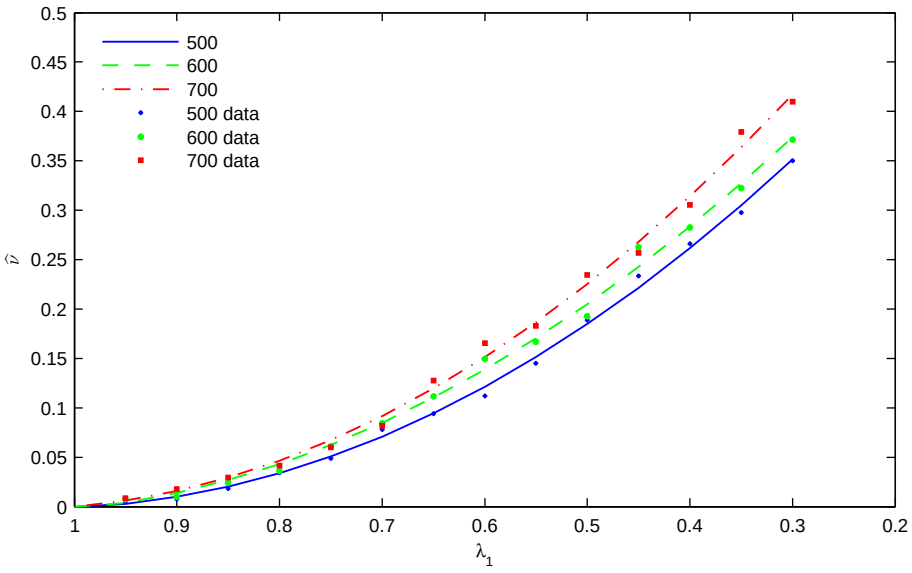

Figure 5.10: Non linear Poisson's coefficient $\widehat{\nu}$ evaluated during compression tests. Fit of experimental data (scattered line).

In view of these definition we have:

$$a = \frac{2}{3}\,\frac{1+\widehat{\nu}}{1-2\hat{\nu}}\,x \tag{5.20}$$

$$s = \frac{1+\widehat{\nu}}{1-2\widehat{\nu}}\,\frac{E}{1+\nu}\,e^{\,k\,\frac{2}{3}\left(\frac{1+\widehat{\nu}}{1-2\widehat{\nu}}\right)^{2}\,x^2-x}\,x \tag{5.21}$$

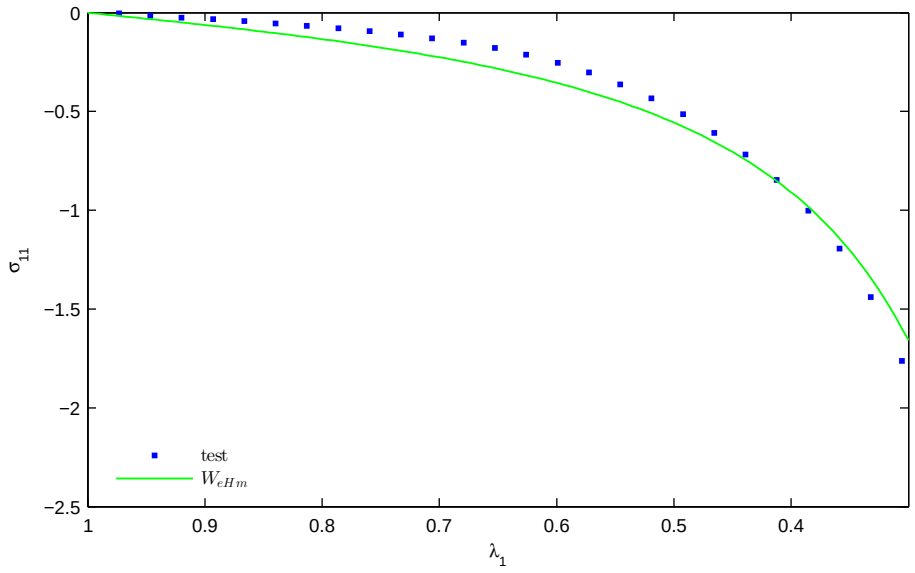

Figure 5.11: Comparison between compression stress corresponding to exponentiated Hencky energy Ψ_{eHm}, equation (5.21), and experimental tests for TDM 500.

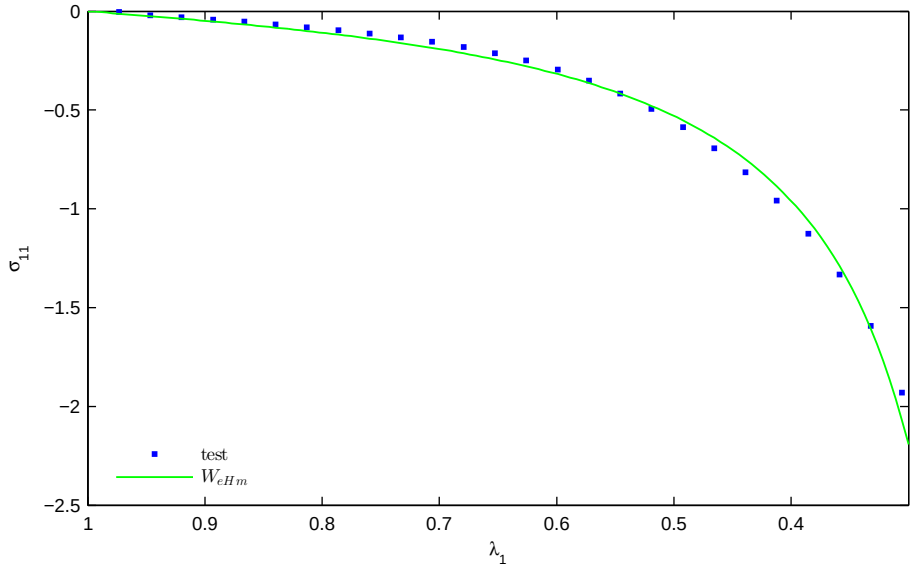

Figure 5.12: Comparison between compression stress corresponding to exponentiated Hencky energy Ψ_{eHm}, equation (5.21), and experimental tests for TDM 600.

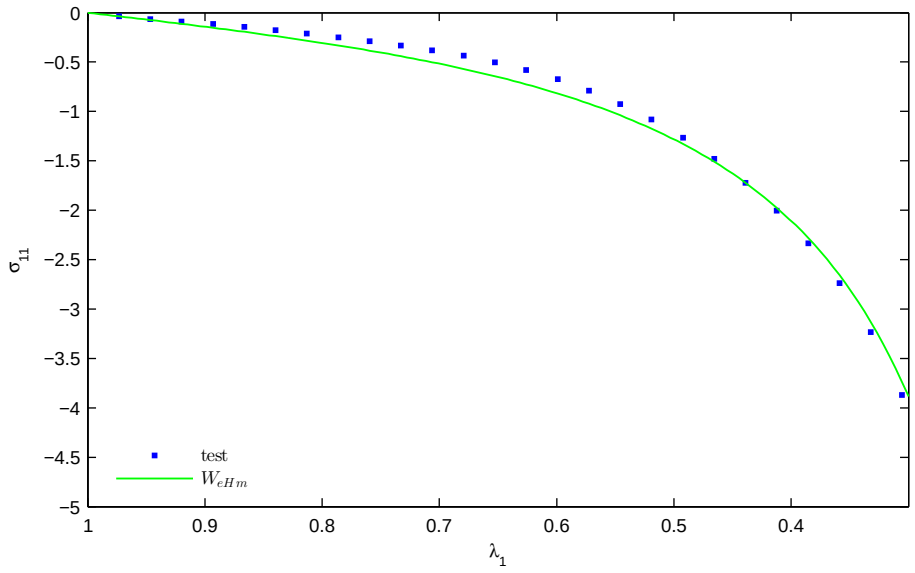

Figure 5.13: Comparison between compression stress corresponding to exponentiated Hencky energy Ψ_{eHm}, equation (5.21), and experimental tests for TDM 800.

Hydrostatic compression

Volumetric tests involved the compression in the axial direction of lubricated cylinder specimens within a rigid cylinder.

Even if both volumetric and deviatoric deformations are present, for natural rubber, the deviatoric stress usually is much smaller than the hydrostatic stress. This is due to a bulk modulus that is several orders of magnitude higher than the shear modulus.

Conversely, TDMs for low applied pressure, are more compressible than natural rubber. For this reason the values of compressibility in this range of pressure might be inaccurate. During the test the force was applied on top of the piston using a MTS810 test machine with a 500 kN load cell at a volume ratio rate $6.7 \cdot 10^{-3} s^{-1}$. Tests were performed on a set of three specimens for every density.

For rubber materials, the volumetric part of the strain energy function most commonly is assumed to be quadratic, which gives a linear relation between pressure and volume change. This is in good agreement with experimental data in the neighborhood of the identity $\mathbf{F} = \mathbb{1}$. However, rubber under large pressure allows for an appreciable volume change [8]. This can be seen by experimentally determined equations of states (EOS), relating the mean stress (the pressure) $\frac{1}{3}\operatorname{tr}(\sigma)$ to the relative volume change $\det \mathbf{F}$.

Considering the exponentiated Hencky energy(5.5), the analytical expression of the pressure $\frac{1}{3}\operatorname{tr}(\sigma)$ is in concordance with the classical Bridgman's compression data for natural rubber as reported in [8, page 497, Fig. 4.47] with $k = 2.5 \cdot 10^9\,\mathrm{Pa} = 2.5\,\mathrm{GPa}$.

Tabor [75] showed that the bulk modulus of rubber is of the order 1 GPa and found the value of the bulk modulus k to be about 2 GPa. Recently, Zimmermann and Stommel [84] found determined experimentally that k is of the order $k = 2.5$ GPa, which can be found in the literature as well (see e.g. [40]).

On the first view, certain threshold values seem unreachable by compression, unless an infinite amount of energy is spent. However, this impression is misleading: stresses and energy remain finite for any stretch $V \in \mathrm{PSym}(3)$. Therefore, in our model the assumption of limited chain extensibility is not needed.

In the neighbourhood of the identity $\mathbf{F} = \mathbb{1}$, the quadratic Hencky energy gives also good results, while in large compression the values obtained using the quadratic Hencky energy are not in agreement with the experimental data. Moreover, the EOS relation corresponding to the quadratic Hencky is not invertible for $\det \mathbf{F} > e$ and it is not able to predict the response for $\frac{1}{3}\operatorname{tr}(\sigma) > \frac{1}{e}$ [81].

TDMs show an important volume change up to a certain value of the pressure then there is a sharp increasing in stiffness. The value of the bulk modulus k before the stiffening is very small due to the presence of voids in the material then it increases reaching values similar to the rubber (Table III). For this reason a different form of the volumetric part of the strain energy is proposed (5.6) to take into account of the large non-linear response.

Using the experimentally determined equation of states, relating the pressure $\frac{1}{3}\operatorname{tr}(\sigma)$ to the relative volume change $\det \mathbf{F}$ we have:

$$\frac{1}{3}\operatorname{tr}(\sigma) = \frac{d}{dt}\left[\frac{\kappa}{2\,\widehat{k}}\, e^{\widehat{k}\,[(\log t)]^2} + \frac{\kappa_1}{m\,\tilde{k}}\, e^{\tilde{k}\left(|\log t|^2\right)^{\frac{m}{2}}}\right]_{t=\det\mathbf{F}} \tag{5.22}$$

$$\frac{1}{3}\operatorname{tr}(\sigma) = \left[\kappa\, e^{\widehat{k}(\log\det\mathbf{F})^2} \cdot \left(\frac{\log\det\mathbf{F}}{\det\mathbf{F}}\right)\right] + \left[\kappa_1\, e^{\tilde{k}\left[|\log\det\mathbf{F}|^2\right]^{\frac{m}{2}}} \cdot \left(\frac{|\log\det\mathbf{F}|^{m-2}\cdot\log\det\mathbf{F}}{\det\mathbf{F}}\right)\right] \tag{5.23}$$

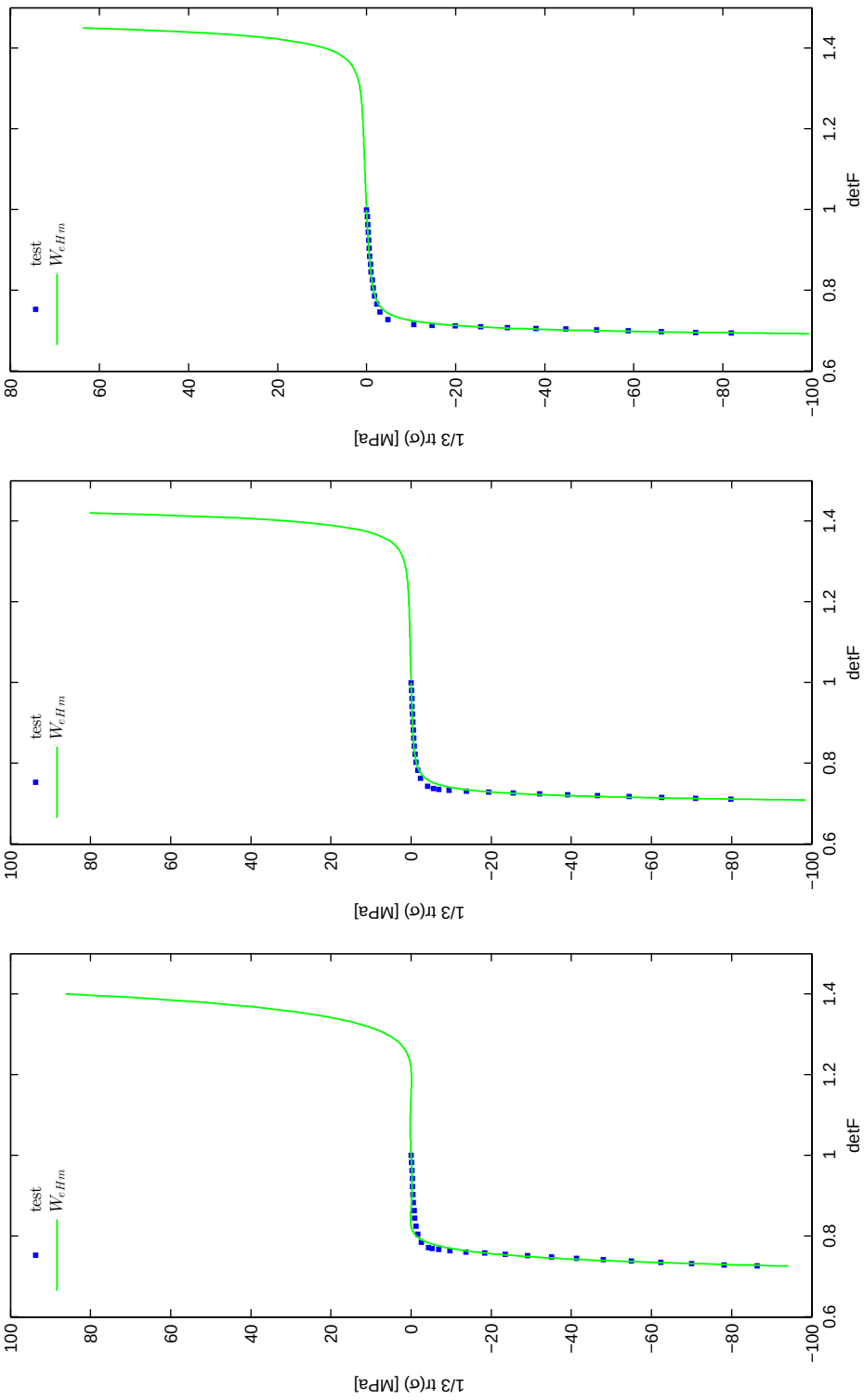

(a) 500 (b) 600 (c) 800

Figure 5.14: Volumetric stress corresponding to equation (5.23) and experimental tests for different densities.

The force deflection plot for each of the tested materials is approximately linear up to a certain value of force, then the stiffness increases holding it to an almost constant value.

5.5 Parameter identification hyperelastic model

The parameter estimation was performed using the non-linear least square (NLS) optimization method to minimize the residuals. The difficulties in a NLS problem is to find a unique set of optimal parameters.

Several numerical algorithms have been used in literature to solve NLS problems [10, 4], they are usually a modification of the Newton method and require an initial guess for the solution. Therefore, when some stopping criteria are met, the iterative technique furnishes an optimal solution.

In this paper we use the function *lsqcurvefit* in the optimization Toolbox of Matlab [54] (See Appendix B). To be able to fit several different sets of data together we use the same modification used by Ogdena et al [67] in which the classical minimization problem is given by:

$$\min_{\mathrm{p}} \left(||\mathbf{P}_{\mathrm{comp}}\left(p\right) - \tau_{\mathrm{comp}}||_2^2 + ||\mathbf{P}_{\mathrm{shear}}\left(p\right) - \tau_{\mathrm{shear}}||_2^2 \right) \tag{5.24}$$

Where $\mathbf{P}_{\mathrm{comp}}$ is the vector of the model stress values which depends on the model parameters p and τ_{comp} being the experimental values of the compression stress while $||\bullet||$ is the standard $l_2 -$ norm. The same for $\mathbf{P}_{\mathrm{shear}}$ and τ_{shear} except that the number of data may be different.

We choose as initial guess the value of the parameters obtained by previous experiment on the TDM (Table III). We imposed positive values as lower bound on the parameters, moreover we choose the one allowed by the mathematical theory.

Table 5.2: Initial guess for parameter identification procedure

$$\widehat{\Psi}_{\mathrm{eHm}}(\mathbf{U}) := \frac{\mu}{k}\, e^{k\,||\,\mathrm{dev}_3 \log \mathbf{U}||^2} + \frac{\kappa}{2\,\widehat{k}}\, e^{\widehat{k}\,[\mathrm{tr}(\log \mathbf{U})]^2} + \frac{\kappa_1}{m\,\tilde{k}}\, e^{\tilde{k}\left([\mathrm{tr}|\log \mathbf{U}|^2]\right)^{\frac{m}{2}}}$$

Material	μ	k	κ	$\widehat{k}$	κ_1	$\tilde{k}$	m
500	0.38	–	6.70	–	297	–	–
600	0.42	–	9.00	–	315	–	–
800	1.00	–	7.90	–	281	–	–

*Parameters obtained from [57]

Table 5.3: Parameters exponentiated-Hencky energy function

$$\widehat{\Psi}_{\mathrm{eHm}}(\mathbf{U}) := \frac{\mu}{k}\, e^{k\,||\,\mathrm{dev}_3 \log \mathbf{U}||^2} + \frac{\kappa}{2\,\widehat{k}}\, e^{\widehat{k}\,[\mathrm{tr}(\log \mathbf{U})]^2} + \frac{\kappa_1}{m\,\tilde{k}}\, e^{\tilde{k}\left([\mathrm{tr}|\log \mathbf{U}|^2]\right)^{\frac{m}{2}}}$$

Material	μ	k	κ	$\widehat{k}$	κ_1	$\tilde{k}$	m
500	0.29	0.20	1.40	0.13	116	231	4
600	0.46	0.20	2.80	0.13	647	1879	6
800	1.48	0.20	4.40	0.13	404	1313	6

Chapter 6

Viscoelasticity

6.1 Theory of finite viscoelasticity

Many materials simultaneously exhibit elastic and viscous material behavior. Indeed TDM when loaded with time dependent external forces reach a state which is a superposition of two different response: a time independent, long term, behavior opposed to a time dependent, short term, behavior.

A general approach, introduced by equation in terms of thermodynamic state-variables: the internal energy is expressed as function of both the current values of strain (stress) and the so-called internal state variables [20] .

Rate effects are introduced through evolution equations, which usually relate time rates-of-change of internal variables to thermodynamic forces, which are the derivatives of the internal energy with respect to each internal variable. Simo proposed a costitutive equation based on internal variable formulation which ha provided a staring point for many successive works ([27],[36],[86]).

In Simo's approach, the internal energy is split according to the multiplicative decomposition of the deformation gradient into dilatational and volume preseving parts.

An advantage of the state-variable formulations is that, in contrast to the other approaches, it is not restricted to isotropic responses. Anisotropic effects could be easily taken into account, e.g., by introducing state variables depending upon fiber orientations as in Holzapfel and Grasser [38].

Based on Green and Tobolsky [31], Lubliner [51] split the free energy of a viscoelastic solid in two parts : the first part describing the rate-independent material behaviour and the second incorporating time-dependent effects. He further assumed a multiplicative decomposition of the deformation gradient into elastic and inelastic parts and interpreted Green and Tobolsky's internal strain as inelastic strain. Although in the framework of elastoplasticity the decomposition of the deformation gradient, into elastic and plastic terms, relies on clear physical assumptions, there is a lack of evidence in the context of viscoelasticity. However, it has been successfully applied in many nonlinear constitutive equations.

An important point in developing models of this form is the choice of the evolution equation for the internal variables.

In the theory of linear viscoelasticity, which is only valid for small deformations and small perturbations away from thermodynamic equilibrium, one can take either the "over-stress" or the inelastic strain as an internal variable. Due to the fact that the relationship between these two is linear and additionally all stress and strain measures coincide for small deformations, the structure of the evolution equation is evident [28].

In the case of large deformations, however,the choice of internal variables and evolution equations is not so evident and not unique. One of the first finite element implementations for such a theory was given by Simo [73]. In contrast to most works, however, he chose the over-stress as the internal variable.

We postulate the existence of a non-equilibrium free energy leads to a non-equilibrium stress which can be derived from a potential.

The advantage of the presented formulation is that it can be easily implemented in a finite element code. This is due to the fact that the evolution equation of finite viscoelasticity has the same structure as the one used in finite deformation associative elastoplasticity and viscoplasticity. Thus, the time integration can be carried out by the exponential mapping algorithm, which has been used in computational elastoplasticity and viscoplasticity. In this context, it is assumed that the deformation gradient can be decomposed as

$$\mathbf{F} = \mathbf{F}_e \mathbf{F}_i \tag{6.1}$$

The inelastic term $\mathbf{F}_i$ introduces an intermediate configuration. However, the decomposition (6.1) is a conceptual one and cannot be determined experimentally since neither $\mathbf{F}_e$ nor $\mathbf{F}_i$ are observable quantities.

The decomposition (6.1) is generally followed by the ansatz on the internal energy for which Ψ is split as the sum of an equilibrium part and an overstress term, i.e.,

$$\Psi = \Psi_{EQ}(\mathbf{C}) + \Psi_{NEQ}(\mathbf{C}_e) \tag{6.2}$$

Here C is the right-Cauchy-Green strain tensor and $\mathbf{C}_e = \mathbf{F}_e^T \mathbf{F}_e$ is the elastic strain in the intermediate configuration. By applying the Coleman and Noll procedure [19] i.e., by restricting the form of the stress tensor in such a way that the Clausius-Plank inequality is verified for every admissible process , the Piola symmetric stress tensor is:

$$\mathbf{T} = \mathbf{T}_e + \mathbf{T}_i \tag{6.3}$$

where $\mathbf{T}_e$ is the equilibrium stress and $\mathbf{T}_i$ is the overstress. In particular, for an internal of the form (6.2), the following relations between $\Psi_{EQ}, \Psi_{NEQ}, \mathbf{T}_e$ and $\mathbf{T}_i$ are valid:

$$\mathbf{T}_e = \frac{\partial \Psi_{EQ}}{\partial \mathbf{C}}, \qquad \mathbf{T}_i = \frac{\partial \Psi_{NEQ}}{\partial \mathbf{C}_i} \tag{6.4}$$

Equation (3.7) is not sufficient to determine the behavior of the material. In order to complete the description, the evolution equations (or flow rules) of the internal variables $\mathbf{F}_e$

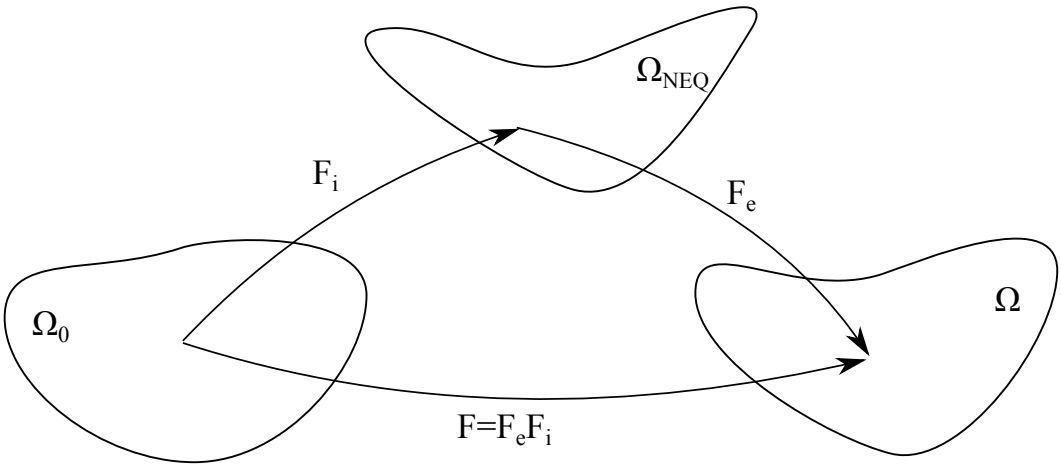

Figure 6.1: The intermediate configuration Ω_{NEQ} is obtained from the deformed configuration Ω by destressing to zero stress. The viscoelastic deformation gradient is decomposed into its elastic and inelastic part, such that $\mathbf{F} = \mathbf{F}_e\mathbf{F}_i$.

and/or $\mathbf{F}_i$, which determine the way viscoelastic processes evolve, must be defined. Often the evolution equations are suitably defined to be efficient with respect to time integration algorithms

6.2 Rheological model for TDM

Here we assume the existence of two viscous mechanism associated to the material: intermolecular resistance and grain interactions.

The first is associated with a Maxwell element including a non-linear spring (A) while the second is associated to a Maxwell element in which a linear spring is included (B).

The choice of modeling the interaction between the rubber particle inside the TDM with a linear law is due to the presence of the binder at the grain interface. The binder acts as an internal constrain allowing only normal contact interaction in between the grains. For this reason no relative rotation neither sliding is allowed in between the grains. A one dimensional rheological model is presented in Figure 6.2.

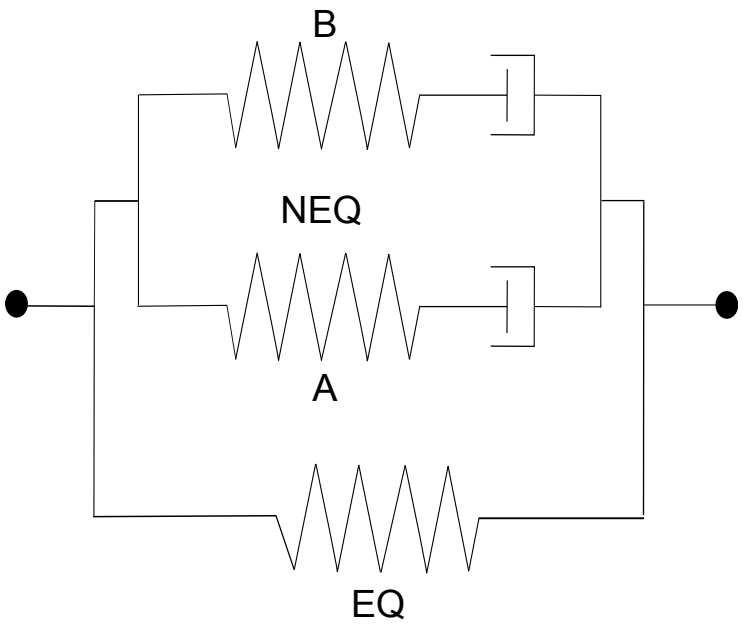

Figure 6.2: One dimensional rheological model for rate-dependent behavior of TDM

If we consider for each viscous mechanism a set of internal variable $\mathbf{F}_i^k$ $(k = A, B)$ that can be viewed as the deformation gradient associated with each the dashpot. we can write the total free energy as:

$$\Psi_{\text{eHm}} = \Psi_{EQ}(\mathbf{C}) + \Psi^A_{\text{NEQ}}(\mathbf{C}^A_e) + \Psi^B_{\text{NEQ}}(\mathbf{C}^B_e) \tag{6.5}$$

Where Ψ_{EQ} represents the strain energy in the "time infinity" spring and Ψ^k_{NEQ} the strain energy in each Maxwell element associated to the "elastic" right Cauchy strain tensor $\mathbf{C}^k_e = [\mathbf{F}^k_e]^T \cdot \mathbf{F}^k_e$.

For most of metals and polymer based materials, the volumetric deformation is purely elastic and the viscous effects are restricted to the isochoric component of the deformation. Hence the strain energy for the Maxwell elements can be written as:

$$\Psi^A_{\text{NEQ}}(\mathbf{C}^A_e) = \frac{\mu_A}{k_A}\, e^{k_A\, ||\, \text{dev}_3 \log \mathbf{C}^{\text{A}}_{\text{e}}||^2} \tag{6.6}$$

$$\Psi^B_{\text{NEQ}}(\mathbf{C}^B_e) = \mu_B\ ||\, \text{dev}_3 \log \mathbf{C}^{\text{B}}_{\text{e}}||^2 \tag{6.7}$$

The fundamental thermodynamic requirement, also called the internal dissipation inequality, can be expressed as:

$$-\,\dot{\Psi} + \frac{1}{2}\,\mathbf{S}\ :\ \dot{\mathbf{C}}\ \geq\ 0. \tag{6.8}$$

If we substitute the assumed functional form (6.5) for the free energy into equation (6.8) and apply the standard Coleman and Noll argument we obtain:

$$\mathbf{S} = \ 2\,\frac{\partial\,\Psi_{EQ}}{\partial\,\mathbf{C}} + 2\,[\mathbf{F}^k_i]^{-1}\cdot\ \frac{\partial\,\Psi^k_{NEQ}}{\partial\,\mathbf{C}^k_e}\ \cdot\,[\mathbf{F}^k_i]^{-T} \tag{6.9}$$

In which the stress is additively decomposed into an equilibrium and a nonequilibrium contribution. From the Coleman and Noll argument we have that the evolution equations for the internal viscous part of the deformation must satisfy the dissipation inequality:

$$2\,\frac{\partial\,\Psi^k_{EQ}}{\partial\,\mathbf{C}^k_e}\;:\left(\mathbf{C}^k_e\cdot\mathbf{l}^k_i\right)\;\geq\;0, \tag{6.10}$$

Where $\mathbf{l}^k_i=\dot{\mathbf{F}}^k_i\cdot[\mathbf{F}^k_i]^{-1}$ is the inelastic part of the velocity gradient $\mathbf{l}^k=\dot{\mathbf{F}}^k\cdot[\mathbf{F}^k]^{-1}$.

According to (6.10) is possible to have an evolution equation that will always satisfy the 2nd Law of Thermodynamics. This is done choosing an expression for $\mathbf{l}^k_i$ such that (6.10) becomes a positive definite quadratic form.

If we assume isotropy the expressions above can be rearranged and expressed entirely in the spatial configuration of the body which is convenient from a computational point of view. If we consider Ψ_{EQ} and Ψ^k_{NEQ} isotropic tensor functions of $\mathbf{C}$ and $\mathbf{C}^k_e$, then the residual inequality can be written as:

$$-\,\tau^k_{NEQ}\;:\;\frac{1}{2}\left(\mathcal{L}_v\,\mathbf{b}^k_e\right)\cdot[\mathbf{b}^k_e]^{-1}\geq\;0 \tag{6.11}$$

Where $\mathbf{b}^k_e=\mathbf{F}^k_e\cdot[\mathbf{F}^k_e]^T$ is elastic relaxing left Cauchy-Green tensor and $\mathcal{L}_v\,\mathbf{b}^k_e$ is its Lie derivative along the velocity field of the material motion.

Finally the evolution equation chosen is:

$$\frac{1}{2}\,\mathcal{L}_v\,\mathbf{b}^k_e\cdot[\mathbf{b}^k_e]^{-1}=[\mathcal{V}^k]^{-1}:\tau^k_{NEQ} \tag{6.12}$$

where $[\mathcal{V}^k]^{-1}=\hat{\mathcal{V}}^{-1}(\mathbf{b}^k_e)$ is an isotropic rank four tensor which has to be positive definite to satisfy (6.12).

In this case $[\mathcal{V}^k]^{-1}$ takes the form:

$$[\mathcal{V}^k]^{-1}=\frac{1}{2\,\eta^k_D}\left(\mathbb{1}^4-\frac{1}{3}\mathbb{1}\otimes\mathbb{1}\right). \tag{6.13}$$

Here $\mathbb{1}^4$ is the fourth order symmetric identity tensor, while η^k_D represents the deviatoric viscosity. It is possibly deformation dependent and has the following properties:

$$\eta^k_D=\hat{\eta}^k_D\left(\mathbf{b}^k_e\right)>0, \qquad\qquad \hat{\eta}^k_D\left(\mathbf{1}\right)=\eta^k_{DEQ} \tag{6.14}$$

Inserting (6.13) in the evolution equation (6.12), we obtain:

$$\mathcal{L}_v\,\mathbf{b}^k_e\cdot[\mathbf{b}^k_e]^{-1}=\frac{1}{\eta^k_D}\,\mathrm{dev}[\tau^k_{NEQ}]. \tag{6.15}$$

To solve the nonlinear evolution law Reese and Govindjee [69] used an integration algorithm, previously proposed by different authors (insert reference), in which the material derivative of $\mathbf{b}^k_e$ is split into an elastic predictor E and an inelastic corrector I.

$$\dot{\mathbf{b}^k_e}=\overline{\left(\mathbf{F}\cdot[\mathbf{C}^k_i]^{-1}\cdot\mathbf{F}^T\right)}^{\cdot}=\underbrace{\mathbf{l}\cdot\mathbf{b}^k_e+\mathbf{b}^k_e\cdot\mathbf{l}^T}_{\mathrm{E}}+\underbrace{\mathbf{F}\cdot\overline{\left([\mathbf{C}^k_i]^{-1}\right)}^{\cdot}\cdot\mathbf{F}^T}_{\mathrm{I}}. \tag{6.16}$$

The operator split, which can be also interpreted as a total motion predictor and a viscous corrector algorithm, first assumes the material time derivative of $\mathbf{C}_i$ equal to zero and the elastic part evolves.

$$(\mathbf{b}_e)_{trial} = (\mathbf{F})_{t=t_n} \cdot \left([\mathbf{C}_i^k]^{-1}\right)_{t=t_{n-1}} \cdot (\mathbf{F})_{t=t_n}^T \tag{6.17}$$

In the inelastic corrector step, the spatial gradient velocity is set to zero, which leads to $\mathcal{L}_v \mathbf{b}_e^k = \dot{\mathbf{b}}_e^k$ (see [69]).

$$\dot{\mathbf{b}}_e^k = -\left(2[\mathcal{V}^k]^{-1} : \tau_{NEQ}^k\right) \cdot \mathbf{b}_e^k. \tag{6.18}$$

Equation (6.18) subjected to the initial conditions of $\left(\mathbf{b}_e^k\right)_{trial}$ from the predictor phase, can be integrated to first order using the exponential map and an Euler method to give:

$$(\mathbf{b}_e)_{t=t_n} = \exp\left(-\frac{\Delta t}{\eta_D^k} \operatorname{dev}[\tau_{NEQ}^k]\right) \left(\mathbf{b}_e^k\right)_{trial} \tag{6.19}$$

This expression gives an implicit relation for $(\mathbf{b}_e^k)_{t=t_n}$. It can be solved easily using standard iterative methods (see Appendix C).

Note that by the isotropy assumption $\mathbf{b}_e^k$ and $(\mathbf{b}_e^k)_{trial}$ share the same set of eigenvectors.

6.3 Simple Shear Test

To study the rate-dependence, TDM specimens were subjected to cyclic processes with constant strain rates. The strain rates applied in these tests have been calculated in terms of the initial dimension of the specimen measured just before the respective test.

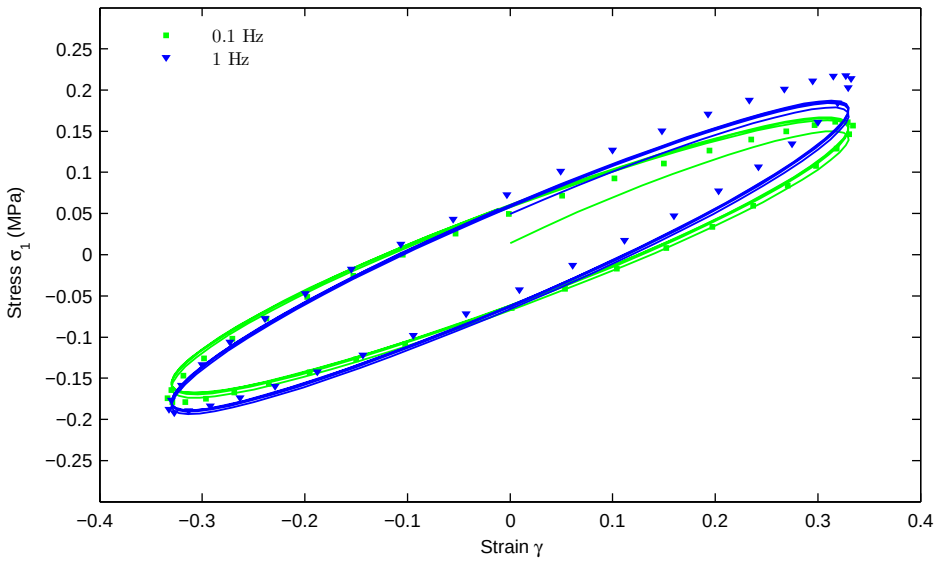

Figure 6.3: Comparison between cyclic shear tests (dot line) and exponentiated Hencky energy Ψ_{eHm} (solid line), equation (5.21), for different frequencies for TDM 500.

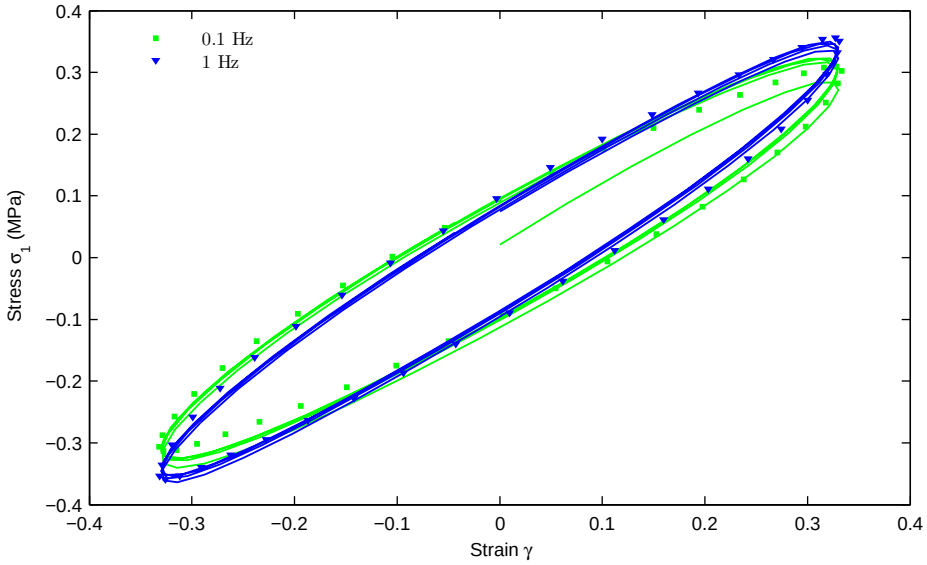

Figure 6.4: Comparison between cyclic shear tests (dot line) and exponentiated Hencky energy Ψ_{eHm} (solid line), equation (5.21), for different frequencies for TDM 600.

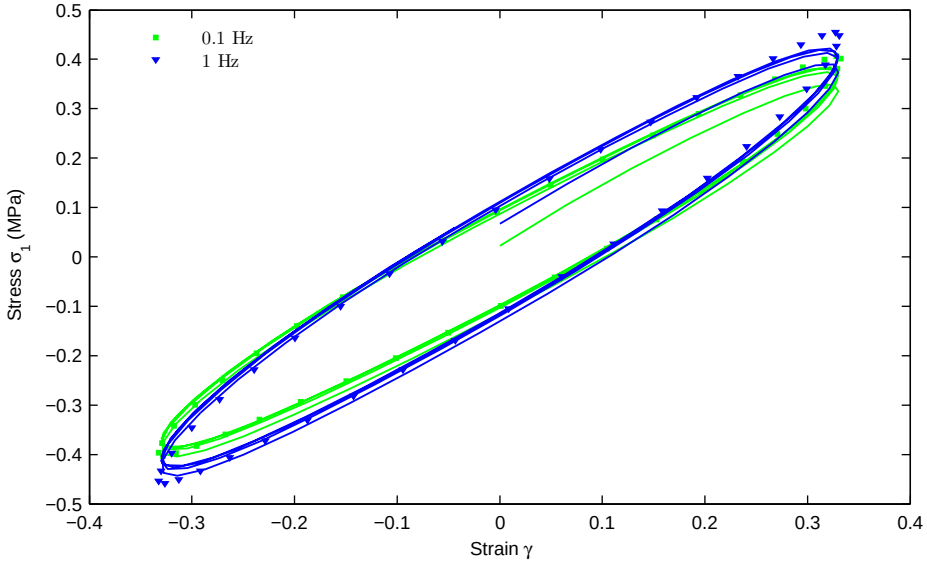

Figure 6.5: Comparison between cyclic shear tests (dot line) and exponentiated Hencky energy Ψ_{eHm} (solid line), equation (5.21), for TDM 800.

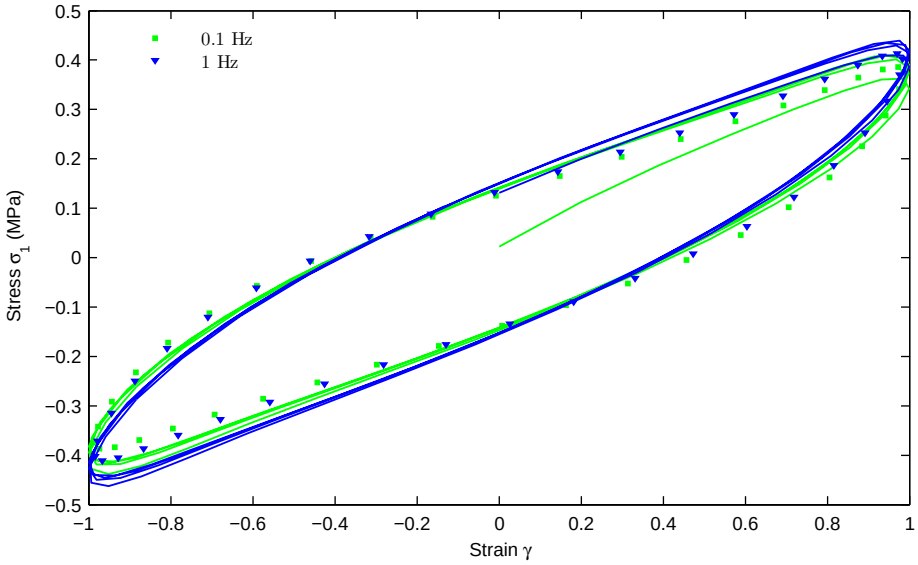

Figure 6.6: Comparison between cyclic shear tests (dot line) and exponentiated Hencky energy Ψ_{eHm} (solid line), equation (5.21), for different frequencies for TDM 500.

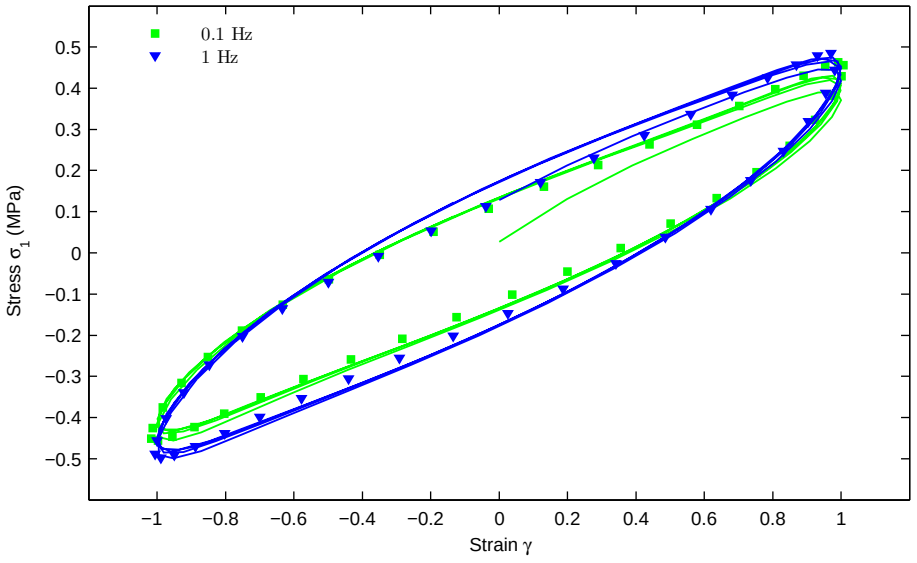

Figure 6.7: Comparison between cyclic shear tests (dot line) and exponentiated Hencky energy Ψ_{eHm} (solid line), equation (5.21), for different frequencies for TDM 600.

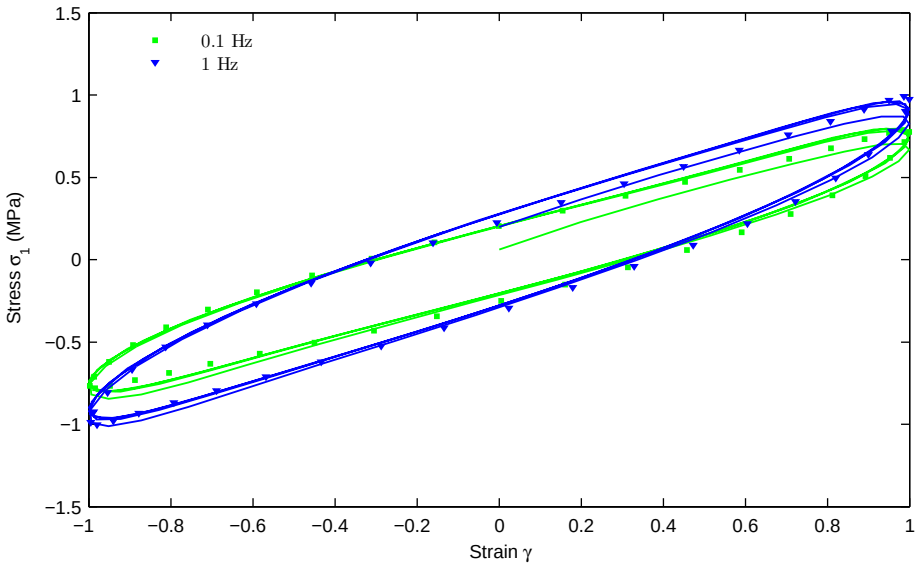

Figure 6.8: Comparison between cyclic shear tests (dot line) and exponentiated Hencky energy Ψ_{eHm} (solid line), equation (5.21), for TDM 800.

Figure 6.6 and Figure 6.4 present the stress–strain responses as obtained from TDM under cyclic shear deformations.

Two tests were conducted in shear, each with a different frequency rate. A comparison of the stress responses indicates a strongly pronounced amplitude-dependent behavior. In addition, the presence of hysteresis along with permanent set is visible.

Moreover the material shows a weak dependence of the response on the strain rates.

6.4 Parameter identification viscoelastic model

For modeling purposes, a common choice is to assume for Ψ_{NEQ} an hyperelastic constitutive equation, here we follow the same idea also because of the good mathematical properties of the exponentiated-Hencky energy we work with.

The fit is done only on shear test which is sufficient to find all the parameters since we assume that volumetric stress does not play a role in the viscous behavior of the material. Following the same procedure used for the hyperelastic function in section 5.5 the minimization problem arising in this section is:

$$\min_{\mathrm{p_A},\mathrm{p_B}} || \left(\mathbf{P}_{\mathrm{A}}\left(p_A\right) + \mathbf{P}_{\mathrm{B}}\left(p_B\right)\right) - \tau_{\mathrm{NEQ}} ||_2^2 \tag{6.20}$$

Where $\mathbf{P}_{\mathrm{A}}$ and $\mathbf{P}_{\mathrm{B}}$ are the stresses in the two Maxwell elements 6.2 and τ_{NEQ} is the values of the stress for the dynamic tests.

The material showed both frequency and amplitude dependency. In the following Tables the values of the parameters for different amplitude are shown. The frequency dependency in the range of frequencies tested can be neglected.

Table 6.1: Parameters for the non equilibrium part of the exponentiated-Hencky energy function for deformation up to 30%

Material	μ_A	k_A	μ_B	η_D^A	η_D^B
500	0.2	2.2	0.35	12	2
600	0.45	2.2	0.5	12	2
800	0.6	2.2	0.6	15	1

Table 6.2: Parameters for the non equilibrium part of the exponentiated-Hencky energy function for large deformations

Material	μ_A	k_A	μ_B	η_D^A	η_D^B
500	0.08	2.2	0.35	12	2
600	0.08	2.2	0.5	12	2
800	0.15	2.2	0.6	15	1

Chapter 7

The problem of vibration induced by railway track

Trains moving along railway tracks are sources of ground-borne vibrations propagated into the surrounding ground. The propagating path of the vibration depends on the ground composition it affects the amplitude and velocity of the propagating vibration. Once the vibrations reach the nearby building they can cause structural damage or disturb sensitive equipment.

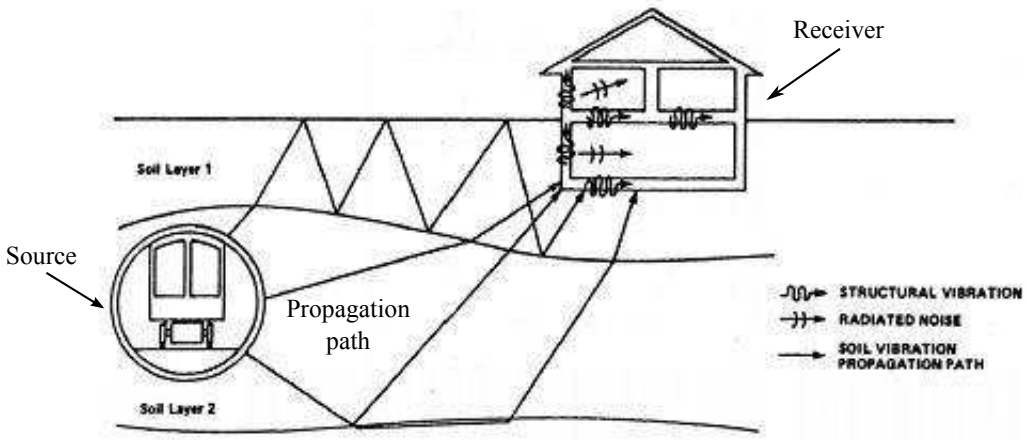

Figure 7.1: Solid shaped mat

Moreover, noise and vibration emission remains a relevant impact factor and they produce complaints from people living above underground lines. Propagation of vibrations generated from moving trains in tunnels into the surrounding ground and to nearby buildings is complex and depends on several factors.

It is common to divide the generation and propagation of train-induced vibrations into three parts (Figure 7.1):

- The source;
- The propagation path;
- The receiver;

During the propagation from the source to the receiver the waves are attenuated in various ways, but amplification may also occur. This aspect is of great interest when dealing with train-induced vibrations and its effects on the surrounding (humans or buildings).

Vibrations are generated at wheel-rail interface. Trains weight is transmitted from wheel to rail and redistributed by the rail, track structure and ground, this load can be defined as static load. When the train moves on the track this force moves along with the train. The static load become a dynamic load due to differences at various parts of the train-track structure system, such as:

- irregularities on the surface of the rail and wheel;
- variations in the support structure beneath the rail

Dynamic loads generate vibrations that are propagated from the track into the surrounding ground. There are many parameters influencing the level and characteristics of train-induced vibrations [23] such as:

- Vibrations induced by the track structure response:

  axle load (weight of train and spacing of wheel axles),

  geometry and composition of the train (type, cargo, length),

  speed of train,

- Wheel-rail interface:

  wheel defects (eccentricity, imbalance, flats, unevenness),

  unsteady riding (bouncing, rolling, pitching, properties of bogie and motor),

  acceleration and deceleration of the train,

- Irregularities on the rail:

  quality of the rail (corrugations, corrosion, unevenness, waviness, joints),

  curves and tiling track (centrifugal forces),

- Variations in support structure:

  geometry and stiffness of the support structure ,

  frost.

As mentioned above, the load generated by trains is due to the sum of a static load, which is the weight of the train, and a dynamic load, generated by irregularities on wheel-rail interface. The dynamic and static forces cause stress waves propagating into the ground below the track. The generated stress waves all have different characteristics depending on where they are generated, i.e. vehicle, wheel, rail, or substructure.

The typical frequency spectra of the vibrations generated by trains in tunnels are from 4 Hz up to a few thousands Hz [30]. Typically, there is one or two vibration peaks at different frequencies where the acceleration levels can reach about 80 to 90 dB.

The amount of vibrations that is transmitted into the building depends on the coupling between the ground and the foundation. Usually there is a reduction (coupling loss) of the vibrations at the transmission from the ground to the building. Slabs-on-grade are in contact with the underlying soil and will be subjected to similar vibrations as the ground, and the coupling loss is therefore determined to be 0 dB for frequencies lower than the resonance frequency of the slab. The coupling loss for lightweight buildings is also determined to be 0. For the other foundations types, the coupling loss varies between 2 and 15 dB depending on frequency and foundation type. For a building supported directly on rock the coupling loss is 0 [48].

The reduction of transmitted vibrations between the ground and building is larger for vertical oscillations than horizontal oscillations since the building is weaker in the horizontal direction. The natural frequency in ordinary dwellings is normally lower than 10 Hz, which is in the same range as for loose soils.

Train-induced vibrations are within that range and thus resonance effects are prominent. Once the vibration has reached the foundation they propagate through the building where the different parts of the building will damp or magnify the vibrations.

Train-induced vibrations can cause damage to buildings in the form of:

- strain
- natural vibrations
- settlements

Strain can be caused by deflection from the train if the track is close to the building. It can also be caused by the stress wave propagating along the ground surface.

As mentioned above, if the train-induced vibrations have a frequency that is near the natural frequency of the building, resonance of the building may arise. The vibrations have to have a reasonable duration for resonance to occur and can generally only be caused by freight trains that are uniformly loaded.

For certain soils train induced vibrations can cause and/or accelerate settlements. Since there are many factors that can contribute to settlements it is usually difficult to determine what part the vibrations is responsible for. Train-induced vibrations can in extreme cases trigger slides, but is never the sole cause.

For old buildings modifications made, e.g. creating opening in walls, together with deterioration of the strength can cause damage. Failure in newer buildings is often caused by unauthorized modification or faults. Consequently, it is not likely that train-induced vibrations cause damage to buildings. If a building is damaged from train-induced vibrations it is usually caused in combination with other factors, e.g. alteration of ground water level, which would have caused damage to the building regardless of the presence of vibrations. The vibrations merely accelerate the process. The damage potential of buildings depends on the age, size, fatigue properties, structural resonance, and type of construction.

The vibration levels required to cause damage to buildings are generally much higher than what humans consider tolerable. Nevertheless, people commonly accuse vibrations to cause cracks within their dwellings although the vibration levels are rarely high enough to be the cause. Many people associate noise with vibrations, and when hearing loud noises this makes them inspect their properties.

There are several measures to reduce vibration generated by trains moving in tunnels. The different measures can be applied at any position along the propagating path, i.e. either at the source, along the path, or at the receiver. The most common measures that can be applied at the source in order to reduce emissions from train traffic on open tracks as well as in tunnels are [23]:

Rail surface

The quality of the surface of the rail is very important with regard to train induced vibration, but also for the comfort of the passengers. Various irregularities, such as short and long pitch corrugations, insulating joints, turnouts, etc. will appear along the rail from the numerous passing of trains.

Kazamaki and Watanabe observed that there was a difference of 10 dB between new rails and wheels compared to corrugated rails and wheels with flats from normal service wear [6]. In order to reduce the vibrations it is therefore important to maintain the rail in good condition, or even use high-strength steel instead. Thus, having a good maintenance program for the rail can be seen as an important and a good measure to reduce vibrations [22].

Rail pads

Rail pads, sometimes also known as “sole” plates or pads, are placed between the rail and the (concrete) sleeper. They are usually made of rubber and their main function is to reduce fatigue cracking of the sleepers, but they are also believed to have a damping effect on vibrations.

The measure here is either to install the pads or to use pads with a different stiffness. For ballasted tracks this measure has been determined to be ineffective in the reduction of vibrations [34].

Rail fastenings

Rail fasteners are used to keep the rail at its designated position on the sleeper. There are various variants that are optimal for different conditions.

Using highly elastic (flexible) rail fastenings will permit larger deflections of the rail beneath the wheel which reduces the mechanical impedance of the superstructure and hence the vibrations [22].

Using flexible fastenings reduces the vibrations between 30 to 50 Hz, where a higher reduction is observed at 50 Hz (about 6 to 10 dB).

Ballast thickness

The main purpose of the ballast is to distribute the pressure from the track. It also provides a foundation for the sleepers holding them in position. Moreover, it has a draining purpose.

The normal height for the ballast is about 0.3 m. An increase of the thickness has no measurable effect [34], while a decrease in thickness leads to deterioration of the attenuation [22].

The Norwegian Geotechnical Institute observed that an increase of the ballast thickness (1 m) increased the attenuation; however, it was believed that the thicker structure gave a greater load distribution and the reduction was concluded not to be caused by damping solely. It has also been observed that newly tampered ballast generates greater attenuation than ballast not tampered for a long time.

This, along with the importance of a smooth rail surface, implies that maintenance is an important aspect of reduction of train-induced vibrations.

Ballast mats

Ballast mats, or sub-ballast mats, are, as the name implies, elastic layers that are placed beneath or inside the ballast bed.

Ballast mats (thickness up to 80 mm) are considered to have high efficiency to attenuate vibrations within the range 16 to 50 Hz where a reduction as high as 20 dB can be reached at 50 Hz [22]. Kazamaki and Watanabe [6] reported a reduction of 5 to 8 dB due to the use of ballast mats. One type of ballast mat applied on concrete base generated reduction of about 10 dB for frequencies above 40 Hz.

Placing the ballast mat higher up within the ballast results in higher attenuation. If the thickness of the ballast is increased from 0.3 to 0.6 m in combination with sub-ballast mat, a reduction of 4 dB can be added. It should be noted that the increase in ballast only have an effect if there is a sub-ballast mat installed [22].

Mass-spring system

Floating-slab-system, is the most effective measure for train-induced vibrations in tunnels [34].

The principle idea is to have a linear harmonic oscillator that has a very low natural frequency. Usually the oscillator is a heavy concrete slab that is isolated from the tunnel invert by rubber bearings or steel springs. A floating slab should have as low natural frequency as possible in order to attenuate the vibrations to as large extent as possible.

It is not practically possible to have a natural frequency lower than 5 Hz; neither should it exceed 14 Hz [22]. Normally the natural frequency is between 8 to 12 Hz.

Hemsworth [34] reported 10 dB attenuation at 16 Hz and 25 dB at 125 Hz, while Kazamaki and Watanabe (1975) reported attenuation levels between 15 to 21 dB. However, Hunt [42] showed, with the aid of numerical analysis, that if the natural frequency of the floating-slab system is not low enough, the attenuation effect would be diminishing. Since most tunnels are unique the required attenuation varies and the slabs are designed to fit with the cross-section of the tunnel. The slabs require a height of 0.8 to 1.4 m and can weigh between 4000 and 9000 kg/m.

Floating slabs can be used for tracks both with and without ballast. A negative aspect with floating-slab-systems is that the system is more expensive than the other systems used to reduce vibrations. It is important that the bearings (or springs) can handle the load efficiently.

7.1 Case of study optimization of railway mat for light-weight line

The goal of this study is to find an optimal solution to reduce the axial stiffness of the TDM rubber mat produced by Isolgomma srl.

The need to expand the application of TDM to light rail systems where the loads are lower than traditional railway system has pushed the need to find a solution where the stiffness of the materials used is lower.

In this section the new material model is not used since is not already implemented in any Finite Element software. Optimization procedure regarding TDMs is very much influenced by the production technology, this makes the problem over-constrained. For these reasons a trial and error procedure is used.

Starting from a simple and easy to produce shape changes are made in order to improve the performance, at every step the analysis are run and solution to implement the performance in the next step are implemented. The procedure converged to a good solution in few steps. The new shape are first tested with static load and then the simulation are run with dynamic ones.

7.2 Mechanical test on elastomeric mats for railway track

UNI 11059 [79] is applied for elastic mats in new railway tracks or as an underballast element or as an under concrete slab element.

The elastomeric mat is designed to reduce vibration induced by railway traffic, it has constant thickness and it has the following characteristics:

- One dimension (the thickness h) is significantly smaller than the other two dimensions (the longitudinal one d_l and the transversal one d_t):

$$\frac{\sqrt{\frac{d_l \cdot d_t}{\pi}}}{h} \geq 10 \tag{7.1}$$

- During the useful life of the railway line loads are orthogonally applied on the mat surface. Two categories of tests are considered.

- Characterization tests that include:

  Static tests;

  Simulation tests (as a function of train speed);

  Forced dynamic tests;

  Dynamic tests of free oscillations

- Performance tests that include:

  Permanent load tests;

  fatigue tests;

  frost strength tests with water;

  atmospheric conditions strength tests;

  adequacy of mats to be put along lines;

  geometric stability of mats.

In the standards the following test loads are considered:

- Nominal initial load (σ_0) it always constantly acts on the railway line and it is produced by the weight of the rack on the elastomeric mat. It approximately assumes values in the range of $0.07 - 0.1MPa$

- Nominal railway load (σ_f) it consists of the accidental load and corresponds to the weight of the train that runs on the line. The standard gives this component as a function of the railway track and of the vehicle.

- Nominal dynamic railway factor (γ_d) it is an amplification factor of the nominal railway load and depends on the railway track type and conditions, on the railway track type and conditions, on train and on dynamic interaction track-train. It varies from 20% to 50%.

Static tests are performed with the application of a slow load. It starts to zero value and increases with linear pattern until its maximum value: three cycles are considered.

Each cycle last two minutes: the first cycle and the second one help to set the specimen, while the mechanical parameters are derived by the third one. The maximum test load is given:

$$\sigma_{max} = \sigma_0 + (1 + \gamma_d) \cdot \sigma_f \tag{7.2}$$

The specimen dimensions for thickness smaller than 50 mm the dimensions of specimens must to be greater than 30 cm x 30 cm and for thickness greater than 50 mm their dimensions depend on the thickness and they must to be greater than (6h) x (6h) in which h is the nominal thickness. The evaluation of the static stiffness is obtained by the following relation:

$$K_{qs} = \frac{\sigma_1 - \sigma_0}{\delta_1 - \delta_0} = \frac{\sigma_f}{\delta_1 - \delta_0} \tag{7.3}$$

In which $\sigma_1 = \sigma_0 + \sigma_f$ and δ_1 is the displacement for the nominal initial load δ_0 is the correspondent displacement and σ_0.

Regarding forced dynamic tests they involve the application of a load $\sigma(t)$ that consists of a static component σ_s and of a dynamic component σ_d that varies sinusoidally with the time:

$$\sigma(t) = \sigma_s + \sigma_d \cdot \sin[(2\pi f) \cdot t] \tag{7.4}$$

Tests have to be performed with two different static and dynamic test load components, in particular the static component is:

$$\sigma_{s1} = \sigma_0 + (1 + \gamma_d) \cdot \sigma_f \tag{7.5}$$

$$\sigma_{s2} = 0.6 \cdot \sigma_0 + (1 + \gamma_d) \cdot \sigma_f \tag{7.6}$$

the dynamic one is:

$$\sigma_{d1} = (0.05 - 0.1) \cdot \sigma_{s1} \tag{7.7}$$

$$\sigma_{d2} = (0.05 - 0.1) \cdot \sigma_{s2} \tag{7.8}$$

In the standard the elastic-viscous-hysteretic model is assumed as the ideal behaviour of the material to evaluate elastic and damping dynamic parameters Figure 7.2.

The elaboration starts from the displacement analysis for each test frequency, it is evaluated considering the mean value of the four transducers and it will be sinusoidal form:

$$\delta(t) = \delta_s + \delta_d \cdot sin[(2\pi f)\, \dot{t} + \psi] + \delta^0(t) \tag{7.9}$$

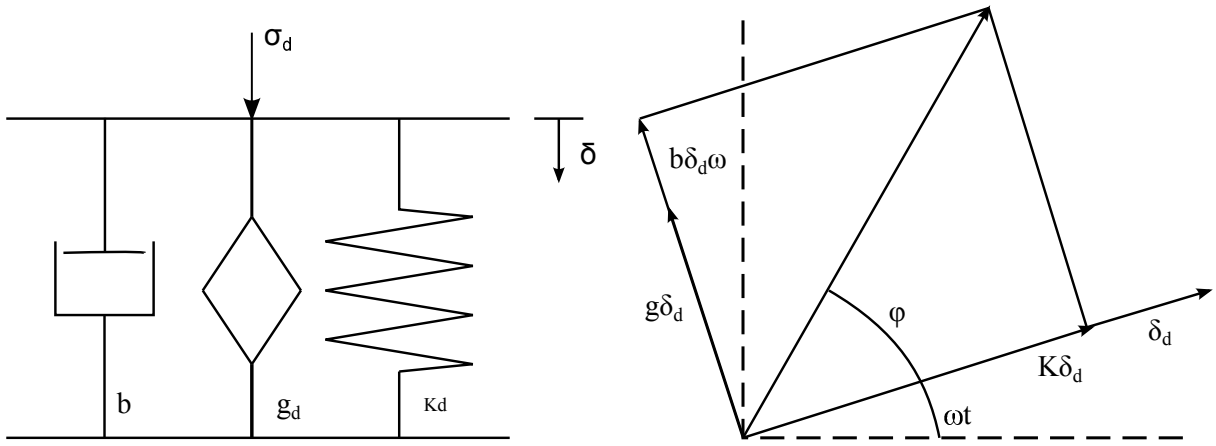

Figure 7.2: Mechanical model UNI 11059

In which δ_s and δ_d are obtained from static and dynamic load respectively while $\delta^0(t)$ is the signal distortion that must be negligible. The spectral transfer functions of the specimen for pads and mats are given by:

$$h(f)^{-1} = \frac{\sigma_d(f)}{\delta_d(f)} \cdot e^{j\psi(f)} \tag{7.10}$$

Considering the model in Figure 7.2 they can be written in the form:

$$h(f)^{-1} = [K_d] + jx[g_d + bx(2x\pi xf)] \tag{7.11}$$

The analytical expressions for the calculation of dynamic parameters are given :

$$K_d \simeq \frac{\sum_{i=1}^{N} [H(f_n)^{-1}]_{Re}}{N} \tag{7.12}$$

7.3 Numerical Simulations

The numerical simulations of the above experiments were performed with the finite element code ABAQUS [30], eight node 3D solid elements with reduced integration (1 integration point) were used to model the TDM pads.

Mesh sensitivity analysis showed negligible change in accuracy keeping equal to one the side ratio and varying the number of elements. The material model used in this section is the compressible Mooney-Rivlin since the new material model presented in the previous sections is not yet implemented in a Finite Element software. Parameters are those given in Tables 5.3. The boundary conditions were defined in conformity with the condition prescribed in Section 7.2.

When modeling a nonlinear hyperelastic material in ABAQUS, the program makes the following assumptions:

- the material behavior is elastic,
- the material behavior is isotropic,
- the simulation includes nonlinear geometrical effects.

The use of hybrid-type elements is highly recommended when dealing with near-incompressible materials. Such elements are based on mixed-type formulations, where independent interpolations for displacement and stress fields are assumed and two sets of governing equations, both equilibrium and compatibility are enforced in weak form.

In ABAQUS, the identification of the hyperelastic material properties can be performed on the basis of experimental stress-strain curves. Four different tests can be used to get an accurate evaluation of the material parameters. These are uniaxial, planar (pure shear test), equibiaxial and volumetric tests.

Clearly, when already known, material parameters can be directly specified in ABAQUS to describe hyperelastic material models. Since the problem of the identification of material parameters has been already addressed in Chap. 4, the second task will be used in this chapter.

7.4 Implicit vs Explicit procedure

Finite Element Analysis (FEA) involving short-time dynamical problems with large deformation, quasi-static problems with large deformations and multiple nonlinearities, or complex contact/impact problems requires the use of either implicit or explicit solution techniques.

Examples of these types of simulations are crashworthiness analysis, drop testing, deep drawing, rolling, extruding, pipe whip, bird strike, fan containment and many more.

The ABAQUS FEA program includes the ability to address both implicit as well as explicit solutions. Both the solution procedures are based on a numerical time integration scheme to solve the discrete dynamical equilibrium equations in terms of displacements, velocities and accelerations, then strains and stresses [35].

Implicit integration schemes (ABAQUS/Standard uses a Hilber-Hughes-Taylor algorithm for implicit integration) assume a constant average acceleration over each step $\Delta t = t_{n+1} - t_n$ where t_n and t_{n+1} are the starting and ending points of the time interval Δt. The governing equations are solved and the resulting accelerations and velocities at t_{n+1} are calculated. Then the unknown displacements at t_n and t_{n+1} are determined.

Explicit integration schemes (ABAQUS/Explicit uses a Central Difference method) assume a linear change of the displacement in each time step. The governing equations are evaluated and the resulting accelerations and velocities at t_n are calculated. Then, the unknown displacements at t are determined. There is one major difference between the two techniques in the equations that are used to solve for displacements at t_{n+1}.

The implicit solution method requires matrix inversion of the structural stiffness matrix, the explicit solution does not.

However, unlike the implicit solution scheme, which is unconditionally stable independently on the time step size, the explicit scheme is stable only for time step size smaller than a critical size evaluated for the analyzed structure. The undamped critical time step size is $2/\omega_n$ (where ω_n is the largest natural circular frequency), which is usually a very small value. This very small time step size requirement for stability thereby makes explicit solutions useful only for very short transient analyses.

But, even though the number of time steps in an explicit solution may be orders of magnitude greater than in an implicit solution, it is significantly more effcient than an implicit solution since no matrix inversion is required. Therefore the choice of the integration scheme strongly relies on the problem under investigation.

7.5 Static tests

The material used in the first part of this study is the TDM 800, for which the parameters for Mooney-Rivlin model are reported in Table 7.2. First we run static tests. The deformation under static load (load of infrastructure with the train not moving) is a limit to our optimization problem.

The loads suggested by the regulations are reported in Table 7.1:

Table 7.1: Static loads UNI 11059

σ_0 (MPa)	σ_f (MPa)
0.4	0.7

The optimal solution needs to be in the best compromise in between static and dynamic properties, moreover the static displacement is a constrain condition to the problem since it has to be in a certain range in order to allow safe and correct functionality of the railway track.

Table 7.2: Parameters for Mooney-Rivlin model used for dynamic simulations

Material	C_{10}	C_{01}	D_1
800	0.186	0.001	0.25

Step 1

The material is very difficult to manufacture in different shapes, the new shape needs to be very regular and keep square angles. Moreover for design limit the height has to be 25 mm and the upper surface, the one in contact with ballast or the slab, needs to be flat. Given all this limit the only parameter that can be changed is the bottom surface of the mat keeping the design simple and admissible for TDM.

In the first variant a simple shape was studied in which the solid shape of the mat (Figure 7.3) is modified introducing three discrete supports (Figure 7.4).

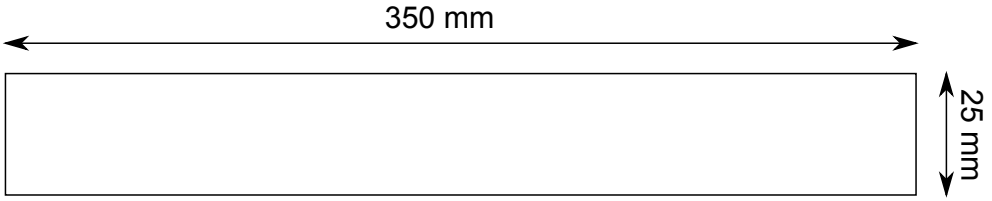

Figure 7.3: Solid shaped mat

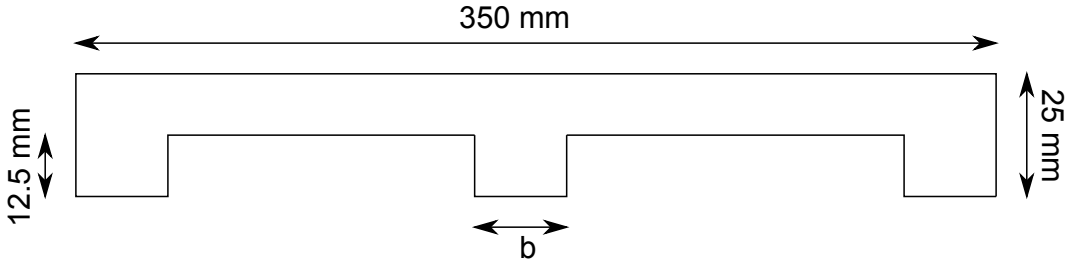

Figure 7.4: First variant

The value of the stiffness K_{qs}, according to the formula (7.3), for the solid mat is 40N/cm^3. The analysis are run changing the value of the width b of the supports Figure 7.4 in order to find the best solution.

Table 7.3 shows the static stiffness of the variants.

Table 7.3: Static stiffness first variant

Material	b (mm)	K_{qs} (N/cm^3)
800	20	6.75
	30	10.0
	40	13.5

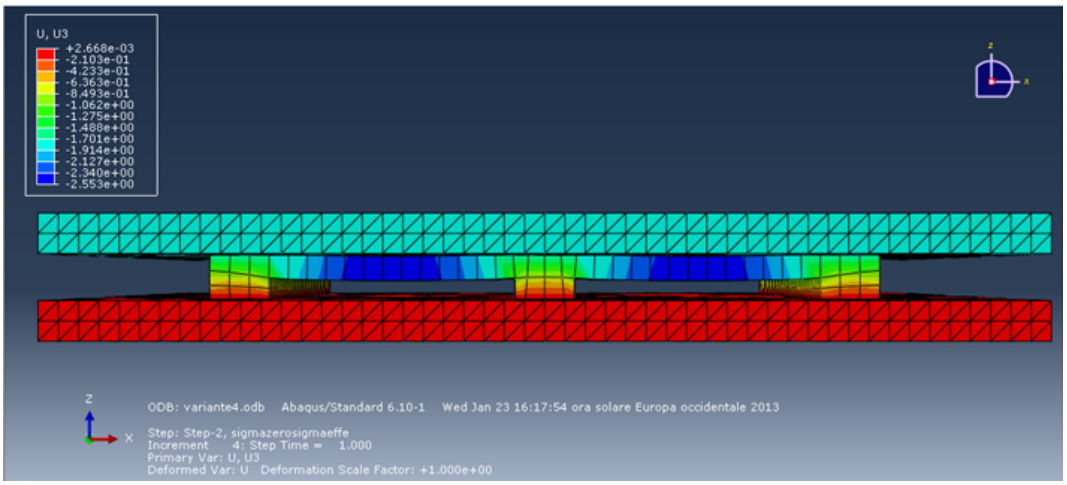

Figure 7.5: Output analysis first variant

Figure 7.5 shows the displacement field of the first variant with b=20 mm subjected to the maximum load Table 7.1.

Step 2

The first variant shows an important vertical displacement in the region in between the two supports, for this reason a second variant was tested in which the number of supports is 4 reducing the distance in between each support Figure 7.6.

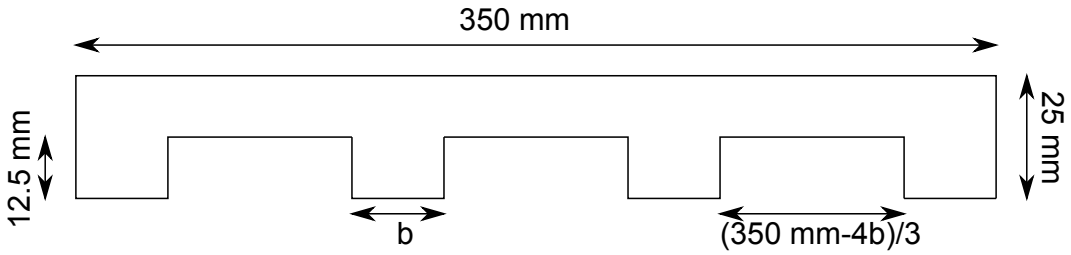

Figure 7.6: Second variant

Also in this variant the width b of the supports varies in between the values of 20 mm to 40 mm.

Table 7.4 shows the results of the static tests for the second variant.

Table 7.4: Static stiffness second variant

Material	b (mm)	K_{qs} (N/cm^3)
800	20	8.75
	30	12.0
	40	18.7

Figure 7.7 shows the displacement field of the second variant with b=30 mm subjected to the maximum load Table 7.1.

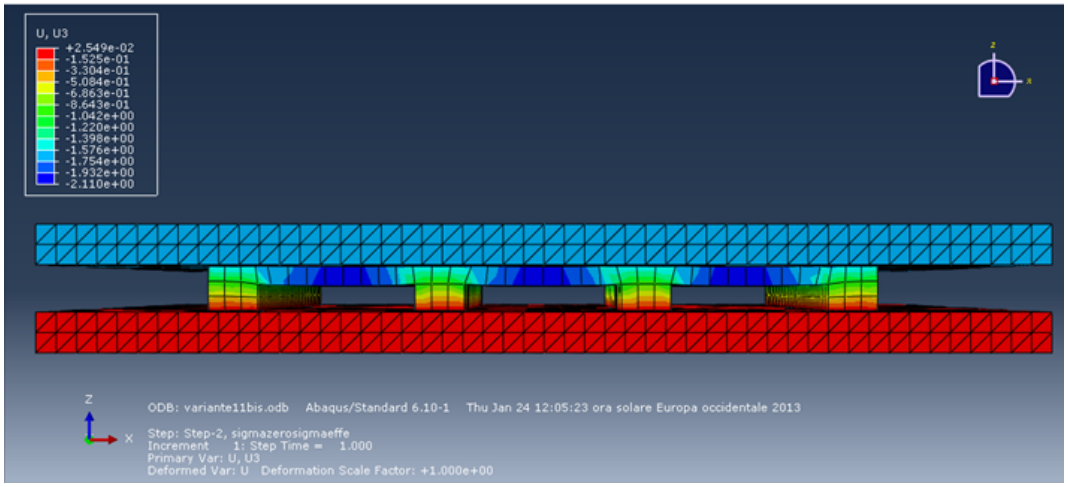

Figure 7.7: Output analysis second variant

Step 3

To further reduce the vertical displacement in between the supports a third variant is considered in which the suopports are staggered in the length of the mat Figure 7.8.

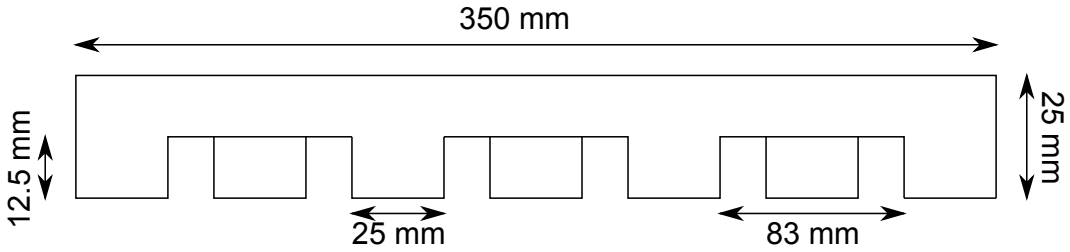

Figure 7.8: Third variant

Also in this variant the width b of the supports varies in between the values of 20 mm to 40 mm.

Table 7.5 shows the results of the static tests for the second variant.

Table 7.5: Static stiffness third variant

Material	b (mm)	K_{qs} (N/cm^3)^3
800	20	8.0
	30	10.0
	40	11.7

Figure 7.9 shows the displacement field of the second variant with b=30 mm subjected to the maximum load Table 7.1.

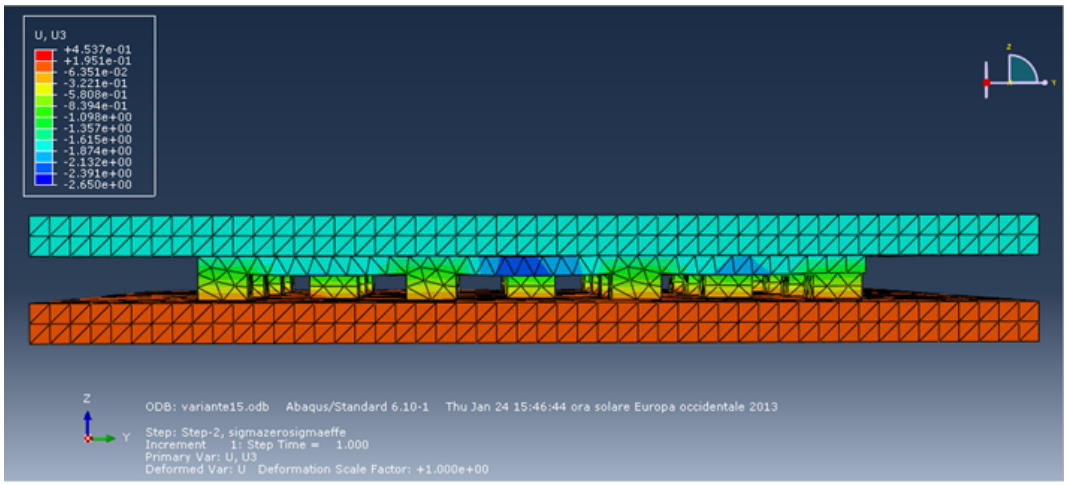

Figure 7.9: Output analysis third variant

Step 4

The third gave good performances and was the best option to move forward for dynamic analysis, but due to difficulties in manufacturing it had to be changed. The foruth variant keeps the same area of the supports but they have different geometry in order to facilitate the production (Figure 7.10-7.11). To reduce the stiffness the TDM 600 was used in this variant.

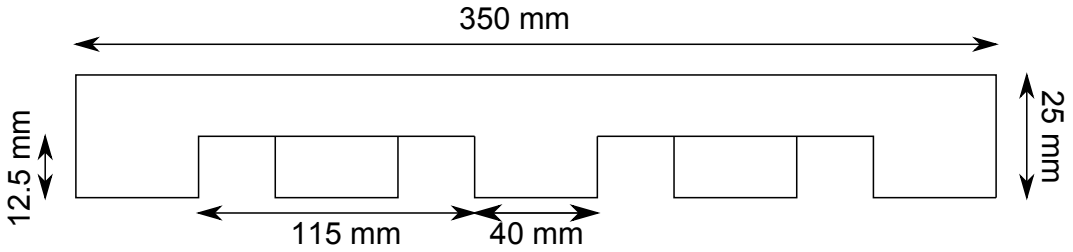

Figure 7.10: Fourth variant

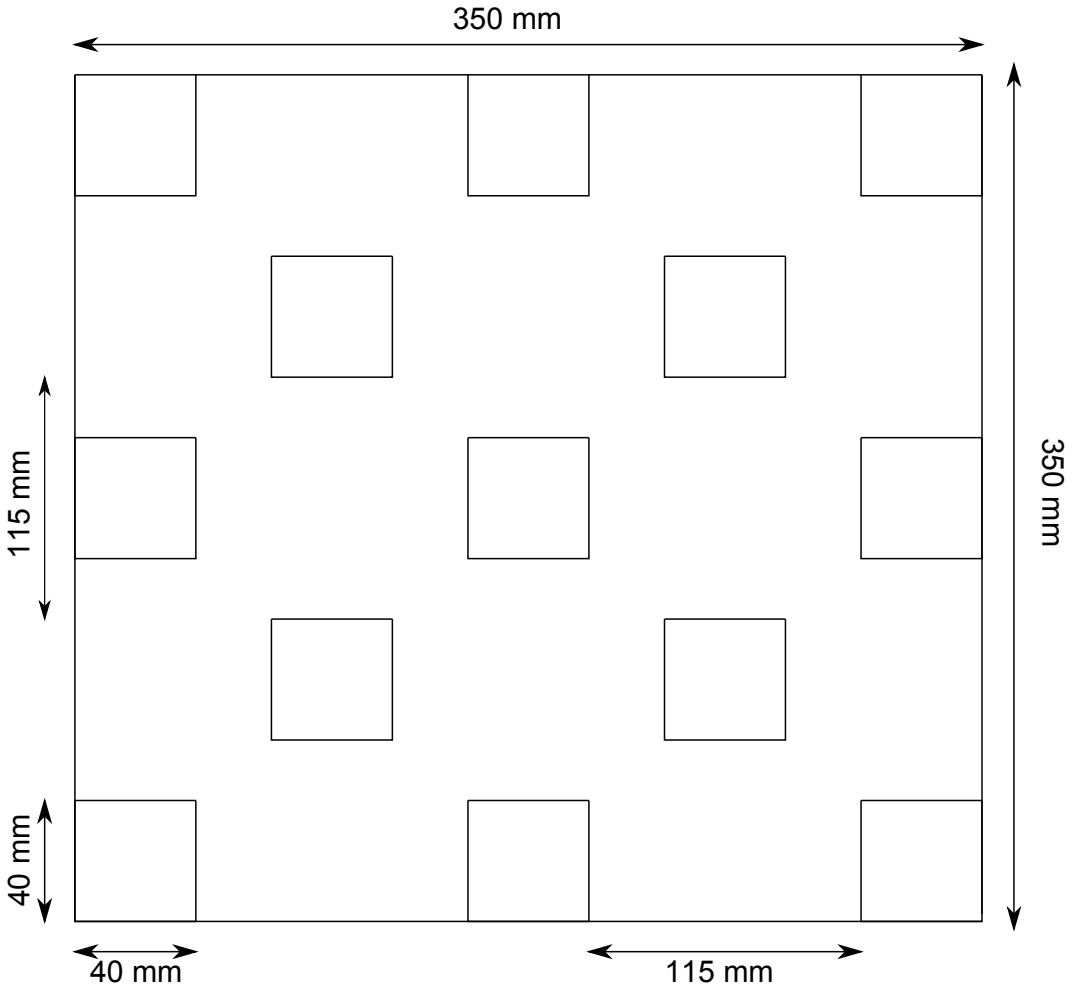

Figure 7.11: Fourth variant different view

The value of the stiffnes for this varinat in the only configuration studied, the one with supports 40 mmx 40 mm is 7.5N/mm^3.

Figure 7.12 shows the displacement field of the fourth variant subjected to the maximum load Table 7.1.

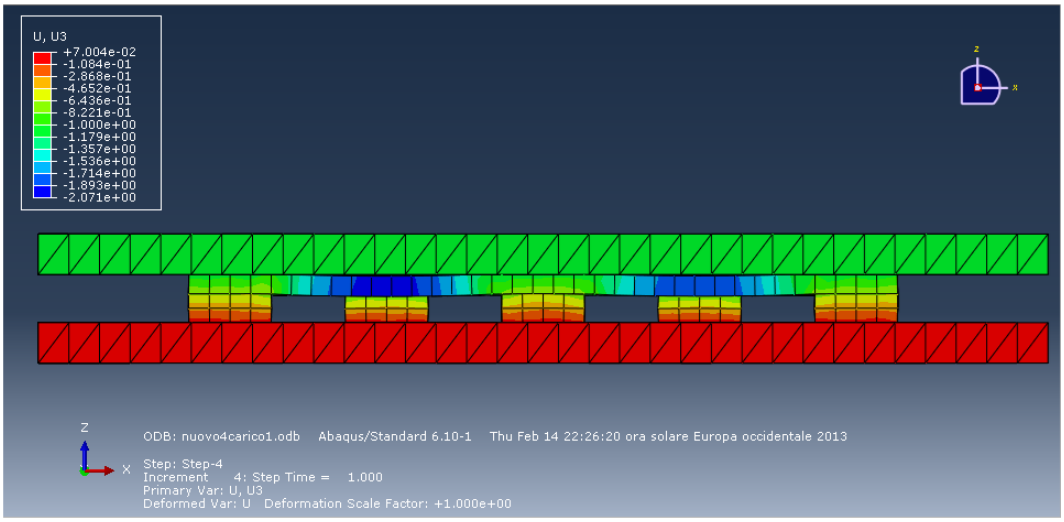

Figure 7.12: Output analysis fourth variant

7.6 Dynamic tests

In this section we study the dynamical behavior of the railway mat, simulating dynamic compression tests as described in section 7.1.

With this aim we introduce the ABAQUS FEA finite viscoelasticity constitutive relation and we investigate the resulting material behavior by means dynamic experiments. Section 4.8.2 of the ABAQUS Theory Manual (Hibbit et al., relation for modeling nonlinear viscoelastic effects in the form:

$$\sigma(t) = \sigma_e + SYM\left\{\mathsf{F}(t)\left[\int_0^t \frac{J(s)}{J(t)}\dot{k}\,(t-s)\,\mathsf{F}^{-1}(s)\sigma_e(s)\mathsf{F}(s)ds\right]\mathsf{F}^{-1}(t)\right\} \tag{7.13}$$

where σ_e is the instantaneous elastic Cauchy stress response, k is the so called viscoelastic kernel, which characterizes the stress relaxation. Also SYM represents the symmetric part of the bracketed term. The relation (7.13) is valid both for compressible and incompressible material only the form of σ_e changes.

Since TDM showed weak frequency dependence, the time relaxation of the solid is assumed to be governed by a one-term Prony series expansion given by:

$$k(t) = \frac{\mu_{\inf}}{\mu_0} + \left(1 - \frac{\mu_{\inf}}{\mu_0}\right) e^{-t/\tau} \tag{7.14}$$

where $\mu_{\inf}$ is the asymptotic value to which the shear modulus settles after an infinite time Table 4.4 and τ is a characteristic time constant which we consider equal to 0.037s.

The mat in the fourth variant is subjected to dynamic load as explained in section 7.2. In a range of frequencies up to 60 Hz.

Table 7.6: Static stiffness third variant

Material	$K_d\,(\mathrm{N/cm^3})$
600	17.2

Chapter 8

Conclusions and Outlook

This thesis aimed at providing information about a new Tire Derived Material with a simple and low cost production cycle.

Experimental tests, mechanical characterization and a new hyperelastic model have been proposed. It was not the objective to provide a full mechanical description, but rather to explore this new material properties and the potential in civil application.

In Chapter 2, the problem of scrap tires is introduced along with the main application of Tire Derived Materials. Moreover, in this chapter, the new material is presented with its production process and its main application are described.

In Chapter 4, an extensive experimental campaign on TDM is described. The tests performed were the only ones allowed by the material composition. Tests revealed lack in tensile strength of the material along with low tensile deformation. This is one of the main limits of TDM which in the current composition can be used in application where subjected to moderate large deformation in stress and compression.

Shear test using the classical dual lap test along with homogeneous compression tests and volumetric tests were performed on the material.

The main outcome of the experimental tests was that the material showed high nonlinearity during hydrostatic compression. This is not usual for rubber and rubber-like materials. This behavior is deemed to be connected to the presence of voids in the TDM which makes it very compressible up to certain value of the volumetric deformation.

To further investigate this behavior another set of compression tests were performed, with the help of optical measurement, the lateral displacement of the sample was measured in order to estimate the Poisson's ratio both in the neighborhood of the undeformed state and for large deformations.

Chapter 5, describes the problem of finding a good hyperelastic model for TDM. Different conventional models are used to model the new material but all failed in describing the behavior for the different deformation state with a unique set of parameters. Moreover the

conventional hyperelastic models in their compressible version are able to describe linear variation of volume with pressure which is in some cases enough accurate to describe rubber or rubber-like materials but not in the case of TDM.

For all these reasons a new hyperelastic model has been introduced. The strain energy function presented here is a variant of the exponentiated Hencky strain energy proposed by Neff et al. [63], which for moderate strains, is as good as the quadratic Hencky model and in the large strain region it improves several important features from a mathematical point of view. One of the advantages of using the proposed form of the exponentiated Hencky energy is that it possesses a set of parameters uniquely determined in the infinitesimal strain regime and an orthogonal set of parameters to determine the nonlinear response that do not interfere with them.

Most of the parameters have a clear physical meaning, we choose the ones suggested by the experimental tests and allowed by the mathematical theory. The advantage is to overcome the difficulties related to finding a unique set of optimal parameters that are usually encountered fitting polynomial forms of strain energies. Moreover, by comparing the predictions from the proposed constitutive model with experimental data we concluded that the new constitutive model gives good prediction.

Chapter 6, covers the viscoelastic problem, a theory of finite viscoelasticity based on multiplicative split of the deformation tensor in an elastic and inelastic part is applied.

The rheological model used to describe the rate dependent material behavior takes into account of the two main dissipative mechanism that happen in the material when loaded with an external force with a finite velocity. The first connected to the grain interaction at the material level and the second connected to the polymer chain resistance at the micromechanical level.

The model is fitted on experimental tests performed on TDM in cyclic simple shear with good results.

Chapter 7 describe a case study in which the problem is to find an optimal solution to reduce the axial stiffness of the TDM rubber mat for railway application produced by Isolgomma srl.

In this section, the new material model is not used since its not already implemented in any Finite Element software. Optimization procedure regarding TDMs is very much influenced by the production technology, this makes the problem over-constrained. For these reasons a trial and error procedure is used.

Starting from a simple and easy to produce shape, changes are made in order to improve the performance, for every change the analysis are run and improvement are implemented in the next step. The procedure converged to a good solution in few steps. The new shape are first tested with static load and then the simulation are run with dynamic ones.

This successful application allowed the company Isolgomma srl. to introduce in its product offers a new one dedicated to light rail.

Final Remarks

The experience gained from studying TDM has lead to important considerations that are summarized here:

- A new material is described with a set of experimental tests. The material can be used for some applications according to its properties. The production process is very easy to implement and requires very low energy consumption and labor making the material very cost efficient.
- A new hyperelastic model is proposed which can describe the behavior of TDM in moderately large deformations. The new strain energy has good mathematical properties and is able to capture the high nonlinear behaviour of TDM when subjected to hydrostatic compression.
- A new shape for TDM is found that allowed us to use it in light weight rail where elastomeric foam have been used.

Outlook

This study leaves some aspect of TDM mechanical characterization still open.

In the future it will be useful to have a micromechanical model of the material which takes into account of the random distribution of the rubber grains and fiber.

The need of such a model is due to the fact that TDMs have potential to improve their performances.

The phenomenological model described in this work allows to design a device with the material we have a michromechanical model would allow to design the material according to specific needs.

Another interesting aspect would be to implement the new model proposed here in a Finite Element software. Many materials have compressible behavior and the mathematical properties of the model makes it very interesting to use in large deformations.

This aspect may be object of future works of the author.

More material testing needs to be done on the TDM, in particular dynamic tests, in order to have a characterization in a wider range of frequencies.

The material is mainly used in railway application where the range of frequencies goes from few Hz to few thousands of Hz.

The dependence of the material response to the amplitude and the frequency of the load is also an aspect that needs to be further investigate. This is still an open problem for rubbers and rubber-like material. As far as the author knows there is no available model

that can describe amplitude and frequency dependency in such a wide range of frequency suitable for Finite Element applications.

Appendix A

Polyconvexity

The mechanical problem (A.1) for a hyperelastic material is to find a displacement field $\mathbf{u}$ out of the set of all admissible displacement fields $\mathbf{u^*}$ that fulfills the boundary conditions on $\partial\Omega$ and that minimizes the total energy Π of the system.

$$u = \arg_{\nu \in \mathbf{u}^*} \min \Pi(\nu) \tag{A.1}$$

$$\Pi(\mathbf{u}) = \int_{\Omega_0} \Psi(\operatorname{grad}(\mathbf{u}))\, d\Omega_0 - \int_{\Omega_0} \rho \mathbf{b} \cdot \mathbf{u} d\Omega_0 - \int_{\Omega_0} \rho \mathbf{t} \cdot \mathbf{u} d\partial\Omega_0 \tag{A.2}$$

Here Ω_0 and $\partial\Omega_0$ are a body and its boundary, respectively, Ψ is the Helmholz free energy, ρ the initial density of the body, $\mathbf{b}$ and $\mathbf{t}$ are volume and surface tractions, respectively and $\mathbf{u}$ is the displacement.

The existence and uniqueness of solutions for the minimization problem (A.1) depends on the functional form of the strain energy density $\Psi(\operatorname{grad}(\mathbf{u}))$.

Several concepts, dealing with the functional dependence of Ψ on the deformation gradient $\mathbf{F} = \operatorname{grad}(\mathbf{u})$, exist that guarantee the existence and uniqueness of a solution of problem (A.1):

$$convexity \rightarrow polyconvexity \rightarrow quasiconvexity \rightarrow rank - one - convexity$$

Each concept from left to right implicates the consecutive, while the inverse is shown not to be true in full generality [21].

The requirement of convexity with respect to $\mathbf{F}$ can be shown to violate fundamental principles of solid continuum mechanics [7], such that this concept cannot be used.

Quasiconvexity is an integral inequality and therefore rather complicated to handle and is only conditional appropriate for the analysis of function.

A more practical notion is the one of polyconvexity, Schroeder and Neff say that [71].

Definition A.1 (Polyconvexity)

"$\mathbf{F} \rightarrow \Psi(\mathbf{F})$ is polyconvex if and only if there exists a function $P : \mathbb{M}^{3x3} x \mathbb{M}^{3x3} x \mathbb{R} \leftarrow \mathbb{R}$ (in general non-unique) such that $\Psi(\mathbf{F}) = P(\mathbf{F}; \operatorname{adj}(\mathbf{F}); \det(\mathbf{F}))$ and the function $\mathbb{R}^{19} \rightarrow$

$\mathbb{R}, \left(\tilde{X}, \tilde{Y}, \tilde{Z}\right) \rightarrow P(\tilde{X}, \tilde{Y}, \tilde{Z})$ is convex for all points $\mathbf{X} \in \mathbb{R}^3$" As a consequence of the above definition we get the additive property of the polyconvex functions for a more restrictive class of energy densities.

Corollary A.1 (Additive polyconvex functions)

" Let $\Psi(\mathbf{F}) = \Psi_1(\mathbf{F}) + \Psi_2(\text{adj}(\mathbf{F})) + \Psi(\det(\mathbf{F}))$. If $\Psi_{,i} = 1, 2$ are convex in the associated variable respectively and $\Psi_3 : \mathbb{R}^+ \rightarrow \mathbb{R}$ is convex in the associated variable as well, then Ψ is altogether polyconvex."

It can be proven that the following Lemma holds [71]:

Lemma A.1 (Convexity and monotone composition)

"Let $P : \mathbb{R}^n \rightarrow \mathbb{R}$ be convex and let $m : \mathbb{R} \rightarrow \mathbb{R}$ be convex and monotone increasing. Then the function $\mathbb{R}^n \rightarrow \mathbb{R}, X \rightarrow m(P(X))$ is convex."

This corollary is one of the main tools in constructing polyconvex strain energies.

A.1 Convexity of the volumetric response of W_{eHm}

In this section we will show the convexity of the second term of the volumetric response $\mathbf{F} \rightarrow e^{\tilde{k}\left(|\log \det \mathbf{F}|^2\right)^{m/2}}$. For the first term the reader can refer to Neff et al. [63]. We first examine the condition under which the more general form $\det\mathbf{F} \rightarrow h\left(|\text{logdet}\mathbf{F}|\right)$ is convex in $\det \mathbf{F}$ (Appendix A.2). Hence, we ask for the second derivative of $\det\mathbf{F} \rightarrow h\left(|\text{logdet}\mathbf{F}|\right)$ to be positive:

$$\frac{d^2}{dt^2} h\left(|\log t|\right) = \frac{d^2}{dt^2}\left(h'\left(|\log t|\right)\frac{\log t}{t|\log t|}\right) = h''\left(|\log t|\right)\frac{\log t^2}{t^2|\log t|^2} - h'\left(|\log t|\right)\frac{\log t}{t^2|\log t|} \geq 0 \quad \text{(A.3)}$$

Obviously, this is the case if and only if $h''\left(|\log t|\right) \geq h'\left(|\log t|\right)$ for all $t > 0$ and hence, if and only if for all $\xi \in \mathbb{R} h''(\xi) \geq h'(\xi)$ Thus, $t \rightarrow h(logt)$ is convex if and only if h grows at least exponentially (see also Appendix A.1).

Fix $n \in \mathbb{N}$ We want to find $\tilde{k}$ such that $h(\xi) = e^{\tilde{k}\xi^n}$ matches the criterion.

$$\tilde{k}^2 n^2 \xi^{2n-2} e^{\tilde{k}\xi^n} + \tilde{k} n(n-1)\xi^{n-2} e^{\tilde{k}\xi^n} \geq \tilde{k} n \xi^{n-1} e^{\tilde{k}\xi^n} \quad \text{(A.4)}$$

which is equivalent to $\tilde{k}n\xi^n - \xi + (n-1) \geq 0$. We compute the minimum of this expression. To this aim we solve the equation $\tilde{k}n\xi^n - \xi + (n-1) = 0$ and we obtain $\xi = \tilde{k}^{-\frac{1}{n-1}} n^{-\frac{2}{n-1}}$

Therefore

$$\min_{\xi\in\mathbb{R}}\left\{\tilde{k}n\xi^n-\xi+(n-1)\right\}=\tilde{k}n\tilde{k}^{-\frac{n}{n-1}}n^{-\frac{2n}{n-1}}-\tilde{k}^{-\frac{1}{n-1}}n^{-\frac{2}{n-1}}+(n-1) \tag{A.5}$$

$$=\tilde{k}^{-\frac{1}{n-1}}n^{-\frac{n+1}{n-1}}(1-n)+(n-1). \tag{A.6}$$

This minimum is nonnegative if and only if $\tilde{k}^{-\frac{1}{n-1}}n^{-\frac{m+1}{m-1}}+1\geq 0$. Thus $\tilde{k}$ has to be chosen such that $\tilde{k}\geq n^{-(n+1)}$.

In conclusion the function $t\to e^{\tilde{k}\xi^n}$ is convex if and only if $\tilde{k}\geq\frac{1}{n^{(n+1)}}$ which for $n=m/2$ means $\tilde{k}\geq\frac{1}{\frac{m}{2}^{(\frac{m}{2}+1)}}$.

A.2 Rank-one-convexity for functions of the type $t\to\xi\left(|\log t|^2\right)$

We consider a generic function $\xi:\mathbb{R}_+\to\mathbb{R}_+$ and we find a characterization of the convexity for the function $t\to\xi\left(|\log t|^2\right)$. In the following let ζ denote the function $\zeta:R_+\to R_+,\zeta(t)=\left(|\log t|^2\right)$. We deduce:

$$\frac{d}{dt}\xi\left(|\log t|^2\right)=\xi'\left(|\log t|^2\right)2\frac{1}{t}\log t, \tag{A.7}$$

$$\frac{d^2}{dt^2}\xi\left(|\log t|^2\right)=4\xi''\left(|\log t|^2\right)2\frac{1}{t^2}\left(\log t\right)^2-2\xi'\left(|\log t|^2\right)2\frac{1}{t^2}\log t+2\xi'\left(|\log t|^2\right)\frac{1}{t^2}$$

$$=2\frac{1}{t^2}\left(2\xi''\left(|\log t|^2\right)\left(\log t\right)^2+\xi'\left(|\log t|^2\right)\left(1-\log t\right)\right) \tag{A.8}$$

where $\xi'=\frac{d\xi}{d\zeta}$. Hence the function $t\to\xi\left(|\log t|^2\right)$ is convex

- on $(1,\infty)$ as a function of t if and only if:
$$2\frac{d^2\xi(\zeta)}{d\zeta^2}\left(\log t\right)^2+\frac{d\xi(\zeta)}{d\zeta}\left(1-\log t\right)\geq 0\qquad\qquad\forall\zeta\in\mathbb{R}_+$$
- on $(0,1)$ as a function of t if and only if:
$$2\frac{d^2\xi(\zeta)}{d\zeta^2}\left(\log t\right)^2+\frac{d\xi(\zeta)}{d\zeta}\left(1+\log t\right)\geq 0\qquad\qquad\forall\zeta\in\mathbb{R}_+$$

Appendix B

Matlab code for parameters optimization

The Matlab file *compression.mat*, *simpleshear.mat* and *volumetric.mat* contains experimental data concerning uniaxial compression (UC) simple shear (SS) and hydrostatic compression (UV). The first and second columns contain, respectively, the vectors of principal stretch (volumetric deformation for hydrostatic compression)and the corresponding stress as read. The following variables are defined:

- L_UC, L_SS, L_UV: stretch values during UC, SS, UV respectively.
- L_max_UC, L_max_SS, L_max_UV: maximum imposed stretch value for UC, SS, UV respectively.
- C=(mu k ... hat_k m): Optimal material parameters.
- P_UC, P_SS, P_UV:Piola-Kirchoof stress values.
- Pol_UC, Pol_SS, Pol_UV: coefficients of the nth order polynomial functions approximating approximating the experimental data.
- PKF_UT, PKF_UC, PKF_PS: Piola-Kirchoof stress values corresponding to L_UC, L_SS, L_UV and calculated by means of the nth order polynomial functions whose coefficients are given by Pol_UC, Pol_SS, Pol_UV.
- r,s,t: number of experimental points. If any of these values is set to 0, the corresponding test is discarded.

The following Matlab script is used to find the optimal parameters following the procedure in Saccomandi and Ogden [67].

```
%Read test data
load('compression.mat')
load('simpleshear.mat')

L_UC=compression(:,1); % Principal stretch load direction
P_UC=compression(:,2); % Stress MPa
ni1=compression(:,3); % Non-linear Poisson's coefficient
L_USS=simpleshear(:,1); % Principal stretch load direction
P_USS=simpleshear(:,2); % Stress MPa
%Uniaxial
Pol_UC=polyfit(L_UC,P_UC,3);
r=length(L_UC);
Lmin_UC=min(L_UC);
L_UC=linspace(1,Lmin_UC,r);
    if r==0
        L_UC=[];
    end
       PKF_UC=polyval(Pol_UC,L_UC);
 %Simple Shear
Pol_US=polyfit(L_SS,P_SS,3);
s=length(L_SS);
Lmax_US=max(L_SS);
L_US=linspace(0,Lmax_US,s);
    if s==0
        L_US=[];
    end
 PKF_US=polyval(Pol_US,L_US);
% Calculation of optimal material parameters deviatoric part
STRETCH=[L_UC L_US]; %overall stretch vector
STRESS=[PKF_UC PKF_US]; %overall stress vector
C0=[0,0]; %Initial guess
lb = [0.1,0.2]; %Lower bound of the optimal ...solution vector
ub = [inf,inf]; %Upper bound of the optimal ...solution vector
optnew=optimset('DiffMaxChange',0.000001,'DiffMinChange',1e-15,...
 'TolFun',1e-15, 'TolX',1e-15,'MaxFunEvals',3000,'MaxIter',3000); %Curve
fit oprtions
[C] = lsqcurvefit(@expHencky_M,C0,STRETCH,STRESS,lb,ub,optnew); %optimal
...solution
```

Published with MATLAB® 7.13

```
function S=expHencky_M(C,STRETCH)
global r s ni1

%material constants
mu=C(1);
k=C(2);
Pol_ni1=polyfit(STRETCH(1:r),ni1',2);
Pol_ni1=Pol_ni1';
ni11=Pol_ni1(1).*STRETCH(1:r).^2+Pol_ni1(2).*STRETCH(1:r)+Pol_ni1(3);
if s==0 %uniaxial
     alpha=2;
     beta=2/3.*((1+ni11)./(1-
2.*ni11)).^2.*(log(STRETCH+(2.*STRETCH.*ni11))).^2-
(log(STRETCH+(2.*STRETCH.*ni11)));
     gamma=(log(STRETCH+(2.*STRETCH.*ni11))).*((1+ni11)./(1-2.*ni11));
 elseif r==0
     alpha=4;
     beta=2.*log(0.5.*sqrt(STRETCH.^2+4)+STRETCH).^2;
     gamma=log(0.5.*sqrt(STRETCH.^2+4)+STRETCH)./sqrt(1./2.*STRETCH.^2+4);

 else
    alpha=[2*ones(r,1)' 4*ones(s,1)'];
    beta=[3/2.*((1+ni11)./(1-
2.*ni11)).^2.*(log(STRETCH(1:r)+2.*STRETCH(1:r).*ni11)).^2-
(log(STRETCH(1:r)+2.*STRETCH(1:r).*ni11))
2.*log(0.5.*sqrt(STRETCH(1:s).^2+4)+STRETCH(1:s)).^2;];
    gamma=[(log(STRETCH(1:r)+2.*STRETCH(1:r).*ni11)).*((1+ni11)./(1-
2.*ni11))
log(0.5.*sqrt(STRETCH(1:s).^2+4)+STRETCH(1:s))./sqrt(1./2.*STRETCH(1:s).^2+
4);];
 end
S=alpha.*mu.*exp(k.*beta).*gamma;
```

Published with MATLAB® 7.13

```
% Calculation of optimal material parameters deviatoric part
load('volumetric.mat')
L_UV=volumetric(:,1); % volume change J
P_UV=volumetric(:,2); % Pressure MPa
%Volumetric
Pol_UV=polyfit(L_UV,P_UV,5);
t=length(L_UV);
Lmin_UV=min(L_UV);
L_UV=linspace(1,Lmin_UV,r);
    if t==0
        L_UV=[];
    end
PKF_UV=polyval(Pol_UV,L_UV);
C0v=[0,0,0,0,0]; %Initial guess
lb=[0.2,0.2,0.2,0.2,2]; %Lower bound
ub=[inf,inf,inf,inf,inf];%upper bound
optnew=optimset('DiffMaxChange',0.000001,'DiffMinChange',1e-15,...
 'TolFun',1e-15, 'TolX',1e-15,'MaxFunEvals',3000,'MaxIter',3000); %Curve
fit oprtions
[C1] = lsqcurvefit(@expHencky_M_vol,C0v,L_UV,PKF_UV,lb,ub,optnew); %optimal
...solution
```

Published with MATLAB® 7.13

```
function P=expHencky_M_vol(C1,L_UV)

%material constants
kappa=C1(1);
hat_k=C1(2);
kappa1=C1(3);
tilde_k=C1(4);
m=C1(5);



P=(C1(1).*(exp(C1(2).*(log(L_UV).^2))).*(log(L_UV)./L_UV))+(C1(3).*(exp(C1(
4).*((log(L_UV).^2).^(C1(5)/2)))).*(((abs(log(L_UV)).^C1(5)-
2).*log(L_UV))./(L_UV)));
```

Published with MATLAB® 7.13

The fitting procedure has been implemented in a .mex file and can be requested to the author (giuseppe.montella@unina.it). The program requires Matlab Compiler to be installed on the computer. It can run the fitting using either the exponentiated Hencky energy proposed by Neff et al [63] or the modification with an extra volumetric term presented in this thesis.

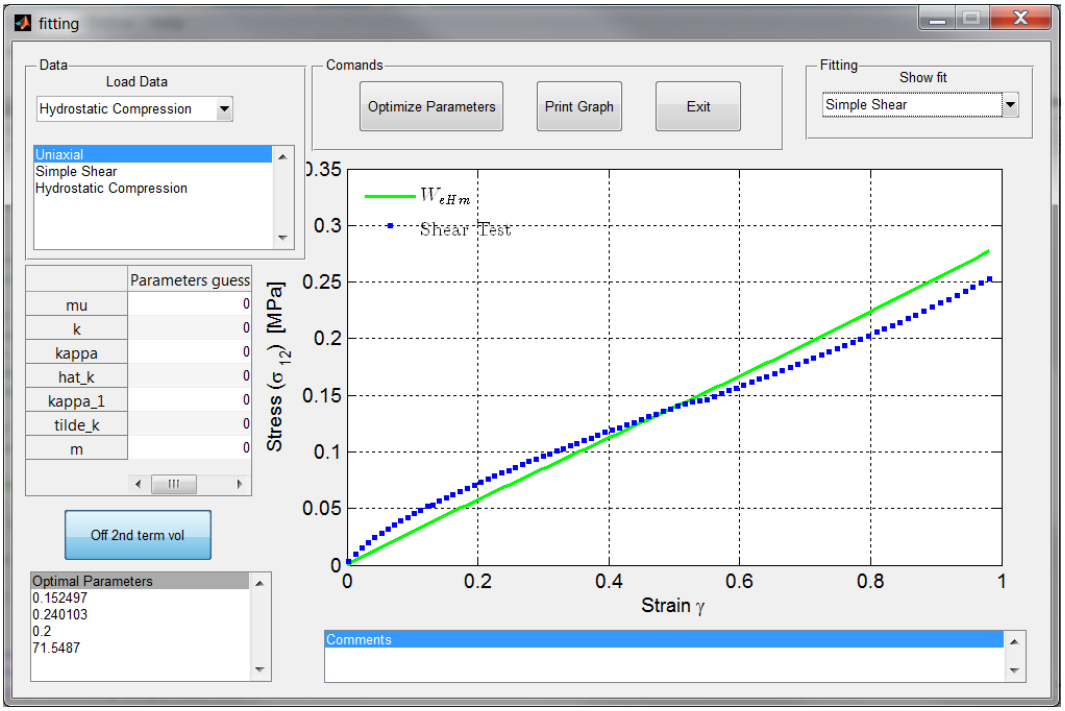

Figure B.1: Standalone program for fitting experimental data with Exponentiated Hencky functions

Appendix C

Matlab code for single Maxwell element

This Matlab code allows to evaluate the response of a single Maxwell element according to the framewrok proposed by Reese and Govindjee [28] and that has been used in this thesis.

- a defines the number of cycles;
- gamma is the amplitude of the imposed displacement;
- mu and k are material parameters;
- nd is the deviatoric viscosity (only deviatoric deformations are considered no contribution to the viscosity from the volumetric deformations);
- Ci is the inelastic right Cauchy-Green tensor;
- ebe is $\mathbf{b}_e = \mathbf{F}_e\mathbf{F}_e^T$;
- ff is the deformation tensor $\mathbf{F}$;
- ebetr is $\mathbf{b}_e$trial. The problem is solved using a numerical tangent.

```
close all
clear all
format long

a=(0:0.2:8*pi);
gamma=(0.33.*sin(a))';  %imposed displacemenet

mu=0.2;    % material parameter
k=2.2;     % material parameter
dt=0.1;    % time interval
nd=13;     %deviatoric viscosity

nstep=length(gamma);

Ci=ones(3,1);
ebe=ones(3,1);


for n=1:nstep
ff=[sqrt(1+(gamma(n)^2/2)+gamma(n)*sqrt(1+(gamma(n)^2/4))) %Deformation
Tensor
    sqrt(1+(gamma(n)^2/2)-gamma(n)*sqrt(1+(gamma(n)^2/4)))
    1];

ebetr=ff./(Ci);  %be trial

c = 0;
res=1;

while res>1e-5 & c<100

ra=ebe-exp(-dt.*((4.*mu.*exp(2.*k.*log(ebe).^2)).*log(ebe))./(nd)).*ebetr;
%residual
i=sqrt(-1);
h=eps;
f= @(ebe) ebe-exp(-
dt.*((4.*mu.*exp(2.*k.*log(ebe).^2)).*log(ebe))./(nd)).*ebetr;
K1=(1./h).*imag(f(ebe+i*h*[1;0;0]));
K2=(1./h).*imag(f(ebe+i*h*[0;1;0]));
K3=(1./h).*imag(f(ebe+i*h*[0;0;1]));
KK=[K1,K2,K3]; %numerical tangent
de=-KK\ra;
res=norm(-ra);
ebe=ebe+de;
c=c+1;

mat1(n,:)= ebe(1); %store first eigenvalue

fprintf('Load Step: %d/%d\n',n,nstep)
fprintf('Newton iteration: %d\n',c)
fprintf('Norm of Residual: %2.4e\n',res)
end
if c==99;
    error('Newton not converging')
end
Ci=ff./(ebe);
```

```
end

figure('Units', 'centimeters','Position',[7 4 14 8])
plot (mat1,'g-');
xlabel('number of steps');
ylabel('be');
set(gca,'Fontsize',7);
```

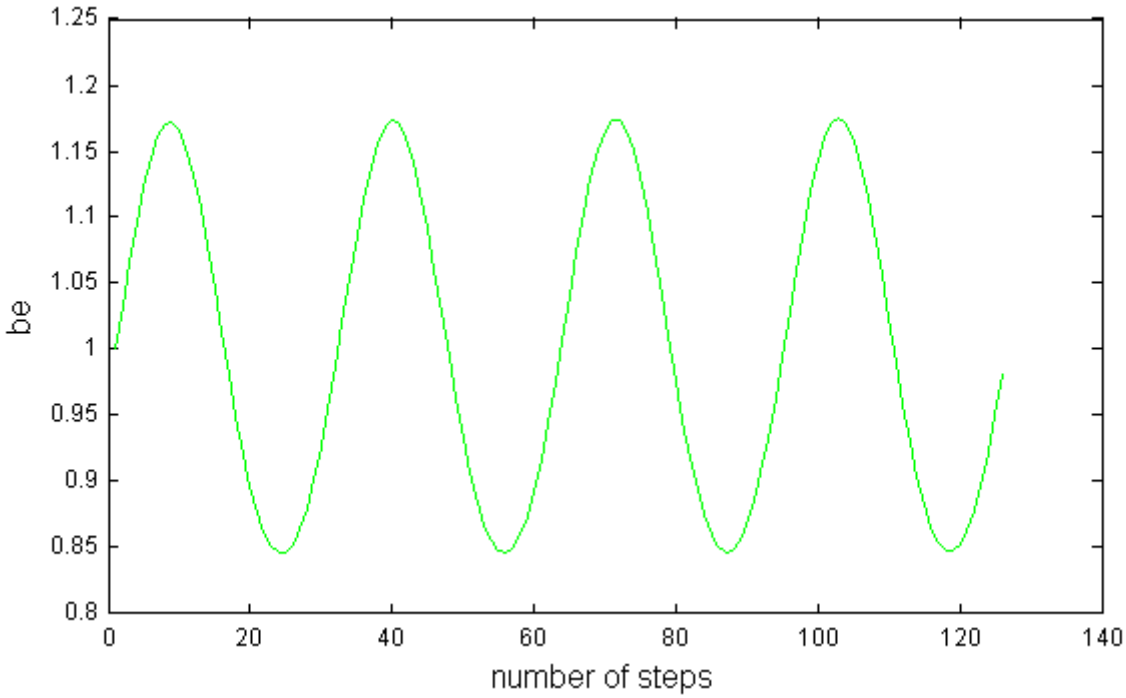

Published with MATLAB® 7.13

Bibliography

[1] ABAQUS/Standard Version 6.10-1. Abaqus/CAE user's manual. Providence, RI, USA: Dassault Systemes simulia Corp.; 2010.

[2] L. Anand. On H. Hencky's approximate strain energy function for moderate deformations. *J. Appl. Mech.*, 46:78-82, 1979.

[3] E.M., Arruda and M.C. Boyce. A three-dimensional model for the large stretch behavior of rubber elastic materials, *J. Mech. Phys. Solids* (1993), 41(2), pp. 389–412.

[4] R.C. Aster, B. Borchers, and C. H. Thurber. *Parameter estimation and inverse problems.* Academic Press, 2013.

[5] ASTM D412 Standard test methods for vulcanized rubber and thermoplastic elastomers — tension ASTM International, West Conshohocken, PA, USA.

[6] J. Avillez, M. Frost, S. Cawser, C. Skinner,A. El-Hamalawi, and P. Shields,(2012). Procedures for estimating environmental impact from railway induced vibration: a review. *American Society of Mechanical Engineers.* (pp. 381-392).

[7] J.M. Ball. Constitutive inequalities and existence theorems in nonlinear elastostatics, volume 1 of Nonlinear Analysis and Mechanics: Heriot-Watt Symposium. Pitman, Edinburgh, 1977b.

[8] J.F. Bell. *Mechanics of Solids: Volume 1: The Experimental Foundations of Solid Mechanics.* Handbuch der Physik. Springer, 1973.

[9] M. Bîrsan, P. Neff, and J. Lankeit. Sum of squared logarithms: An inequality relating positive definite matrices and their matrix logarithm. *J. Inequal. Appl.*, 2013(1):168, 2013.

[10] A. Björck, *Numerical methods for least squares problems.* Siam, 1996.

[11] M.C. Boyce and E.M. Arruda. Constitutive models of rubber elasticity: a review *Rubber Chemical Technology*, 73(2000), 504-522.

[12] G.L. Bradley, P.C. Chang, G.B. Mckenna. Rubber modelling using uniaxial data. *J. Appl. Polymer Sci* (2001). 81, 837–848.

[13] R. Brown. Physical testing of rubber (2006), 4th ed., Springer–Verlag, London.

[14] A. Calabrese, M. Spizzuoco, G. Serino, G. Della Corte, G. Maddaloni Shaking table investigation of a novel, low-cost, base isolation technology using recycled rubber. *Structural Control and Health Monitoring*, 22 (2015), 107-122.

[15] A.Calabrese, G. Serino, S. Strano, M. Terzo Investigation of the seismic performances of an FRBs base isolated steel frame through hybrid testing, World Congress on Mechanical Engineering 2013 Vol. III, London, UK.

[16] A.I. Camille Utilization of recycled crumb rubber as fine aggregates in concrete mix design. *Construction and Building Materials*, 42 (2013), 48-52.

[17] D.J. Charlton ,J. Yang,K. The K. A review of methods to characterize rubber elastic behavior for use in finite element analysis. Rubber Chemistry and Technology (1993).

[18] Y.C. Chen. Stability and bifurcation of homogeneous deformations of a compressible elastic body under pressure load. *Math. Mech. Solids*, 1(1):57–72, 1996.

[19] B.D. Coleman, and W. Noll, (1963). The thermodynamics of elastic materials with heat conduction and viscosity. *Arch. Rational Mech. Anal.*, 13, 167–178.

[20] B.D. Coleman, and W. Noll, (1961) Foundations of linear viscoelasticity *Rev. Modern Phys*, 33, 239–249

[21] B. Dacorogna. Polyconvex, quasiconvex and rank one convex functions. *Applied Mathematical Sciences* volume 78 , pages 155-263. Springer New York, 2007

[22] F. Deischl, L. Eisenmann,and L. Steinbeisser, (1995). Vibration problems in structures: practical guidelines. Bachman, H. Basel: Birkäuser Verlag.

[23] C. Esveld. Modern railway track. MRT-Productions, Netherlands (2001).

[24] ETRMA European Tire & Rubber Industry Statistics Edition 2013, European Tyre & Rubber Manufacturers' Association Brussels, Belgium.

[25] P. J. Flory. Thermodynamic relations for high elastic materials. *Trans. Faraday Sot* (1961). 57,829-838.

[26] A. N. Gent and P. B. Lindley. The compression of bonded rubber blocks. Proceedings of the Institution of Mechanical Engineers (1959), Vol. 173(3), pp. 111-122.

[27] S. Govindjee, and J.C. Simo, (1992). Mullins effect and the strain amplitude dependence of the storage modulus. *Int. J. Solids Struct.*, 29, 1737–1751.

[28] S. Govindjee and S. Reese A presentation and comparison of two large deformation viscoelasticity models. *J. Eng. Mater. Technol.*, 119, 251-255 (1997).

[29] J. Gough, A.H. Muhr, A.G. Thomas Effect of compressible filler on the elastic properties of rubber. Constitutive Models for Rubber III (2003), Busfield & Muhr (eds), 283-289.

[30] S.L. Grassie, R.W. Gregory, D. Harrison, K.L. Johnson (1982). The dynamic response of railway track to high frequency vertical excitation *Journal Mechanical Engineering Science* Vol. 24 No 2.

[31] M. Green and A. Tobolsky (1946). A new approach to the theory of relaxing polymeric media. *J. Chem. Phys.*, 14, 80–92.

[32] N. Hataf, M.M. Rahimi Experimental investigation of bearing capacity of sand reinforced with randomly distributed tire shreds. *Construction and Building Materials*, 20 (10) (2005), pp. 910–916.

[33] H. Hencky. *Zur Theorie plastischer Dehnungen und der hierdurch im Material hervorgerufenen Nachspannungen. Z. Angew. Math. Mech.*, 4(4):323-334, 1928.

[34] B. Hemsworth (2000). Reducing groundborne vibrations: state-of-the-art study. *Journal of Sound and Vibration*, 231(3), 703–709.

[35] D.Hibbit, B. Karlsson, & P. Sorensen, (2007). ABAQUS/Theory Manual. Hibbitt, Karlsson & Sorensen, Inc., Rhode Island, 6th edn.

[36] G. A. Holzapfel (1996). On large strain viscoelasticity: Continuum formulation and finite element applications to elastomeric structures. *Internat. J. Numer. Methods Engrg.*, 39, 3903–3926.

[37] G.A. Holzapfel Nonlinear Solid Mechanics: A Continuum Approach for Engineering Chichester: J. Wiley & Sons (2000), p. 440.

[38] G.A. Holzapfel and T.C. Gasser (2001). A viscoelastic model for fiber-reinforced composites at finite strains: Continuum basis, computational aspects and applications. *Comput.Meth. Appl. Mech. Eng.*, 190, 4379–4403.

[39] C.O. Horgan and J.G. Murphy Compression tests and constitutive models for the slight compressibility of elastic rubber-like materials. *International Journal of Engineering Science*, 47 (2009), 1232-1239.

[40] C. Horgan and J. Murphy. On the volumetric part of strain-energy functions used in the constitutive modeling of slightly compressible solid rubbers. *Int. J. Solids Struct.*, 46(16):3078–3085, 2009.

[41] C. O. Horgan, J. G. Murphy, On the volumetric part of strain-energy function used in the constitutive modeling of slightly compressible solid rubbers. *Interational Journal of Solids and Structures* (2009). 46, 3078–3085.

[42] H.E.M Hunt, M.F.M. Hussein, (2007) Ground borne vibration transmission from road and rail systems prediction and control. Handbook of Noise and Vibration

[43] Isolgomma s.r.l. Applications of Tire derived material. Retrieved from: http://www.isolgomma.com/eng/referenze.php (Accessed : 10 February 2015).

[44] C.S. Jog and K.D. Patil. Conditions for the onset of elastic and material instabilities in hyperelastic materials. *Arch. Appl. Mech.*, 83:1–24, 2013.

[45] D.F. Jones and L.R.G. Treloar. The properties of rubber in pure homogeneous strain. *J. Phys. D: Appl. Phys.*, 8(11):1285, 1975.

[46] P.A. Kakavas. Prediction of the nonlinear Poisson function using large volumetric strains estimated from a finite hyperelastic material law. *Polymer Eng. Sci.*, 40(6):1330–1333, 2000.

[47] J.M. Kelly, A. Calabrese, G. Serino . Design criteria for fiber reinforced rubber bearings, 15th World Conference on Earthquake Engineering, Lisbon, Portugal (2012).

[48] L.G. Kurzweil,(1979). Ground-borne noise and vibration from underground rail systems. *Journal of Sound and Vibration*, 66(3), 363–370.

[49] J. Lankeit, P. Neff, and Y. Nakatsukasa. The minimization of matrix logarithms: On a fundamental property of the unitary polar factor. *Lin. Alg. Appl.*, 449(0):28 – 42, 2014.

[50] D. Lo Presti Recycled Tyre Rubber Modified Bitumens for road asphalt mixtures: A literature review. *Construction and Building Materials*,49 (2013), 863-881.

[51] J. Lubliner, (1985). A model of rubber viscoelasticity. *Mech. Res. Commun.*, 12, 93–99.

[52] P. Ludwik. *Elemente der technologischen Mechanik.* Springer, 1909, *https : //www.uni − due.de/imperia/md/content/mathematik/ag$_n$eff/ludwik − elementetechnologischemechanik.pdf*.

[53] MATLAB 2014b. Image Processing Toolbox Users Guide.

[54] MATLAB 2014b. Optimization Toolbox Users Guide.

[55] V.M. Makarov, V.F. Drozdovski Reprocessing of tyres and rubber wastes. Recycling from the rubber products industry. Ellis Horwood, Chichester, UK 1991.

[56] G. Montella, G. Mastroianni, G. Serino Experimental and Numerical Investigations on Innovative Floating-slab Track Including Recycled Rubber Elements, International Conference on Noise and Vibration Engineering, Leuven, Belgium (2012). 2869-2880.

[57] G. Montella, A. Calabrese, G. Serino. Mechanical characterization of a Tire Derived Material: Experiments, hyperelastic modeling and numerical validation. *Constr. Build. Mater.*, 2014(66):336, 2014.

[58] M. Mooney. A theory of large elastic deformation. *Journal of Applied Physics*, 11(9), pp. 582-592, 1940.

[59] P. Neff, B. Eidel, F. Osterbrink, and R. Martin. A Riemannian approach to strain measures in nonlinear elasticity. *C. R. Acad. Sci.*, 342:254–257, 2014.

[60] P. Neff, B. Eidel, F. Osterbrink, and R. Martin. Geometry, solid mechanics and logarithmic strain measures. The Hencky energy measures the geodesic distance of the deformation gradient $F \in \mathrm{GL}^+(n)$ to $\mathrm{SO}(n)$ in the unique left invariant Riemannian metric on $\mathrm{GL}(n)$ which is also right $\mathrm{O}(n)$-invariant. *in preparation*, 2015.

[61] P. Neff and I.D. Ghiba. The exponentiated Hencky-logarithmic strain energy. Part III: Coupling with idealized isotropic finite strain plasticity. *in preparation*, 2014.

[62] P. Neff and I.D. Ghiba. Loss of ellipticity in additive logarithmic finite strain plasticity. *Preprint arXiv:1403.3843, submitted*, 2015.

[63] P. Neff, I.D. Ghiba, and J. Lankeit. The exponentiated Hencky-logarithmic strain energy. Part I: Constitutive issues and rank–one convexity. *to appear J. Elasticity*, 2015.

[64] P. Neff, I.D. Ghiba, J. Lankeit, R. Martin, and D. Steigmann. The exponentiated Hencky-logarithmic strain energy. Part II: Coercivity, planar polyconvexity and existence of minimizers. *to appear in Z. Angew. Math. Phys.* , 2015.

[65] P. Neff, Y. Nakatsukasa, and A. Fischle. A logarithmic minimization property of the unitary polar factor in the spectral norm and the Frobenius matrix norm. *SIAM J. Matrix Analysis*, 35:1132–1154, 2014.

[66] R.W. Ogden. *Non-Linear Elastic Deformations.* Mathematics and its Applications. Ellis Horwood, Chichester, 1. edition, 1983.

[67] R.W. Ogden, G. Saccomandi, I. Sgura. Fitting Hyperelastic Models to Experimental Data. *Computational Mechanics*, 2004(34):484, 2004.

[68] S.D. Poisson. *Traité de Mécanique, 2.* 1811.

[69] S. Reese and S.Govindjee. A theory of finite viscoelasticity and numerical aspects. *Int. J. Solids Structures*, 35(26-27):3455–3482, 1998.

[70] R.S. Rivlin. Large elastic deformations of isotropic materials. IV. Further developments of the general theory, *Philosophical Transactions of the Royal Society of London* (1948) A241, 379-397.

[71] J.Schröder and P. Neff Invariant formulation of hyperelastic transverse isotropy based on polyconvex free energy functions. *International Journal of Solids and Structures*, 40(2):

[72] F. Sidoroff, (1974). Nonlinear Viscoelastic Model with an Intermediate Configuration. *Journal Mécaniques*, 13, 679–713.

[73] J.C. Simo, (1987). On a fully three-dimensional finite-strain viscoelastic damage model: Formulation and computational aspects. *Comput. Meth. Appl. Mech. Eng.*, 60, 153–173.

[74] C.W. Smith, R.J. Wootton, and K.E. Evans. Interpretation of experimental data for Poisson's ratio of highly nonlinear materials. *Exp. Mech.*, 39(4):356–362, 1999.

[75] D. Tabor. The bulk modulus of rubber. *Polymer*, 35(13):2759–2763, 1994.

[76] L.R.G. Treloar. Stress-strain data for vulcanised rubber under various types of deformation. *Trans. Faraday Soc.*, 40:59–70, 1944.

[77] L.R.G. Treloar. The elasticity and related properties of rubbers. *Rep. Prog. Phys.*, 36(7):755, 1973.

[78] L.R.G. Treloar. *The physics of rubber elasticity*. Oxford University Press, 1975.

[79] UNI 11059, 2003 Elementi antivibranti. Materassini elastomerici per armamenti ferrotranviari. Indagini di qualifica e controllo delle caratteristiche meccaniche e delle prestazioni.

[80] U.S. Environmental Protection Agency Innovative uses of scrap tires. Retrieved from: http://www.epa.gov/osw/conserve/materials/tires/science.htm (Accessed : 17 Dec 2014).

[81] C. Vallée. Lois de comportement élastique isotropes en grandes déformations. *Int. J. Eng. Sci.*, 16(7):451–457, 1978.

[82] C. Vallée, D. Fortuné, and C. Lerintiu. On the dual variable of the Cauchy stress tensor in isotropic finite hyperelasticity. *Comptes Rendus Mecanique*, 336(11):851–855, 2008.

[83] K. C. Valanis and R. F. Landel. The strain-energy function of a hyperelastic material in terms of the extension ratios. *J. Appl. Phys.* (1967), 38, 2997–3002.

[84] J. Zimmermann and M. Stommel. The mechanical behaviour of rubber under hydrostatic compression and the effect on the results of finite element analyses. *Arch. Appl. Mech.*, 83(2):293–302, 2013.

[85] O. H. Yeoh. Some forms of the strain energy function for rubber. *Rubber Chemistry and technology*, Volume 66, Issue 5, November 1993, Pages 754-771.

[86] J. Yoshida, M. Abe, and Y. Fujino, (2004). Constitutive Model of High-Damping Rubber *Materials. J. Eng. Mech.*, 130, 129–141.